COMPUTATIONAL STUDIES OF OPTICAL PROPERTIES OF SOME SILICON NANOSTRUCTURES

Ph.D. THESIS

by

SAPNA

DEPARTMENT OF CHEMISTRY
INDIAN INSTITUTE OF TECHNOLOGY ROORKEE
ROORKEE – 247667, INDIA
JULY, 2018

भारतीय प्रौद्योगिकी संस्थान रुड़की
INDIAN INSTITUTE OF TECHNOLOGY ROORKEE

COMPUTATIONAL STUDIES OF OPTICAL PROPERTIES OF SOME SILICON NANOSTRUCTURES

A THESIS

Submitted in partial fulfilment of the
requirements for the award of the degree

of

DOCTOR OF PHILOSOPHY

in

CHEMISTRY

by

SAPNA

DEPARTMENT OF CHEMISTRY
INDIAN INSTITUTE OF TECHNOLOGY ROORKEE
ROORKEE – 247667, INDIA
JULY, 2018

भारतीय प्रौद्योगिकी संस्थान रुड़की
INDIAN INSTITUTE OF TECHNOLOGY ROORKEE

©INDIAN INSTITUTE OF TECHNOLOGY ROORKEE, ROORKEE- 2018
ALL RIGHTS RESERVED

INDIAN INSTITUTE OF TECHNOLOGY ROORKEE ROORKEE

CANDIDATE'S DECLARATION

I hereby certify that the work which is being presented in the thesis entitled **"COMPUTATIONAL STUDIES OF OPTICAL PROPERTIES OF SOME SILICON NANOSTRUCTURES"** in partial fulfilment of the requirements for the award of the Degree of Doctor of Philosophy and submitted in the Department of Chemistry of the Indian Institute of Technology Roorkee, Roorkee is an authentic record of my own work carried out during a period from July, 2012 to July, 2018 under the supervision of Dr. P. P. Thankachan, Associate Professor,and Dr. Pallavi Debnath, Assistant Professor, Department of Chemistry, Indian Institute of Technology Roorkee, Roorkee.

The matter presented in this thesis has not been submitted by me for the award of any other degree of this or any other Institute.

(SAPNA)

This is to certify that the above statement made by the candidate is correct to the best of our knowledge.

(P. Debnath)
Supervisor

(P. P. Thankachan)
Supervisor

The Ph. D. Viva-Voce examination of **Ms. SAPNA**, Research Scholar has been held on ……………….

Chairman, SRC **Signature of External Examiner**

This is to certify that student has made all the corrections in the thesis.

Signature of Supervisors **Head of the Department**

Dated: ________

भारतीय प्रौद्योगिकी संस्थान रुड़की
INDIAN INSTITUTE OF TECHNOLOGY ROORKEE

Dedicated to my Parents

Abstract

The present thesis contains an account of some theoretical studies on silicon nano-systems. After a review of some uses and calculations silicon nanoclusters (SiNCs) a brief introduction to the theoretical methods used is given. Some preliminary calculations of the E_{gap} by several methods are followed by calculations of polarizability and complex dielectric constants and refractive indices. For these we use two sets of systems: (i) a set of open silanes and (ii) and a set of sila-diamondoids. An anomalous behavior is observed in the frequency dependence of optical properties in the case of sila-diamantane and ascribed tentatively to the relatively more compact structure. The thesis concludes with a study of one-photon absorption (OPA) and two-photon absorption (TPA) of silicenes with substitutions, and some concluding remarks.

भारतीय प्रौद्योगिकी संस्थान रुड़की
INDIAN INSTITUTE OF TECHNOLOGY ROORKEE

Acknowledgements

At the outset, I would like to express my sincere and deepest sense of gratitude to my supervisor Dr. P. P. Thankachan, for his meticulous guidance. He provided me unwavering encouragement and support in various ways. I feel privileged to have ample time and intellectual conversations with a brilliant person like him. I appreciate the way he has changed my whole perspective towards research and personal life. I would like to thank his sister and brother-in-law for their presence and support in every possible way.

I would like to convey sincere gratitude to my co-supervisor Dr. Pallavi Debnath, for her consistent guidance and support after the retirement of Dr. P. P. Thankachan. I admire her enthusiasm and attitude towards research. I appreciate her valuable suggestions which would help me develop as a sincere and independent researcher in future.

I take this opportunity to express my sincere thanks to Prof. M. R. Maurya, present Head of the Department, Prof. Anil Kumar, past Head of the Department, Prof. Ravi Bhushan, Department of Chemistry, for providing me research facilities, lab space even in the absence of Dr. P. P. Thankachan and their consistent guidance to finish my research work.

I feel privileged to express the gratitude to the Student Research Committee (SRC) members, Prof. M. R. Maurya (Chairman) and Dr. P. Jeevanandam (Internal Expert) of the Department of Chemistry and Prof. A. K. Sen (External Expert) of the Department of Earth Sciences, for taking out time from their schedules to advise me on my research work.

I would like to express unfeigned thanks to Prof. S. K. Nath, Head of Centre for Nanotechnology for extending the centre’s research facilities and for giving me permission to avail the software facility while carrying out my research work.

I am thankful to the non-teaching staff of the Department of Chemistry, Mr. S. P. Singh, Mr. Tiwari, Ankur, Mr. MadanPal, Mr. Ramesh and all other staff members for their countless assistance and cooperation over these years.

I would like to specially thank Dr. C. N. Ramachandran, Dr. K. R. Justin Thomas, Dr. R. K. Dutta and Dr. R. K. Pedentti, for moral support.

I am thankful to The Head, Institute Computer Centre (ICC) for providing me high performance computing (HPC) facility. I would like to express special thanks to Dr. Navneet Kumar Gupta (System Programmer) for helping me sorting out problems related to HPC and supporting me to complete my research work.

I specially thank Dr. Soumita Talukdar, Dr. Surinder Pal Kaur, Dr. Varun Kundi and Dr. Nishant Kumar Verma, Dr. Pinki Sharma, Dr. Abhishek Baheti, and Divya Yadav for their tremendous support both in presence and absence. I thank my MSc friends for always encouraging me and supplying doses of tranquilizers through humour whenever I needed.

I would like to deeply thank Pooja Kesari, Shailza Singh, Pallavi Singh, Priyanka Gunjan, Neetu, Savita, for helping and encouraging me during last crucial years. I thank my friends and juniors, Varinder, Shubrajyotsna, Niyati, Anjali, Nity, Neethu, Mandeep Kaur, Nabi Ahamad, Prakhar Shukla, Vinit, Mohan Tiwari, Sujith, Ankita, Azfar, Deepika Das, Deepika Malwal, Ishita, Anita, Toshi for assistance and support.

I would also like to acknowledge Ankit Ranjan for helping me tackle the challenges faced during these years. I thank Abhishek Singh Tomar, Ashish Bagoria, Uditya Raj and Vandan Kothari to remain always there for any help. I would also like to thank Govind Babu Srivastava, Poonam for help and support.

I owe special mention and deepest thanks to Coach Daljit Singh and Satish Saini for bringing the best and worst out of me and motivating me all these years.

Further, I would like to thank my parents who have always believed in me and supported me immensely. I deeply express my heartfelt gratitude for their eternal love and blessings. I appreciate the love, care and support of my brothers Yashpal Bondwal and Umesh Bondwal for always standing by my side and encouraging me to achieve my goals. I thank my sister-in-law, Sarita Bondwal for her support.

I would like to express profound gratitude to my uncle Rajbir Singh Bondwal and my aunt Krishna Devi for consistently inspiring me to aspire for higher education. I thank my cousins Vishal Bondwal and Varun Bondwal for their love, care and support.

All adjectives are small to express my gratitude to my father Fateh Singh Bondwal and my mother Prabha Devi for bringing me up as a kind and strong individual. Despite of all the hardships, they provided me all the comforts throughout my academic journey. I admire them for their immense patience, perseverance, support and never giving up attitude. I dedicate this thesis to them.

I would like to acknowledge the research funding by Indian Institute of Technology Roorkee, India and Student Aid Committee for awarding me fellowship for carrying out my research work all through.

Finally, I thank ALMIGHTY GOD for providing me inner strength and peace to keep going with positivity.

SAPNA
IIT ROORKEE
July, 2018

Table of Contents

Candidate's Declaration

Abstract i

Acknowledgements iii

List of Abbreviations xi

List of Figures xiii

List of Tables xv

List of Publications xvii

List of Conferences/Workshops xix

Chapter 1 Introduction **1**
- 1.1 Quantum Confinement 2
- 1.2 Silicon Quantum Dots (SiQDs) 4
- 1.3 Theoretical Studies 5
- 1.4 Sila-Diamondoids: Silicon analogues of Diamondoids 7
- 1.5 Applications of Silicon Quantum Dots 9
- 1.6 Silicene: Silicon analogue of Graphene 9
- 1.6 1.6.1 Silicene derivatives 10
  - 1.6.2 Bandgap-tuning in Silicene 11
- 1.7 Applications of Silicene 11
- 1.8 Objectives of the present work 12

Chapter 2 Theoretical Background **13**
- 2.1 The Schrödinger Equation 13
- 2.2 Hartree-Fock Method 14
- 2.3 Post-Hartree Fock Methods 16
- 2.4 Density Functional Theory (DFT) Methods 17
  - 2.4.1 Generalized Gradient Approximation (GGA) 18
- 2.5 Time-Dependent Density Functional Theory (TDDFT) 19
- 2.6 Solid-State Calculations 21
  - 2.6.1 Supercell Approach 22
  - 2.6.2 Pseudopotentials 23

Chapter 3 Silicon Quantum Dots: Model systems **25**
- 3.1 Introduction 25

3.1.1 HOMO-LUMO Energy Gap 25
3.2 Computational Details 26
3.3 Results and Discussion 26
3.3.1 Linear silanes 26
3.3.2 Comparison of linear and branched silanes 28
3.3.3 Comparison of linear and cyclic silanes 30
3.4 Conclusion 33

Chapter 4 Structural, Electronic and Optical properties of model Silicon quantum dots: a Computational Study 35
4.1 Introduction 35
4.2 Computational Details 35
4.3 Results and Discussion 37
4.3.1 Polycyclic Silanes 37
4.4 Studies of Static mean Polarizability of model SiNCs 38
4.5 Optical Properties 41
4.5.1 Optical Spectra 42
4.5.1.1 Dielectric Function 42
4.5.1.2 Refractive Index (n) 44
4.5.1.3 Extinction Coefficient (k) 47
4.6 Conclusion 48
Appendix 4.I 49
Appendix 4.II 50

Chapter 5 Bandgap Tuning and Two-Photon Activity of push-pull derivatives of silyl substituted silicene monolayer 51
5.1 Introduction 51
5.2 Computational Details 52
5.3 Model Silicene Systems 54
5.3.1 Unsubstituted 54
5.3.2 Substituted 55
5.4 Theoretical Concepts 55
5.4.1 One-Photon Absorption (OPA) Process 55
5.4.2 Two-Photon Absorption (TPA) Process 55
5.4.3 Λ Parameter 56
5.5 Results and Discussion 57
5.5.1 Unsubstituted 57
5.5.2 Substituted 60
5.5.2.1 Bandgap tuning 60
5.5.2.2 OPA/TPA properties 62
5.6 Conclusion 72

Chapter 6 Concluding Remarks 75

References 77

भारतीय प्रौद्योगिकी संस्थान रुड़की
INDIAN INSTITUTE OF TECHNOLOGY ROORKEE

List of Abbreviations

QDs	Quantum Dots
SiQDs	Silicon Quantum Dots
SiNCs	Silicon Nanoclusters
HF	Hartree-Fock
SCF	Self-consistent field
MCSCF	Multi-configuration self-consistent-field
DFT	Density Functional Theory
KS	Kohn Sham
TDDFT	Time-Dependent Density Functional Theory
MPn	n^{th} order Møller Plesset method
MBPT	Many Body Perturbation Theory
CC	Coupled Cluster
CI	Configuration Interaction
XC	Exchange-correlation
B3LYP	Becke's 3-parameter exchange functional with Lee-Yang-Parr correlation functional
PBE	Perdew Burke Ernzerhof functional
CAM-B3LYP	Coulomb-attenuating method Becke 3-parameter Lee-Yang-Parr functional
LDA	Local Density Approximation
GGA	Generalized Gradient Approximation
CASTEP	Cambridge Serial Total Energy Package
FFT	Fast Fourier Transform
PPs	Pseudopotentials
USPPs	Ultrasoft Pseudopotentials
OPA	One-Photon Absorption
TPA	Two-Photon Absorption
SOS	Sum-over States

भारतीय प्रौद्योगिकी संस्थान रुड़की
INDIAN INSTITUTE OF TECHNOLOGY ROORKEE

List of Figures

3.1. The gas phase optimized geometry of the linear silanes at B3LYP/6-31G(d) level of theory. 27

3.2. The gas phase optimized geometries of branched silanes at B3LYP/6-31G(d) level of theory. (a) isomers of linear *n*-Si_4H_{10} (b) isomers of linear *n*-Si_5H_{12} (c) isomers of linear *n*-Si_6H_{14}. 29

3.3. Gas phase optimized geometries of cyclic silanes, Si_nH_{2n} (n=5 and 6) at B3LYP/6-31G(d) level of theory in gas phase. I- *envelope*- Si_5H_{10} (C_s), II- *twist*-Si_5H_{10}(C_2), III- *chair*- Si_6H_{12} (D_{3d}), IV- *boat*- Si_6H_{12}(C_{2V}), V- *twist boat*- Si_6H_{12} (D_2) and VI- *half chair*- Si_6H_{12} (C_2). 31

4.1. Gas phase optimized geometries of (a) acyclic clusters containing diamond like core and (b) series of sila-diamondoids, $Si_{2(2n+1)}H_{4(n+2)}$ (n = 1, 2,…4) at B3LYP/6-31G(d) level of theory. 37

4.2. Imaginary part (ε_2) of the complex dielectric function of (a) acyclic SiNCs, SiH_4, Si_5H_{12} and $Si_{17}H_{36}$ (b) hydrogenated sila-diamondoids, Si_6H_{12}, $Si_{10}H_{16}$, $Si_{14}H_{20}$, $Si_{18}H_{24}$. 43

4.3. Frequency dependence of the real part of the refractive index (n) of hydrogenated sila-diamondoids, Si_6H_{12}, $Si_{10}H_{16}$, $Si_{14}H_{20}$, $Si_{18}H_{24}$. 44

4.4. Size dependence of the real part of the refractive index (n) of dehydrogenated sila-diamondoids, Si_{10}, Si_{14}, Si_{18} and sila-diamantane, $Si_{14}H_{19}$ with one apical hydrogen missing (one surface dangling bond). 45

4.5. Frequency dependence of Extinction coefficient (k) (a) hydrogenated sila-diamondoids (b) dehydrogenated sila-diamondoids. 46

4.6. Extinction coefficient, **k** (imaginary part of refractive index) of acyclic SiNCs (a) Si_5H_{12} and (b) $Si_{17}H_{36}$. 47

5.1. Optimized geometries of silicene systems terminated at the edges by hydrogen or by H and one -SiH_3 or –SiH_2SiH_3 groups denoted as S, S_0 and S_1 respectively. The lines correspond to the coordinate axes. 52

5.2. Gas phase optimized geometries of the model systems S_1 substituted with D/A pair at PBE/6-31G(d) level of theory. 53

5.3. A schematic representation of the tuned HOMO, LUMO energy levels and HOMO-LUMO energy gaps of silicene derivatives (summarized from Table 5.3 and Table 5.6). 61

List of Tables

3.1. HOMO-LUMO gaps of *n*-silanes Si_nH_{2n+2}(n=1, 2, ..., 6) at different levels of theory. 28

3.2. HOMO-LUMO gaps of linear and branched silanes at different levels of theory. 29

3.3. HOMO-LUMO gaps of linear Si_5H_{12} and cyclic Si_5H_{10} at different levels of theory. 32

3.4. HOMO-LUMO gaps of linear Si_6H_{14} and conformers of cyclohexasilane, Si_6H_{12} at different levels of theory. 32

4.1(a). Static mean polarizabilities ($Å^3$), static mean polarizability per atom and HOMO-LUMO gaps (eV) in a series of sila-diamondoids. 39

4.1(b). Static mean polarizability $\bar{\alpha}$ ($Å^3$), static mean polarizability per atom $\bar{\alpha}/n_c$ ($Å^3$) and HOMO-LUMO gaps (eV) in a series of sila-Diamondoids calculated at CAM-B3LYP/6-31++G** level of theory. 40

4.2(a) Static mean polarizability, $\bar{\alpha}$ ($Å^3$), static mean polarizability per atom and HOMO-LUMO gaps, E_{gap} (eV) in a series of the acyclic silanes with tetrahedral symmetry. 40

4.2(b) Static mean polarizability, $\bar{\alpha}$ ($Å^3$), Static mean polarizability per atom and HOMO-LUMO gaps, E_{gap} (eV) in a series of the acyclic silanes at CAM-B3LYP/6-31++G** level of theory. 40

4.3. HOMO-LUMO gap, E_g (eV) of sila-diamondoids and non-cyclic SiNCs with T_d symmetry at B3LYP/6-31G (d) level of theory, optical bandgap, E_p (eV) obtained from the maximum of the plot of ε_2 as a function of photon energy and the maximum value of imaginary part of the complex dielectric function ($\varepsilon_{2\,(max)}$). 44

5.1. The nomenclature of model substituted silicene systems, different acceptor and donor groups, and their structure. 54

5.2 OPA parameters of first five excited states f_i (i = 1, 2, …, 5) of the model systems, S, S_0 and S_1 (with representative MO picture of S_1) calculated at level of theory CAMB3LYP/cc-pVDZ in gas phase. 58

5.3 Parameters for TPA of first five excited states f_i (i = 1, 2, …, 5) of the systems S, S_0 and S_1 in gas phase calculated at the level of theory CAMB3LYP/cc-pVDZ: HOMO, LUMO energies (a.u.), (HL)gap (eV), Excitation energy (E), TPA cross-section (σ_{TPA}) and transition probability (δ_{TPA}). 59

5.4 TPA tensor components (S_{ij}) of the first five excited states f_i (i = 1, 2, …, 5) of silicene systems, S, S_0 and S_1 the systems calculated at level of theory CAM-B3LYP/cc-pVDZ in gas phase. 60

5.5(a) OPA parameters of first five excited states f_i (i = 1, 2, …, 5) of the model silicene system $S_1A_1D_1$ in gas phase calculated at level of theory CAMB3LYP/cc-pVDZ, and MO contour plots of $S_1A_1D_1$. 62

5.5(b) Parameters for OPA of first five excited states f_i (i = 1, 2, …, 5) of the model silicene system $S_1A_2D_1$ in gas phase calculated at level of theory CAMB3LYP/cc-pVDZ, and MO-contour plots of $S_1A_2D_1$. 63

5.5(c) Parameters for OPA of first five excited states f_i (i = 1, 2, …, 5) of the model silicene system $S_1A_1D_2$ in gas phase calculated at level of theory CAMB3LYP/cc-pVDZ, and MO-contour plots of $S_1A_1D_2$. 64

5.5(d) Parameters for OPA of first five excited states f_i (i = 1, 2, …, 5) of the model silicene system $S_1A_2D_2$ in gas phase calculated at level of theory CAMB3LYP/cc-pVDZ, and MO-contour plots of $S_1A_2D_2$. 65

5.5(e) Parameters for OPA of first five excited states f_i (i = 1, 2, …, 5) of the model silicene system $S_1A_3D_3$ in gas phase calculated at level of theory CAMB3LYP/cc-pVDZ, and MO-contour plots of $S_1A_3D_3$. 66

5.5(f) Parameters for OPA of first five excited states f_i (i = 1, 2, …, 5) of the model silicene system $S_1A_4D_4$ in gas phase calculated at level of theory CAMB3LYP/cc-pVDZ, and MO-contour plots of $S_1A_4D_4$. 67

5.5(g) Parameters for OPA of first five excited states f_i (i = 1, 2, …, 5) of the model silicene system $S_1A_5D_5$ in gas phase calculated at level of theory CAMB3LYP/cc-pVDZ, and MO-contour plots of $S_1A_5D_5$. 68

5.6 TPA parameters of first five excited states f_i (i = 1, 2, …, 5) of all the systems S_1 substituted with D/A pair in gas phase calculated at level of theory CAMB3LYP/cc-pVDZ: HOMO, LUMO energies (a.u.), (HL)gap (eV), Excitation energy (E), TPA cross-section (σ_{TPA}) and transition probability (δ_{TPA}). 70

5.7 TPA tensor components (S_{ij}) of the first five excited states f_i (i = 1, 2, …, 5) of system, S_1 substituted with D/A pair calculated at level of theory CAM-B3LYP/cc-pVDZ in gas phase. 71

List of Publications

Publication(s) related to Thesis

1. **Sapna Bondwal**, Pallavi Debnath and Pompozhi Protasis Thankachan; "Structural, Electronic and Optical properties of model silicon quantum dots: a computational study." *Phys. E Low Dimens. Syst.*, 2018, **103**, 194.

2. **Sapna Bondwal**, Pallavi Debnath and Pompozhi Protasis Thankachan; "Bandgap tuning and two-photon activity of push-pull derivatives of silyl substituted silicene monolayer," manuscript in preparation.

Publication(s) not related to Thesis

1. Venkateshwar Rao Tamula, Sapna Bondwal, Priyanka Bisht, Chandrashekar Pendem, and Jagdish Kumar: "Oxidation of sulfides to sulfones with hydrogen peroxide in the presence of acetic acid and Amberlyst 15." *Reac. Kinet. Mech. Cat.*, 2012, **107**, 449.

List of Conferences/ Workshops

1. Attended International Conference on ‘*Chemistry with Computers’*, *IIIT Hyderabad, India*, January 18-19, 2014.
2. Attended *Theoretical Chemistry Symposium*, *CSIR-NCL*, *Pune*, *India*, December 18-21, 2014.
3. S. Bondwal, P. Debnath and P. P. Thankachan, Nature of transition in model silicon quantum dots, *International Conference on Nanotechnology: Ideas, Innovations & Initiatives*-2017, *Indian Institute of Technology Roorkee*, *Roorkee, India* December 6-8, 2017. (Received third position in the oral presentation, under the theme Computational Nanotechnology).

INDIAN INSTITUTE OF TECHNOLOGY ROORKEE

Chapter 1

Introduction

“The problems of chemistry and biology can be greatly helped if our ability to see what we are doing, and to do things on an atomic level, is ultimately developed—a development which I think cannot be avoided.”

Richard Feynman

Since the advent of this century, science and engineering has seen increasingly rapid interest in materials at nanoscale as made explicit by Richard Feynman [1] in 1959 in his famous Caltech lecture “There’s plenty of room at the bottom: an invitation to enter a new field of physics.”

The prefix “nano” means one billionth part of something. By convention, a nanostructure is an object with size (at least in one of the directions) in the range between 1 and 100 nm. Nanostructures encompass objects with sizes ranging from single atoms (size of an atom ≈ 0.1 nm) to large clusters comprising up to 10^8 atoms or molecules. Sharp changes in material properties like physical, electronic, magnetic properties occur in switching from macroscale to the nanoscale material structures; forms a formidable reason behind strong interest in the latter. These dramatic changes in properties are due to small size, where surface effects become dominant and quantum size effects occur.

1.1 Quantum Confinement

The word quantum-confinement is made up of two words, quantum which reflects the atomic regime of particles and confinement involves restrictions to the motion of such randomly moving particles like electrons or holes in specific dimensions. The quantum-confinement effect comes into picture when the particle is squeezed into increasingly smaller dimensions comparable with the spatial extent of allowed electronic motion. Consequently, confined particles tend to feel the constraints of the confined boundaries, and respond to the changes in size by adjusting their energy. The length scale where quantum confinement effects are observed, ranges from 1—25 nm for typical semiconductors. As the restrictions on the particle motion approaches quantum-confinement regime, the energy levels become discrete resulting in widening of bandgap. Bandgap increases as size decreases and blue shift is observed in the absorption/emission spectrum. This phenomenon is called as the quantum size effect.

When a semiconductor is irradiated with light of energy equal to or higher than that of the bandgap, electrons get excited to conduction band while holes stay in the valence band and the resultant electron-hole pair is called an ‘exciton’. By the analogy of hydrogen atom, the most probable distance between electron and hole in an exciton, is termed as exciton Bohr radius of a particular semiconductor. Bohr radius of a particle, which may refer to electron or hole in a nanostructure like nanocrystal, is expressed as [2],

$$a_B = \varepsilon \frac{m}{m^*} a_0 \tag{1.1}$$

where, ε denotes the material dielectric constant and, m^* and m correspond to the effective mass and rest mass of the particle, respectively. a_0 is the Bohr radius of hydrogen atom.

Quantization effects become more prominent when size of the semiconductor is near to and below Bohr exciton radius of bulk semiconductor leading to strong dependence of the properties of materials on its size and shape [3]. The shift energy gap of nanoparticle ($E_{g(nano)}$) from that of bulk ($E_{g(bulk)}$) can be expressed in terms of the Brus equation [4], which takes into account Coulomb interaction between electron and hole in exciton and polarization terms in the Hamiltonian for first excited state, and is given by:

$$E_{g(nano)} = E_{g(bulk)} + \frac{\hbar^2 \pi^2}{2R^2}\left(\frac{1}{m_e^*} + \frac{1}{m_h^*}\right) - \frac{1.86\, e^2}{\epsilon R} \tag{1.2}$$

where R is radius of semiconductor, m_e^* and m_h^* are the effective masses of electron and hole, respectively, $\hbar$ is the reduced Plank constant, e is the electron charge and ε corresponds to semiconductor dielectric constant.

A semiconductor with radius $R << a_o$, corresponds to strong confinement regime, while $R >> a_o$, corresponds to weak confinement regime. So, the phenomenon of quantum confinement occurs when exciton is squeezed to a dimension that approaches critically the domain of quantum measurements.

Unlike a periodic bulk system, electronic picture of quantum confined system is characterized by discrete energy levels much like a many-electron atomic system. Such quantum confined systems in which charge carriers are confined in all the three dimensions and length scale lies below Bohr radius is defined as *'quantum dot'*. The term 'quantum dot' was coined in 1986 by Reed [5] and was first discovered in a glass matrix and in colloidal solution [6] by Alexey , Efros [7] and Louis Brus [8,9]. Quantum confinement effect in clusters was first evidenced through spectroscopic studies on CuCl clusters grown in silicate glasses which indicated a blue shift (up to 0.1eV) of absorption spectrum relative to the bulk [10]. On similar terms, there can be two other types of confined systems: *quantum wires* where motion of charge carriers are restricted only to one dimension, and *quantum wells* where charge carriers are allowed to move rather in only two spatial dimensions.

The material of choice exhibit different phenomena of interest, corresponding to different length scales and time scales; accordingly simulation procedures have to be developed to effectively describe the properties and behavior of materials. Theory throws light on the fundamentals behind innovation, design and fabrication of a particular material, by incorporating aspects of physics, chemistry, materials science and engineering. The structural, electronic and optical properties of new materials can be described accurately by first-principles methods [11]. The present study focuses on small length scales, for which it is possible to employ first-principles or ab-initio many-body quantum-mechanical methods. In particular, in this thesis, we shall present results from calculations using density-functional theory (DFT) [12]. DFT is an extremely popular method and its ability to deal with challenging problems in a fairly good and cost effective manner. With ongoing advances in theoretical methods and availability of improved computational resources every other day, the possibility of simulating greater number of atoms using DFT has increased in last decade. DFT is found to be capable in producing reliable results in less time in a wide variety of calculations, concerning diverse fields such as materials science [13], biology [14], molecular physics [15], nanotechnology [16] and many more, thus, maintaining a balance between accuracy and computation time.

The emerging field of nanoscience and nanotechnology allows modelling of systems of different sizes, thus offering opportunities to researchers for exploring novel properties shown by a material at different sizes. But at the same time, corresponding size of systems that can be probed and controlled experimentally has become quite challenging. The current scenario, suggests a possible meeting point between first-principles simulations and experiment. Electronic structure calculations provide valuable insights into the properties of novel nanostructures such as quantum dots, nanowires and nanotubes [17,18], to name a few. Electronic properties of nanoscale materials depend strongly on atomistic details of the system under consideration, therefore, first-principles simulations are necessary for obtaining qualitatively and quantitatively correct results, which can direct experimentalists to further realize the material of choice.

Extensive theoretical research, have successfully led to the development of more sophisticated, stable, accurate and computationally inexpensive simulation procedures based on first-principles methods, in order to deal with present scientific problems [19,20]. Therefore, theoretical approaches can be routinely used not only to explain experimental findings but also to predict the properties of proposed model nanostructures [21], thus allowing design of new devices. [22, 23].

1.2 Silicon Quantum Dots (SiQDs)

Silicon is a ubiquitous electronic material due to its abundance and relatively benign character. The economic feasibility and retention of semiconducting properties over a wide range of temperatures makes it a material of choice in Si based technology. The current knowledge of Si properties and the sophistication of Si technology are impressive [24]. The manufacture of complex architectures of Si based integrated circuits and devices has progressed exponentially. Researchers have made tremendous efforts in the area of microelectronics to implement innovative ideas and design unique devices in cost effective ways [25].

Bulk silicon exhibits indirect transitions between the valence band states and the conduction band states and their occurrence involves phonon-assisted transitions and non-radiative relaxation processes [26]. Indirect transitions require simultaneous absorption/emission of phonon in order to satisfy momentum conservation rules which make occurrence of radiative recombination processes less probable. Hence, the indirect bandgap of silicon curtails its optical efficiency and makes it less interesting for light emitting devices. In 1990, Canham [27] observed visible luminescence in porous silicon which led researchers to explore the nature of transitions occurring in nanosized silicon [28]. It has been found that a type of transition intermediate between indirect and direct transitions can be observed when the size of silicon crystal is reduced to nano-dimension owing to the relaxation in selection rules which govern transitions from valence band states to conduction band states [29−31]. The **k** conservation rules are relaxed at nanoscale due to strong quantum confinement effect. Quantum confinement and surface effects stimulate direct transitions in silicon nanoclusters [32,33]. Further, hydrogenation leads to the widening of energy gap and enhances the stability of the silicon nanocluster [34, 35]. The silicon atom on the surface of the nanocluster has free valence state which encroach the bandgap region, predominantly the region near the band edges, giving rise to several intermediate transitions [36]. Hence, the energy gaps are reduced compared to fully hydrogenated counterparts [37].

The dangling bond behaves as an electron-hole recombination center. The recombination process can take place both radiatively and non-radiatively [38] depending upon the bandgap of nanocluster. Non-radiative recombination process occurs through two possible channels: Intrinsic Auger recombination [39] and extrinsic recombination on the neutral surface dangling bond [40]. Lannoo and coworkers have made detailed studies on the effect of the presence of surface dangling bonds on the surface of silicon nanoclusters and state that for silicon nanoclusters with bandgap less than 2.2eV, the presence of one neutral dangling bond leads to non-radiative capture of electron (or hole) [41]. So, phonon-assisted transitions become dominant as in bulk silicon. Also, the existence of localized states [42] of the form of ‘self trapped states’ [43] which behave as luminescent centers in confined systems leads to radiative recombination processes. In case of silicon nanoclusters, the mixing of different **k** states is such that optical properties intermediate between indirect bandgap and direct bandgap material can also be observed [44].

1.3 Theoretical Studies

The electronic structure of nanomaterials has been investigated by various theoretical methods. These include *ab-initio* molecular structure calculations at different levels such as Hartree-Fock, Moller-Plesset perturbation theory and so on, semi-empirical methods and density functional theory using different functionals.

In the studies based on the structure and stability of a nanocluster, the stable structure is determined by searching the configuration which realize the global energy minimum and so corresponds to the ground state energy [45]. Isomeric configurations with energy values in the range very near to the ground state energy makes it complicated to predict the stable nanocluster. First-principles studies dealing with such a situation is addressed by Matsko et al. [46]. They performed calculations with DFT, hybrid functionals, Hartree-Fock methods, and GW-approximation methods. Their analysis of energetic of SiNCs terminated by hydrogen $Si_{10}H_{2n}$ ($0 \leq n \leq 11$), shows that, the structure loses its compactness and becomes loosely packed and branched on hydrogen termination, and isomer energy ordering exhibits considerable sensitivity towards many-electron effects. The exchange-correlation (XC) contribution is subject to approximations such as the standard local-density approximation [47] and generalized-gradient approximation [48] which may affect the accurate description of the energies of the structure under study. So, it is essential to include XC contribution. The use of hybrid functional like B3LYP [49] is often considered as a very accurate approach for the description of nanoclusters.

Grossman applied quantum Monte Carlo methods to calculate the total energy of SiNCs. Their results show that the energetics of nanocluster can be affected significantly by proper description of the electron correlation effects [50]. Seminario and coworkers [51] employed sophisticated compound methods G1-G4, CBS and W1 as well as density functional theory to calculate the electronic and charge states of silicon nanoclusters (Si_n, with n in the range 1 to 96) and found that B3PW91 functional yields results comparable with those of the compound methods and agree well with the experimental data. Lehtonen and Sundholm [52], studied excited state properties of SiNCs $Si_{29}H_{24}$, $Si_{29}H_{36}$, and $Si_{35}H_{36}$ at the DFT level using first-order linear-response-theory approach. Frank-Condon shift for the first excited state of $Si_{29}H_{24}$ was reported to be in agreement with the experiments while the shifts for $Si_{29}H_{36}$, and $Si_{35}H_{36}$ were smaller than the experimental values. Further DFT studies on the recently synthesized molecule $Si_{14}C_{24}H_{72}$ which is sila-adamantane (Si_{10}) capped by twelve methyl groups and four trimethylsilyl groups were also done by the same research group [53]. They have used Becke-Perdew functional and triple- Zeta quality basis sets augmented with polarization functions for the optimization of this structure and also for related hydrogen terminated nanoclusters with Si_{10} cage at the centre. The excitation spectra of these systems were studied using TDDFT level by employing functionals of GGA type and the silicon nanoclusters with fused adamantane units, and found to have weaker oscillator strengths than small capped adamantane cage. In a recent work by Niaz and Zdetsis [54], the energy gaps of a large number of spherical quantum dots obtained from DFT calculations using B3LYP functional have been fitted to a formula of the form $(A + B)/ D$ where A and B are parameters to be fitted and D is the estimated diameter of quantum dot and energy gaps of elongated quantum dots to an analogous formula of the form $A + BN^{-1/3}$ where N is the number of atoms involved. This work has been extended by them to test other functionals later. Gopir and coworkers [55] performed DFT based study of quantum confinement effects and electronic properties of small silicon quantum dots in the ground state condition using numerical basis sets. They also examined DOS and deduced the HOMO-LUMO gaps of SiQDs. Baturin et al. [56] reported a very interesting study of atomic structure and stability of the ensemble of SiNCs $Si_{10}H_{2m}$ (m = 0–12) using evolutionary structure searching through USPEX code and DFT. Their calculations show that the Si atom arrangement in $Si_{10}H_{16}$ closely resembles the diamond crystal structure and the ensemble of clusters with Si_{10} core remains uniform after hydrogen termination only if concentration of hydrogen corresponds to stable compositions, $Si_{10}H_{14}$, $Si_{10}H_{16}$, $Si_{10}H_{20}$, or $Si_{10}H_{22}$. They have also studied thermodynamical properties of small SiNCs passivated by hydrogen and oxygen by tracing the connection between geometry and passivation degree using graph theory.

Petkov and coworkers [57] investigated structure-property correlation in Si nanoparticles by a simulation set up involving high-energy synchrotron X-ray diffraction coupled to atomic pair distribution function analysis and computer simulations and determined the atomic-scale structure of silicon nanoparticles obtained by two different synthetic route.

For saving time the inner electrons are sometimes represented by effective core potentials or pseudopotentials in a vast number of calculations [58] [59]. Wang et al. [60] have shown a simple linear-in-size method which enables calculation of eigensolutions of the Schrödinger equation in a desired window and studied the near-gap electronic structure of SiQDs using plane waves pseudopotenial approach. Further, Andrea Dal Corso developed a well-tested library of projector augmented-wave (PAW) and ultrasoft pseudopotentials (PPs) for all elements of periodic table from H to Pu [61].

1.4 Sila-Diamondoids: Silicon analogues of Diamondoids

The literature from last few decades is well equipped with findings on carbon based nanomaterials like carbon dots, carbon nanotubes, carbon nanosheets, fullerenes, graphene [62], to name a few. Carbon belongs to group IV of the periodic table. It exists in two allotropic forms namely, diamond and graphite. The diamond structure has adamantane as basic unit. The basic structure of adamantane comprises of three connected cyclohexane rings arranged in “armchair” configuration. It is the simplest diamondoid.

Nanodiamondoids is a new class of nanomaterials which find applications in various fields, namely, chemical, biological and medicinal [63]. Peter and coworkers [64] extracted novel carbon based material from petroleum, which finds application as an electron emitter. Self-assembled monolayers of molecular diamonds on metal substrates have excellent electron-emission properties [65]. Monochromatic electron photoemission from large self-assembled monolayers of a functionalized diamondoid tetramantane-6-thiol, was reported to have applications in technologies such as electron microscopy, electron lithography and field emission flat panel displays [66].

Silicon analogues of diamondoids is a new class of molecules which has recently raised curiosity of researchers. The present scenario of electronics and information technology compels researchers to find new silicon based novel devices. The exploration in this area is still in its infancy. Synthesis of exact analogues of diamondoids, namely, sila-adamantane, sila-diamantane and so on has been a great challenge for experimentalists and most of the studies are theoretical. Recently, Fischer et al. [67] made an important contribution by successfully synthesizing four-fold silylated, molecule, $C_{24}H_{72}Si_{14}$, derived from sila-adamantane, $Si_{10}H_{16}$. In 2006, Lehtonen and Sundholm provided earliest theoretical results of the optical properties of sila-adamantane based on the DFT and coupled-cluster theory (CC) [68]. The first-principles investigation of Zope and coworkers [69] further developed renewed interest in this area. They found that DFT based studies of structural, electronic and vibrational properties of $C_{24}H_{72}Si_{14}$ give results in agreement with the recent available data [70]. They have speculated that sila-adamantane could serve as a template for novel class of materials called sila-diamondoids, and predicted, sila-diamondoids to be nanostructures derived from the bulk diamond structure of silicon which could be potential candidates in molecular electronics and nanotechnology. A comparative study of the optoelectronic properties of adamantane ($C_{10}H_{16}$) with hydrogen terminated sila-($Si_{10}H_{16}$) and germa- adamantane ($Ge_{10}H_{16}$) as calculated by DFT was done by the research group of Farah Marushi [71]. They have shown that electron affinity for $C_{10}H_{16}$ is negative while that for $Si_{10}H_{16}$ and $Ge_{10}H_{16}$ are positive.

Very recently, vibrational and thermodynamic properties of adamantane and two silicon analogues, $C_9Si_1H_{16}$ and $Si_{10}H_{16}$ using DFT formalism considering both GGA and LDA were investigated by Miranda et al. [72]. Their results from quantum mechanical calculations agree well with the available experimental and theoretical data and indicate that all the derived molecular systems studied by them could be synthesized, but the synthesis of sila-adamantane, besides being more favorable, occurs spontaneously, above 630K. The spatial confinement influences the structural, electronic and optical properties of nanosystems. Katin and coworkers studied the spatial confinement effects on the structural characteristics and optical spectra of $Si_{18}H_{12}$ and $Si_{19}H_{12}$ isomers using DFT methods [73].

Emerging interest in silicon analogues of carbon based nanomaterials like sila-diamondoids has led us to attempt to investigate the optical properties, namely static mean polarizability and complex dielectric function and complex refractive index of sila-diamondoids [74].

1.5 Applications of Silicon quantum dots

Silicon quantum dots have an important role to play in vast number of applications. For example, SiNCs doped using phosphorous and boron show highly tunable infrared plasmon resonances that can be tuned by altering the doping density [75]. Surface functionalized SiQDs are important for electroluminescene and photoluminescence application. Carrier transport properties in films of alkyl ligand-terminated SiNCs have been studied, which show the potential in device applications [76]. It is crucial and challenging to maintain a surface chemistry of SiNPs capable of conjugating with a biological moiety when it comes to biological applications. Tu et al. [77] were able to synthesize SiQD nanoparticles with antifouling coatings for immunostaining on liver cancer cells.

1.6 Silicene: Silicon analogue of Graphene

The elemental 2D materials usually have names ending ‘ene’, such as carbon based 2D material named as graphene has been studied extremely in the last few decades [78, 79]. It is one-atom thick single planar graphite sheet, possess a peculiar electronic structure of π and π* bands, forming a Dirac cone at the Fermi energy at the Brillouin zone corner (K points), resulting in charge carriers, which behave like massless relativistic particles [80]. High mobility of charge carriers independent of concentration and temperature permits its use in high-speed electronic devices. The isolation of single layer [81] in the year 2004 prompted researchers to speculate whether Si and Ge also have low-dimensional allotropes. It became quite appealing for researchers to find possibilities for creating 2D hexagonal lattices of Si and Ge called as silicene and germanene, respectively. In this respect, silicene is an interesting example of 2D nanomaterial which has graphite-like phase, with artificial honeycomb lattice made up of Si atoms [82]. The name *silicene* was first coined by Verri and Vonn in 2007 in their work on electronic structure of silicon-based nanostructures [83,84].

Last decade has been extensively devoted to explore the structure, stability and various properties like electronic, optical, mechanical etc. of the silicon counterpart of graphene, called as ‘Silicene’ [85−87]. It is very well known that graphene has planar structure, whereas, silicene has a puckered structure [88]. Silicene has not been synthesized unmodified in the free-standing form. Most of the evidences of its existence involve supporting templates. The structural, electronic, mechanical, topological, optical, magnetic, transport properties of unmodified free-standing silicene are primarily theoretical in nature.

Graphite despite having outstanding electronic properties, cannot be integrated in electronic devices due to zero bandgap. The switching mechanism in conventional transistor technology for logic operations implicates presence of an energy gap in the electronic structure. “Gap issue” acts as stimulus to further exploration of silicene. The constitutive high affinity of Si-lattice with the existing Si-based technology makes it a potential candidate for electronics applications and acts as a driving force behind the efforts to achieve synthetic Si-lattice. Recently, Haussai et al. [89] reviewed structural, electronic and vibrational properties of free-standing silicene, as predicted from first principles calculations. They have also discussed about the theoretical studies on the interaction of silicene with different substrates. Free-standing silicene is a hypothetical form. It has been predicted to possess massless Dirac fermions and to exhibit an experimentally accessible quantum spin Hall effect [90]. It is a big challenge for researchers to realize such properties in the experimentally synthesized silicene. Synthesis of a single layer silicene is challenging as it is very unstable. Therefore, it is grown on metallic substrates and cannot be exfoliated from substrates. Since 2012, Ag (111) substrate for growing silicene films, is very much in debate. In this context, Wu Ke-Hui [91] wrote a very nice and brief review which discusses all the plausible structural models and properties of silicene and clarifies concerned issues.

The nature of substrate strongly influence the crystal and hybrid structure of the Si honeycomb lattice, hence the properties so observed are different from those predicted from the isolated 2D structures [92]. So, free-standing, stable silicene materials needs to be discovered in order to achieve unique properties. A systematic discussion on the effect of substrate on the structural and electronic properties of silicene, from theoretical point of view was done by Jing and coworkers [93]. Li Hui and coworkers studied the structural and electronic properties of silicene films on Ag (111) including single layer and multilayer by employing STM and first-principles calculations [94]. They have also done pioneering work on hydrogenation of silicene and showed that it is easier than hydrogenation of graphene and silicene can be used for hydrogen storage [95]. The properties predicted from the standalone buckled structure of free-standing silicene are destroyed in the silicene realized on metallic substrates due to the lattice distortion and interaction with the subtstrate. Neek-Amal et al. [96] made interesting attempts for the realization of free-standing silicene using bilayer graphene.

1.6.1 Silicene derivatives

Organosilicon nanosheet allows introduction of organic groups on the silicon surface yielding unique functional materials. Organosilicon nanosheets modified with phenyl groups having an atomic thickness which can uniformly disperse in organic solvents have been reportedly synthesized [97].

1.6.2 Bandgap-tuning in Silicene

Oxygen adatoms tune the bandgap to semiconducting from semimetallic type in silicene monolayers which are grown on Ag (111) surfaces [98]. It was observed through low temperature STM results that the adsorption configurations and oxygen adatoms amounts on the grown silicene surface are crucial for engineering the bandgaps, dominated by various buckled structures in silicene layers. Mokkath et al. [99] investigated structural, electronic and optical properties of silicene using TDDFT and found that unlike graphene, silicene molecules prefer buckled structure and has strong optical response from visible to the ultraviolet spectral range, thus can be used for sunlight harvesting. They have also identified molecular plasmons in silicene.

1.7 Applications of Silicene

DFT based studies, were performed, on the optical properties of 2D pure as well as doped buckled nanosheets, by varying the concentrations of dopants, Al and P in silicene nanosheets, where the buckling effect influences the electron energy loss spectra [100]. Also, the calculated maximum values of absorption coefficient of doped systems are higher than the pristine ones. These results suggest the potential of silicene as building block for optoelectronic device fabrication. Band structure based DFT calculation were performed on 2D analogues of graphene: stanine, germanene, and silicone, and graphene itself [101], where complex refractive index and complex dielectric function were calculated. From these functions optical observables like reflection, absorption, optical conductivity and energy loss function, were studied. Graphene optical response was lying more in UV region while for other materials, optical response was shifted in IR and visible regions. Potential applications of such materials in optical and optoelectronic industries are also predicted. DFT and cluster models with van der Waals dispersion corrections and inclusion of solvent effects are employed for the investigation of electronic and optical properties of graphene, boron nitride (BN), silicene, phosphorene functionalized with antitubercular chemotherapeutic pyrazinamide (PZA) [102]. It was found that PZA favours covalent functionalization on silicene, whereas physisorbed on graphene, BN and phosphorene and such 2D materials are predicted to be useful for potential drug delivery applications.

Motivated by the current scenario in silicene based technology, we have also made an attempt to model novel derivatives based on organofunctionalized silicene and investigated their non-linear optical properties. We have appended the free-standing silicene monolayer having buckled structure as expected, with donor and acceptor pair and studied charge-transfer properties, one-photon absorption and two-photon absorption activity. Our results show that buckled monolayer with Si=Si bonds show signatures of TPA activity and bandgaps can also be tuned with different donor-acceptor pairs to visible range of electromagnetic spectrum. We propose, such models of silicene can serve as potential candidates in application of two-photon active materials and other silicon based technology. As per the present status of work in this research area, theoretical investigation on the non-linear optical behavior of freestanding silicene derivatives has not been done so far. The proposed push-pull derivatives showing signatures of two-photon activity are also new.

1.8 Objectives of the present work

The present work has the following objectives

1) To investigate the effect of quantum confinement in silicon nanoclusters by studying their optical properties and static mean polarizability.
2) To investigate the one-photon and two-photon activity in silicene substituted with donor-acceptor push-pull derivatives.

Chapter 2

Theoretical Background

2.1. The Schrödinger Equation

The properties of small systems can only be dealt with using Quantum Mechanics [103-110]. At the lowest level we use non-relativistic quantum mechanics, most commonly in its formulation due to Schrödinger, where the state of a system of electrons and nuclei is fully described by a function of electron coordinates (denoted by **r**) and nuclear coordinates (denoted by **R**) and time t. The state function $\Psi\ (\boldsymbol{r}, \boldsymbol{R}, t)$ satisfies the equation

$$i\hbar\ \frac{d\Psi\ (\boldsymbol{r}, \boldsymbol{R}, t)}{dt} = \hat{\mathrm{H}}\ \Psi\ (\boldsymbol{r}, \boldsymbol{R}, t) \tag{2.1}$$

called the time-dependent Schrödinger equation. In a stationary state, where the time dependence of Ψ is of the form

$$\Psi\ (\boldsymbol{r}, \boldsymbol{R}, t) = \psi(\boldsymbol{r}, \boldsymbol{R}) e^{-iEt/\hbar} \tag{2.2}$$

The equation reduces to

$$\hat{\mathrm{H}}\ \Psi\ (\boldsymbol{r}, \boldsymbol{R}) = E\ \Psi\ (\boldsymbol{r}, \boldsymbol{R}) \tag{2.3}$$

called the time-independent Schrödinger equation. The operator $\hat{\mathrm{H}}$ is called the Hamiltonian operator and it will be observed that the time-independent Schrödinger equation is of the form of an eigenvalue equation.

For a molecular system with N electrons and M nuclei, using atomic units (i.e. setting $e = \hbar = m_e = 4\pi\varepsilon_0 = 1$), the Hamiltonian operator has the form

$$\hat{\mathrm{H}} = \sum_{i}^{N} \frac{1}{2}\nabla^2 - \sum_{i}^{N}\sum_{A}^{M} \frac{Z_A}{r_{iA}} + \sum_{i}^{N}\sum_{j>i}^{N} \frac{1}{r_{ij}} \qquad (2.4)$$

where the first term corresponds to the kinetic energy of electrons, second term represents the electrostatic interactions between nuclei and electrons and last term represents the electron-electron repulsive interactions.

Unfortunately, an exact solution of the Schrödinger equation is not possible when more than two particles are present. So, for a many-electron atom or a molecule, first we use the Born-Oppenheimer approximation, and separate the nuclear and electronic motions. As the nuclei are much slower moving than the electrons, we assume the nuclei to be stationary and solve the problem of electronic motion in the field of stationary nuclei, thus getting the electronic energy, $E_e(\boldsymbol{R})$ as a function of nuclear coordinates. This forms the potential energy for nuclear motion (essentially vibrational, rotational and translational motions of the molecule). The configuration of the nuclei that corresponds to a minimum of $E_e(\boldsymbol{R})$ gives the equilibrium geometry of the molecule, and suitable algorithms (called optimization methods) can be used to locate the equilibrium geometry of the molecule beginning from a suitable starting geometry.

The solution of the electronic Schrödinger equation itself is rigorous. The lowest acceptable method from a theoretical standpoint is the Hartree-Fock method.

2.2. Hartree-Fock (HF) Method

In this method, each electron in an N electron system is assumed to move under the average field of (N-1) electrons; instantaneous electronic repulsions are treated in an average way. The wave function of an N-particle system can be written as

$$\psi_e(\boldsymbol{r_1}, \boldsymbol{r_2}, \ldots, \boldsymbol{r_N}) = \Phi_1(\boldsymbol{r_1})\Phi_1(\boldsymbol{r_2}) \ldots \Phi_1(\boldsymbol{r_N}) \qquad (2.5)$$

which is known as the Hartree product. This form of the wave function would be exact if the Hamiltonian where the sum of one particle operators and the particle themselves were distinguishable. However, indistinguishability of electrons imposes certain requirements on the wave functions, which cannot be satisfied by the simple Hartree product functions. As electrons are fermions, the wave function is required to be antisymmetric with respect to the interchange of the particles. A Slater determinant function

$$\psi_e = \frac{1}{\sqrt{N!}} \begin{vmatrix} \chi_1(1) & \chi_1(2) \dots & \chi_1(N) \\ \chi_2(1) & \chi_2(2) \dots & \chi_2(N) \\ \vdots & \vdots & \vdots \\ \chi_N(1) & \chi_N(2) \dots & \chi_N(N) \end{vmatrix} \tag{2.6}$$

(where the $\chi_i(N)$ are one-electron functions or orbitals) is the simplest to satisfy this requirement. Formally, χ_i is a spin orbital defined either as

$$\chi_i = \phi_m \alpha \quad \text{or} \quad \chi_i = \phi_m \beta \tag{2.7}$$

where, ϕ is the spatial orbital and α and β are the spin functions corresponding to $m_s = {}^1\!/_2$ and $m_s = -{}^1\!/_2$ respectively. The best wave function of a system can be obtained by minimizing the expectation value of energy with respect to variations in the spin orbitals, subject to requirements of orthonormality. A trial wave function is built as a slater determinant of spin orbitals χ_i (i=1, 2, ...N) which can be chosen to satisfy

$$f(\chi_i) = \varepsilon_i \chi_i \tag{2.8}$$

where f is a Fock operator, but it is built out of the other orbitals as well, so this is not a simple eigenvalue equation and needs to be iteratively solved. Formally,

$$f_i = h_i + \sum_{j \neq i} (J_j - K_j) \tag{2.9}$$

where J_j and K_j are the two electron Coulomb and exchange operators and h_i is the one-electron part. The ε_i can be identified with orbital energies but because of double counting of interactions $\sum \varepsilon_i$ is not the total electronic energy, infact we may see that

$$E = \sum_i \langle i|h|i\rangle + \frac{1}{2} \sum_i \sum_j \langle ij|ij\rangle - \langle ij|ji\rangle \tag{2.10}$$

where $\langle ij|ij\rangle$ are Coulomb integrals and $\langle ij|ji\rangle$ are exchange integrals. By varying the orbitals χ_i successively till the energy values converge- we get the Hartree-Fock wavefunction.

In atomic systems the orbitals were earlier improved using numerical integration. However, in molecular systems it is more convenient to choose the initial trial orbitals as linear combinations of basis functions and effect of the variations as changes of coefficients. Currently, the basis sets are generally chosen as Gaussian functions because of ease of integral evaluations. Once the orbitals χ_i are expanded in terms of basis functions.

$$\chi_i = \sum_a c_{ai}\phi_a \tag{2.11}$$

The SCF equations assume the form

$$\bar{F}\bar{C} = \bar{S}\bar{C}\bar{\varepsilon} \tag{2.12}$$

where, $\bar{F}$, $\bar{S}$ and $\bar{C}$ are matrices such that

$$\bar{F}_{ab} = \int \phi_a\,(1)f(1)\,\phi_b(1)\,d\boldsymbol{r}_1 \tag{2.13}$$

$$\bar{S}_{ab} = \int \phi_a\,(1)\,\phi_b(1)\,d\boldsymbol{r}_1 \tag{2.14}$$

and $\bar{C}$ is a square matrix of the expansion coefficient C_{ai}. $\bar{F}$ and $\bar{S}$ are called the Fock matrix and the overlap matrix. $\bar{\varepsilon}$ is a diagonal matrix of the orbital energies: $\varepsilon_{ij} = \varepsilon_i\delta_{ij}$.

The equation $\bar{F}\bar{C} = \bar{S}\bar{C}\bar{\varepsilon}$ is solved by a transformation that reduces it to the form $\bar{F}'\bar{C}' = \bar{C}'\bar{\varepsilon}'$ appropriately followed by a diagonalisation. This was formulated by Roothaans [110] and co-workers.

2.3. Post-Hartree Fock Methods

The Hartree-Fock method has two drawbacks: (i) The use of finite basis sets limits the accuracy of the wave functions, and (ii) The HF procedure does not account for correlation of electronic motions, particularly between electrons of opposite spins. This is because it is an essentially one-electron method which treats electron-electron interactions in an averaged way only. However, electrons of similar spins are kept apart by the exchange interaction. There are methods to include correlation, the chief of which is the configuration interaction method which works not with a single Slater determinant but with a linear combination of Slater determinants. The choice of appropriate configurations (SD’s) is a formidable task. A simpler method uses a limited number of configurations but varies the coefficients and the orbitals simultaneously. This is known as the Multi-configuration SCF method (MCSCF). Other methods used are Many-Body Perturbation Theory (MBPT), one version is due to M⌀ller & Plessett. In the MP methods the sum of the Fock operators is the zeroth order function, and H-$\sum f_i$ is taken as the perturbation; the first-order (MP1) energy corresponds to Hartree-Fock energy and the real corrections begin with MP2. Usually, MP2, MP4 methods are the highest order methods tried, as when the order of perturbation theory involved rises the computational costs does, too. Another approach is the Coupled Cluster (CC) methods.

2.4. Density Functional Theory (DFT) Methods

The prohibitive cost of getting wave functions significantly better than HF has resulted in the development of a semi-empirical treatment called Density- functional theory [12, 110]. DFT originated from the Thomas-Fermi statistical model of the atom which was proposed independently by Thomas [111] and Fermi [112] in 1927 and its logical foundations were laid by the theorems of Hohenberg and Kohn for a system of many electrons in its ground (time-independent) state [113, 114]. DFT takes the electron density $\rho(\boldsymbol{r})$ to completely define the observable state of the system rather than the wave function and a correspondence between the electron density $\rho(\boldsymbol{r})$ and the external potential $V_{ext}(\boldsymbol{r})$ is established. The energy of the system is expressed as a functional of density, and the correct energy minimizes this functional in the variational sense. Formally,

$$E[\rho] = T[\rho] + V_{ext}\,[\rho] + U[\rho] \tag{2.15}$$

where the first term $T[\rho]$ is the kinetic energy functional, the second term, $V_{ext}\,[\rho]$ is the potential energy functional and the third term $U[\rho]$ gives the contribution from electron-electron interaction. All the components of $E[\rho]$ include classical terms.

However, the problem with the density-functional method is that it is impossible to define the kinetic energy functional without an orbital model. Kohn and Sham therefore introduced a Hartree-Fock like self-consistent-field (SCF) scheme defining density $\rho(\boldsymbol{r})$ as

$$\rho(\boldsymbol{r}) = \sum_{i=1}^{N} \left|\phi_i^{k-s}\,(\boldsymbol{r})\right|^2 \tag{2.16}$$

They derived a set of equations satisfied by $\phi_i^{k-s}\,(\boldsymbol{r})$ or Kohn-Sham (KS) orbitals by a variational method:

$$\left[-\frac{1}{2}\nabla_i^2 + V_{eff}(\boldsymbol{r})\right]\phi_i^{k-s}\,(\boldsymbol{r}) = \varepsilon_i\phi_i^{k-s}\,(\boldsymbol{r}) \tag{2.17}$$

where ε_i is the KS eigenvalue. The V_{eff} appearing in the Hamiltonian has a form

$$V_{eff}(\boldsymbol{r}) = V_{ext}(\boldsymbol{r}) + U_{el}(\boldsymbol{r}) + V_{xc}(\boldsymbol{r}) \tag{2.18}$$

where $U_{el}(\boldsymbol{r}) = \int \frac{\rho(\boldsymbol{r}')}{|r-r'|}d\boldsymbol{r}'$ and $V_{xc}(\boldsymbol{r}) = \frac{\delta E_{xc}(\boldsymbol{r})}{\delta\rho}$ is called the exchange-correlation potential. The KS equations are solved starting from an initial set of KS orbitals, yielding a KS potential via $V_{xc}(\boldsymbol{r}) = \frac{\delta E_{xc}(\boldsymbol{r})}{\delta\rho}$ and an initial density from $\rho(\boldsymbol{r}) = \sum_{i=1}^{N}\left|\phi_i^{k-s}\,(\boldsymbol{r})\right|^2$ which enables to obtain an improved set of KS orbitals from $[-\frac{1}{2}\nabla_i^2 + V_{eff}(\boldsymbol{r})]\,\phi_i^{k-s}\,(\boldsymbol{r}) = \varepsilon_i\phi_i^{k-s}\,(\boldsymbol{r})$ and hence a new improved $\rho(\boldsymbol{r})$ iteratively. Once self-consistency is achieved the total energy of the system is calculated from

$$E[\rho] = T[\rho] + V_{ext}\,[\rho] + U[\rho] \tag{2.19}$$

In the original Kohn-Sham formulation the exchange-correlation energy has been described inaccurately. Although this method has been used by solid state theorists till the 90's, simple approximations have been made for exchange-correlation functional in order to make the calculations practically more appropriate for molecular systems. The local density approximation (LDA) [47] is the most basic of all the approximations to the exchange-correlation functional and can be expressed as

$$E_{XC}^{LDA}[\rho] = \int \rho(\boldsymbol{r})\epsilon_{XC}^{unif}[\rho(\boldsymbol{r})]d\boldsymbol{r} \tag{2.20}$$

where, $\epsilon_{XC}^{unif}[\rho(r)]$ is the exchange-correlation energy per particle of the uniform electrom gas density $\rho(\boldsymbol{r})$. The quantity $\epsilon_{XC}^{unif}[\rho(\boldsymbol{r})]$ can further be splitted into exchange and correlation contributions.

$$\epsilon_{XC}^{unif}[\rho(\boldsymbol{r})] = \epsilon_{X}^{unif}[\rho(\boldsymbol{r})] + \epsilon_{C}^{unif}[\rho(\boldsymbol{r})] \tag{2.21}$$

2.4.1. Generalized Gradient Approximation (GGA)

The Generalized Gradient approximation [48] involves the gradient of the density ($\nabla\rho(\mathbf{r})$), at a particular point **r** as a supplement to the density, also at **r**. It is more logical in the sense that it accounts for the inhomogeneity of the true electron density. The functional form of GGA can be expressed as

$$E_{XC}^{GGA}[\rho] = \int \rho(\boldsymbol{r})\, \epsilon_{XC}[\rho(\boldsymbol{r})]d\boldsymbol{r} + \int F_{XC}\,[\rho(\boldsymbol{r}), \nabla\rho(\boldsymbol{r})]d\boldsymbol{r} \quad (2.22)$$

where the second term is the correction term to the exchange correlation. All GGA functional are not parametrized by fitting experimental data. For instance the Perdew Burke Ernzerhof (PBE) functional is a standard GGA functional which achieves the inclusion of gradient correction without fitting to reference data on atoms and molecules and is used for its general applicability in a wide range of applications. In the context of Silicon nanoclusters, PBE [115] functional has been used extensively and is seen to show results quite in agreement with the experimental results [116].

Another refinement which is currently very popular is the hybrid functional which includes a fixed fraction of the Hartree-Fock exchange energy. The most popular of this is the B3LYP [50] functional, which is combination of Becke's three-parameter exchange functional and Lee. Yang and Parr's correlation functional which are both gradient corrected. The functional is given by the equation:

$$E_{XC}^{B3LYP} = E_{XC}^{LDA} + a_0(E_X^{HF} - E_X^{LDA}) + a_X(E_X^{GGA} + E_X^{LDA}) + a_C(E_C^{GGA} - E_C^{LDA}) \quad (2.23)$$

where, E_X^{HF} is the Hartree-Fock exact exchange functional, a_0= 0.20, a_X = 0.72 and a_C= 0.81 are the three empirical parameters determined by fitting the predicted values to a set of atomization energies, ionization potentials, proton affinities, and total atomic energies: E_x^{GGA} and E_C^{GGA} are generalized gradient approximations: Becke 88 exchange functional and the correlation functional of Lee, Yang and Parr, and E_c^{LDA} is the local-density approximation to the correlation functional. Further, long-range corrected functional like, CAM-B3LYP is also becoming popular in polarizability calculations [117, 118].

2.5. Time-Dependent Density Functional Theory (TDDFT)

DFT is confined to the studies of the ground state properties which involve non-perturbative phenomena. The electronic excitations to higher energy states are not adequately accessible through standard DFT formalism. TDDFT formulation is applicable to the excited state studies which involve time-dependent perturbative phenomena, for example, optical properties such as absorption, emission and response to time-dependent fields such as laser fields. In this approach, the (non-relativistic) time-dependent Schrödinger equation for the many-electron wave function $\Psi(t)$ is solved.

$$H(t)\psi(t) = i\frac{\partial\psi(t)}{\partial t} \tag{2.24}$$

where,

$$H(t) = T + V_{ee} + V_{ext}(t) \tag{2.25}$$

$$T = -\frac{1}{2}\sum_{i=1}^{N}\nabla_i^2 \tag{2.26}$$

$$V_{ee} = \frac{1}{2}\sum_{i\neq j}^{N}\frac{1}{|\boldsymbol{r}_i - \boldsymbol{r}_j|} \tag{2.27}$$

$$V_{ext}(t) = \sum_{i=1}^{N} v_{ext}(\boldsymbol{r}_i, t) \tag{2.28}$$

The central theorem of TDDFT is the Runge-Gross Theorem [119] which proves that there is a one to one mapping between the external (time-dependent) potential, $V_{ext}(t)$ and the electronic one body density $\rho(t)$ for many body systems. It states that the densities $\rho(\boldsymbol{r}, t)$ and $\rho'(\boldsymbol{r}, t)$ evolving from a common initial state $\psi_0 = \psi$ (t = 0) under the influence of two external potentials $V_{ext}(\boldsymbol{r}, t)$ and $V'_{ext}(t)$ are always different provided that the potentials differ by more than a purely time-independent function. Here the external potentials are expandable using the Taylor series about the initial time t = 0 i.e.

$$V(\boldsymbol{r}, t) = \sum_{k=0}^{\infty}\frac{V_k(\boldsymbol{r})}{k!}(t - t_0)^k \tag{2.29}$$

Thus,

$$\Delta V_{ext}(\boldsymbol{r}, t) = V(\boldsymbol{r}, t) - V'(\boldsymbol{r}, t) \neq c(t) \tag{2.30}$$

In analogy to DFT formalism, time-dependent potentials can be written as a functional of the density i.e. $V(\boldsymbol{r}, t) = V[n, \psi_0](\boldsymbol{r}, t)$ where *n* is the time-dependent density. Subsequently, time-dependent Hamiltonian of the system, the wave-function and desired observable properties can be expressed as a density functional. An assumption of a non-interacting system which can produce time-dependent density equal to that for the interacting system also works here as in case of ground-state DFT such that

$$n(\boldsymbol{r},t) = \sum_{\mathrm{j}=1}^{\mathrm{N}} \left|\phi_{\mathrm{j}}(\boldsymbol{r},\mathrm{t})\right|^2 \tag{2.31}$$

which satisfies the time-dependent Kohn-Sham equation.

$$\frac{\partial \phi_j(\boldsymbol{r},t)}{\partial t} = \left[-\frac{\nabla^2}{2} + V_{KS}[n;\ \phi_0](\boldsymbol{r},t)\right]\phi_j(\boldsymbol{r},t) \tag{2.32}$$

Here, $V_{KS}[n;\ \phi_0](\boldsymbol{r},t)$ is the external potential of the non-interacting system which produces the density of the real system. It is further decomposed into three terms, the external time-dependent field, time-dependent Hartree potential and the exchange-correlation potential.

$$V_{KS}[n;\ \phi_0](\boldsymbol{r},t) = V_{ext}[n;\ \psi_0](\boldsymbol{r},t) + \int d^3r'\,\frac{n(\boldsymbol{r}',t)}{|\boldsymbol{r}-\boldsymbol{r}'|} + V_{xc}[n;\ \psi_0,\phi_0](\boldsymbol{r},t) \tag{2.33}$$

The last term is approximated by some standard functionals of density, the Kohn- Sham initial state and the true initial state. The knowledge of this term is equivalent to the exact solution of all the time dependent Coulomb interacting problems.

2.6. Solid-State Calculations

A solid is an extended periodic system, the electronic structure of which is characterized by the band structure, which defines the energies of electron orbitals for each point in the Brillouin zone. The orbital energies can be calculated using ab-initio and semi-empirical methods so the same can be applied to band structure calculations except that the calculation of energy for the entire list of points in the Brillouin zone demands high computation cost.

The computational chemical methods can be used in the same way as for molecules but with two implications. First, utilization of translational symmetry of the solid and second is the possibility of using completely delocalized basis functions such as plane waves as an alternative to the molecular atom-centered basis functions. In solids the core electrons can be treated approximately as it has minimal effect on the properties of interest in the solid. Furthermore, the implicit inclusion of core states into a pseudopotential makes the use of plane-waves much more appropriate and flexible for electronic structure calculations. Further, the solid-state calculations can use the Hartree–Fock method, some post-Hartree–Fock methods, particularly Møller–Plesset perturbation theory to second order (MP2) and DFT.

CASTEP [120] is a state-of-the-art quantum mechanics-based program which provides robust and efficient implementation of density functional theory using the concept of plane wave basis set, pseudopotential description of the electron-ion interaction, supercell approach with periodic boundary conditions, the iterative schemes for the self-consistent electronic minimization. Fast-Fourier transform (FFT) is extensively used for evaluation of the terms of the Hamiltonian. The most popular DFT expressions are implemented for the exchange-correlation functional. First-principles quantum mechanical calculations can be performed to investigate the properties of solids, surfaces, dielectric matrices, semiconductors using less tedious procedures. Typical applications involve studies of surface chemistry, structural properties, band structure, density of states, and optical properties. The spatial distribution of the charge density and wave functions of a system can also be studied. It can also be used to perform spectroscopic studies like IR, NMR and Raman, thermodynamic studies, linear response calculations, phonon-dispersion calculations, transition state searching, defects studies and many more. In the present study, CASTEP has been employed for the calculation of optical properties namely, complex dielectric function, complex refractive index and bandgaps through band structure calculations.

The major requirement for running a calculation in CASTEP is to build a periodic 3D model structure of the system of interest. The system of interest in our study is a molecular system, for that a supercell approach with periodic boundary conditions is required in CASTEP input scheme. Further, the imposition of symmetry constraints can enhance the performance.

2.6.1. Supercell Approach

In CASTEP, plane wave basis functions represent the Kohn-Sham functions and various other quantities (such as charge density). As a result, it implicitly assumes an infinite crystal and impose the Born-von Karman periodic boundary condition on the Kohn-Sham wave functions. The isolated molecules are assumed to be placed in a 3D box which provides an artificial periodic environment to the system and the length of the box is chosen sufficiently large so that the charge densities associated with molecules in the neighboring supercells have very small overlaps. The periodic boundary conditions are imposed to apply the Bloch's theorem, which states that in a periodic system each electronic wave function can be written as a product of a cell-periodic part and a wavelike part [121]

$$\psi_i\,(\boldsymbol{r}) = e^{ik\boldsymbol{R}}\psi_i(\boldsymbol{r}) \tag{2.34}$$

The cell periodic part, $\psi_i\,(r)$, is a linear combination of plane waves basis functions. The wave vectors of the discrete set of plane waves are reciprocal lattice vectors of the crystal:

$$\psi_i(\boldsymbol{r}) = \sum C_{i,\boldsymbol{G}}\, e^{i\boldsymbol{G}.\boldsymbol{R}} \tag{2.35}$$

Therefore, each electronic function can be written as a sum of plane waves, exp [i (**k**+**G**)•**R**]. The simplified form of the Kohn-Sham equations is involved in which kinetic energy is diagonal, the various potentials (electron-ion, Hartree, exchange-correlation) are described in terms of their Fourier transforms.

$$\sum[|\mathbf{k}+\boldsymbol{G}|^2\, \delta_{\boldsymbol{G}\boldsymbol{G'}} + V_{ion}(\boldsymbol{G}-\boldsymbol{G'}) + V_H(\boldsymbol{G}-\boldsymbol{G'}) + V_{xc}(\boldsymbol{G}-\boldsymbol{G'})]C_{i\mathbf{k}+\boldsymbol{G'}} = \varepsilon_i C_{i\mathbf{k}+\boldsymbol{G'}} \tag{2.36}$$

The derivative of the total energy with respect to atomic displacements is easy to calculate using plane wave basis set. The convergence of plane-wave basis set calculations can be improved by systematically adding more basis functions.

2.6.2. Pseudopotentials

In a solid, ionic cores containing nuclei and tightly bound core electrons are arranged periodically and valence electrons move freely around the ionic cores. While analyzing the wave functions it is found that the valence-electron wave functions are orthogonal to core-electron wave functions. All electron wave functions of valence electrons exhibit rapid oscillations in the core region in order to satisfy the orthogonality constraint. The representation of such wave functions using plane wave basis set demands large size of basis set [122] and is impractical in that sense.

In the pseudopotential approach ion cores are considered to be *frozen* and the properties of the solids are assumed to be dictated by valence electrons. The pseudopotential approximation replaces core electrons and the strong Coulomb potential by a weaker pseudopotential that acts on a set of pseudo wave functions. This potential can be represented with only a small number of Fourier coefficients. The pseudopotentials which can be represented accurately using small number of Fourier coefficients are soft and vice verse. We have employed ultrasoft pseudopotentials [123] as implemented in CASTEP, for calculating the optical properties.

भारतीय प्रौद्योगिकी संस्थान रुड़की
INDIAN INSTITUTE OF TECHNOLOGY ROORKEE

Chapter 3

Silicon Quantum Dots: Model Systems

3.1 Introduction

In nanosystems like quantum dots the gap between the highest occupied molecular orbital (HOMO) and the lowest unoccupied molecular orbital (LUMO) is taken to be the representative of the bandgap in crystals. Theoretical work has concentrated on various aspects of the HOMO-LUMO gap in systems of interest. We investigate a few selected small systems with a view to identify the methods that correspond better with experiments for purposes of studying the correspondence with some of the properties that we investigate in the next chapter.

3.1.1 HOMO-LUMO Energy Gap

In quantum dots, the spatial confinement of the wave function in three dimensions results in discrete energies as compared to bands in extended periodic systems [124-127]. The electronic picture entirely changes and resembles that of a many electron atomic system. As a consequence of the quantum confinement, discrete energy levels (with different quantum numbers) arise at the band edges of both the valence band and the conduction band and the bandgap increases as the size of the semiconductor quantum dot decreases which further imparts drastic changes to the optical properties as a function of size of the quantum dot [128]. In such a physical situation, the difference between HOMO and LUMO can be considered as the energy gap for a transition from valence band to conduction band. The dependence of HOMO-LUMO gaps on the size of the silicon quantum dot allows us to manipulate the optical properties by tuning the HOMO-LUMO gaps [129-131]. Here we discuss these gaps in various model systems of SiNCs using different theoretical methods.

In this chapter, several open Silicon hydrides, cyclosilane conformers are studied as models of Silicon quantum dots (SiQDs). The gap between HOMO and LUMO is evaluated at different levels of theory namely, *ab-initio*, semi-empirical, and DFT and compared with available spectroscopic estimates. Pseudopotential methods have also been used to assess the correctness of results in comparison with all electron calculations.

3.2 Computational Details

Ground state geometry optimizations for all the clusters studied have been performed at different levels of theory such as semi-empirical (PM3), *ab-initio* methods such as Hartree-Fock (HF) and Møller-Plesset (MP2) and DFT. The 6-31G (d) basis set was used with both MP2 and HF methods. In DFT, Becke's 3-parameter exchange functional with Lee-Yang-Parr correlation functional (B3LYP) and PBE functional were used in conjunction with 6-31G (d) basis set as implemented in Gaussian 09 software package [132]. All geometry optimizations have been performed in gas phase along with symmetry constraints. Geometry optimizations employing Dunning basis, D95 [133-136] and effective core potential based basis sets LANL2DZ (D95 *i.e.* Dunning double zeta basis on 1st row and Los Alamos ECP+DZ on Na-La) and SHC (D95V on 1st row and Goddard Medley ECP on 2nd row) have also been performed with B3LYP functional in order to compare the results with those obtained from the all-electron calculations. All the optimized geometries correspond to true minima on the potential energy surface as confirmed by frequency calculations.

3.3 Results and Discussion

We begin with the study of HOMO-LUMO gaps of homologous series of linear, branched and cyclic silanes taking these as models for a limiting case of SiQDs.

3.3.1 Linear silanes

The gas phase optimized geometries of linear silanes, Si_nH_{2n+2} (n = 1, 2, ...6) at B3LYP/6-31G (d) level of theory with respective point group symmetry are shown in Fig 3.1. The

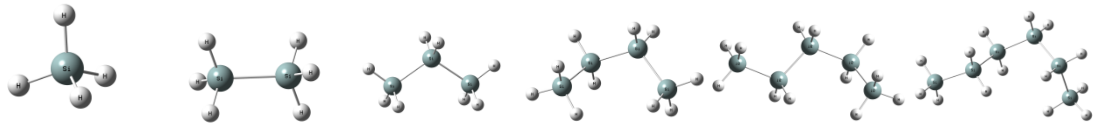
SiH_4 (T_d) Si_2H_6 (D_{3d}) Si_3H_8 (C_{2V}) *n*-Si_4H_{10} (C_2) *n*-Si_5H_{12} (C_1) *n*-Si_6H_{14} (C_1)

Fig. 3.1 The gas phase optimized geometry of the linear silanes at B3LYP/6-31G (d) level of theory.

variation of HOMO-LUMO gaps with size (no. of Si atoms) among linear silanes at different levels of theory is given in Table 3.1. From the table, it can be seen that HOMO-LUMO gap (in eV) for B3LYP/6-31G(d) level of theory decreases with the increase in number of silicon atoms. A similar trend is also observed at all the other levels of theory. The decrease in the HOMO-LUMO gap with an increase in the number of silicon atoms is mainly because of the size of silicon quantum dot which plays a crucial role while studying their electronic behavior. A consistent definition of the size of the quantum dot can be given through the empirical relation which associates the effective size with the diameter of the sphere which has mass density of bulk Si and contains same number of Si atoms as the QD [137]

$$d(N_{Si}) = \left(\frac{3}{4\pi\rho}\right)^{1/3} N_{Si}^{1/3} = 3.3685 N_{Si}^{1/3} \quad (\text{Å}) \tag{3.1}$$

Average spacing between occupied states (ΔE) in small clusters is given as

$$\Delta E = \frac{4E_f}{3n} \tag{3.2}$$

where, E_f is fermi energy and *n* is the number of valence electrons. Thus, as the number of valence electrons increases or the number of atoms in the cluster increases, the energy gap decreases.

Table 3.1. shows variation of HOMO-LUMO gaps with size of *n*-silanes calculated at different levels of theory. The number of silicon atoms *n* are varied between 1 to 6. The results from calculations using *ab-intio* methods are shown in first two rows. The next five (3-7th) rows present results from DFT calculations using different functional and basis sets. HOMO-LUMO gap values from fifth until seventh row correspond to pseudopotential basis sets. The results in eighth row are obtained from semi-empirical method, while ninth row results are calculated using DFT functional at higher basis set. The last three rows in Table 3.1 contain earlier theoretical results and estimates from spectroscopy [138]. It is seen that most of the methods used overestimate the HOMO-LUMO gap, where MP2 methods give results with highest discrepancy. DFT calculations with aug-ccpVDZ basis produce results close to experiments for SiH_4, while the use of smaller 6-31G(d) basis set gives more reasonable estimates. CCSD results from literature give results comparable with the DFT results at PBE/6-31G(d) level of theory, while for Si_2H_6 the agreement of CCSD results with experiment is better. Thus, we conclude that the use of PBE functional with the modest 6-31G (d) basis set gives estimates of the band gaps that are qualitatively satisfactory. The ECP basis sets LANL2DZ and SHC also are seen to overestimate the HOMO-LUMO gap. The results from SHC basis set in particular are close to the semi-empirical PM3 values.

Table 3.1 HOMO-LUMO gaps (eV) of *n*-silanes Si_nH_{2n+2} (n = 1, 2,...6) at different levels of theory.

No.	Method/Basis-set	SiH_4	Si_2H_6	Si_3H_8	*n*-Si_4H_{10}	*n*-Si_5H_{12}	*n*-Si_6H_{14}
1	HF/6-31G(d)	17.80	14.79	13.67	13.35	9.94	12.65
2	MP2/6-31G(d)	17.76	14.85	13.73	13.48	12.82	12.77
3	B3LYP/6-31G(d)	10.99	8.67	7.71	7.47	6.92	6.90
4	PBE/6-31G(d)	9.15	7.04	6.20	5.98	5.48	5.46
5	B3LYP/LANL2DZ[a]	11.52	7.59	8.28	8.05	7.50	7.47
6	B3LYP/D95[b]	11.40	8.82	7.92	7.64	7.09	7.07
7	B3LYP/SHC[c]	11.33	8.71	7.81	7.52	6.97	6.95
8	PM3	12.41	8.64	7.88	7.64	9.12	7.15
9	PBE/aug-cc-pVDZ	7.97	6.61	5.91			
10	CCSD/aug-cc-pVD (Liter.)[138]	9.28	7.67				
11	PBE/aug-cc-pVQZ(Liter.) [138]	8.06	6.92	5.99			
12	Experimental[139]	8.8	7.56	6.63			

[a] [b] [c]Effective Core Potential based basis set, [a](D95 i.e Dunning split valence basis on 1st row and Los Alamos ECP+DZ on Na-La) ,[b](Dunning basis) and [c](D95V on 1st row and Goddard Medley ECP on 2nd row)

Based on the data on the lower silanes, specifically the correspondence with spectroscopic estimates of the HOMO-LUMO gaps, our work in the next chapter, uses DFT results with PBE functional and moderately sized basis sets for comparison and correlation purposes.

3.3.2 Comparison of linear and branched silanes

The gas phase optimized geometries of isomers of linear *n*-Si_4H_{10}, *n*-Si_5H_{12} and *n*-Si_6H_{14} at B3LYP/6-31G (d) level of theory are shown in Fig 3.2.

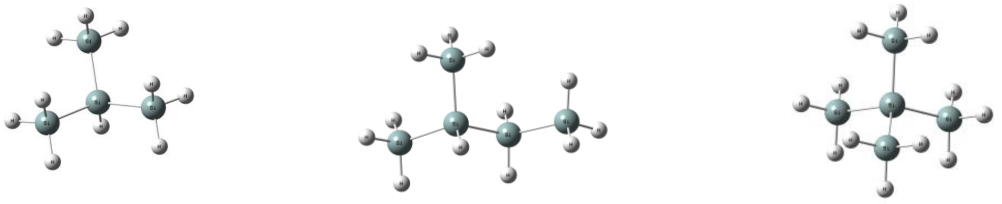

***iso*- Si_4H_{10} (C_1)** ***iso*-Si_5H_{12} (C_1)** ***neo*-Si_5H_{12} (T_d)**

(a) **(b)**

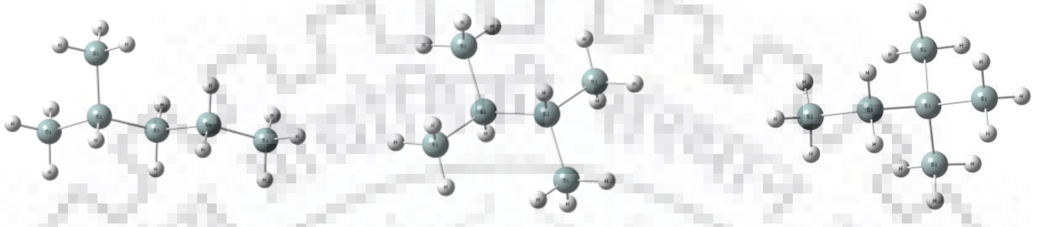

***iso*- Si_6H_{14} (C_1)** **Si_6H_{14} (C_{2h}) (*branched*)** ***neo*-Si_6H_{14} (C_1)**

(c)

Fig. 3.2 The gas phase optimized geometries of branched silanes optimized at B3LYP/6-31G(d) level of theory (a) isomers of linear *n*-Si_4H_{10} (b) isomers of linear *n*-Si_5H_{12} (c) isomers of linear *n*-Si_6H_{14}

The branched isomers of linear silanes have been optimized at different levels of theory and basis sets as done in the case of linear silanes. We study the effect of branching on the HOMO-LUMO gaps in *n*-silanes by comparing the HOMO-LUMO gap of *n*-silane with two

Table 3.2 HOMO-LUMO gaps (eV) of linear and branched silanes at different levels of theory

Method/Basis-set	*n*- Si_4H_{10}	*iso*- Si_4H_{10}	*n*- Si_5H_{12}	*iso*- Si_5H_{12}	*neo*-Si_5H_{12}	*n*- Si_6H_{14}	*iso*- Si_6H_{14}	Si_6H_{14} (branched)	*neo*-Si_6H_{14}
HF/6-31G(d)	13.35	13.51	9.94	12.76	13.44	12.65	12.21	12.67	12.76
MP2/6-31G(d)	13.48	13.61	12.82	12.88	13.46	12.77	12.33	12.80	12.85
B3LYP/6-31G(d)	7.47	7.57	6.92	6.96	8.11	6.90	6.51	6.82	6.95
PBE/6-31G(d)	6.00	6.07	5.48	5.51	6.06	5.46	5.10	5.36	5.49
B3LYP/LANL2DZ	8.04	8.10	7.50	7.52	8.11	7.47	7.08	7.37	7.52
B3LYP/D95	7.64	7.68	7.09	7.12	7.61	7.07	6.67	6.95	7.12
B3LYP/SHC	7.52	7.59	6.97	7.01	7.56	6.95	6.55	6.84	7.03
PM3	7.64	5.93	9.12	7.05	7.28	7.15	6.76	6.88	4.91

of the isomers as shown in Fig. 3.2, and also examine the consistency of the same effect at different levels of theory and basis sets. The HOMO-LUMO gaps of linear silanes with respective branched isomers at various levels of theory and basis sets are shown in Table 3.2. In case of Si_4H_{10} and Si_5H_{12}, the HOMO-LUMO gaps are found to increase with branching at all levels. We may correlate it with the more compact structures of the branched compounds [140]. However, in the case of Si_6H_{14} the *iso*-isomer deviates from this tendency at all the levels of theory while the branched and *neo* isomers deviate at some levels of theory. It is also observed, that, the values increase with further increase in branching from *iso* to *neo* isomer indicating an increase in the degree of compactness with branching except at some levels of theory.

3.3.3. Comparison of linear and cyclic silanes

The shapes of the conformers of the cyclic silanes namely, cyclopentasilane, Si_5H_{10}, and cyclohexasilane, Si_6H_{12} corresponding to their linear conterparts (linear silanes) *n*-Si_5H_{12} and *n*-Si_6H_{14}, respectively are shown in Fig.3.3. Cyclopentasilane has two predominant conformations, envelope (C_s) and twist (C_2). The structure I and II in Fig. 3.3 show the optimized geometries of envelope and twist conformers calculated at B3LYP/6-31G (d) level of theory in gas phase, respectively. The twist conformer has three Si atoms in plane and one above the plane and one below the plane. The envelope conformer has four Si atoms in plane and one above and below the plane of the ring. Haixing and coworkers [141] examined the impact of ring conformations of cyclopentasilane substituted with alkyl groups and studied its capability of controlling the conductance.

The structures III, IV, V and VI represent different conformers of cyclohexasilane optimized at B3LYP/6-31G(d) level of theory, namely, chair, boat, twist boat and half chair, respectively. The chair conformer of cyclohexasilane is the global minimum on the potential energy surface followed by twist boat and boat conformer. Half-chair conformer corresponds to a transition state structure, connecting the chair and twist boat minima, as it has exactly one imaginary vibrational frequency. Cyclohexane was the first molecule whose conformations were recognized in 1890 by H. Sachse and the silicon analogue of cyclohexane i.e. cyclohexasilane, Si_6H_{12} was prepared nearly 30 years ago by Hengge and Kovar through reduction of Si_6Cl_{12} with $LiAlH_4$ [142]. The conformational study of the silicon analogues of cyclohexane is an active area of research these days. Recently, Tekautz and coworkers [143] reported a combined DFT and Raman spectroscopic study of the chair, boat and twist conformations of cyclohexasilane and reported that chair conformer is the most stable conformer.

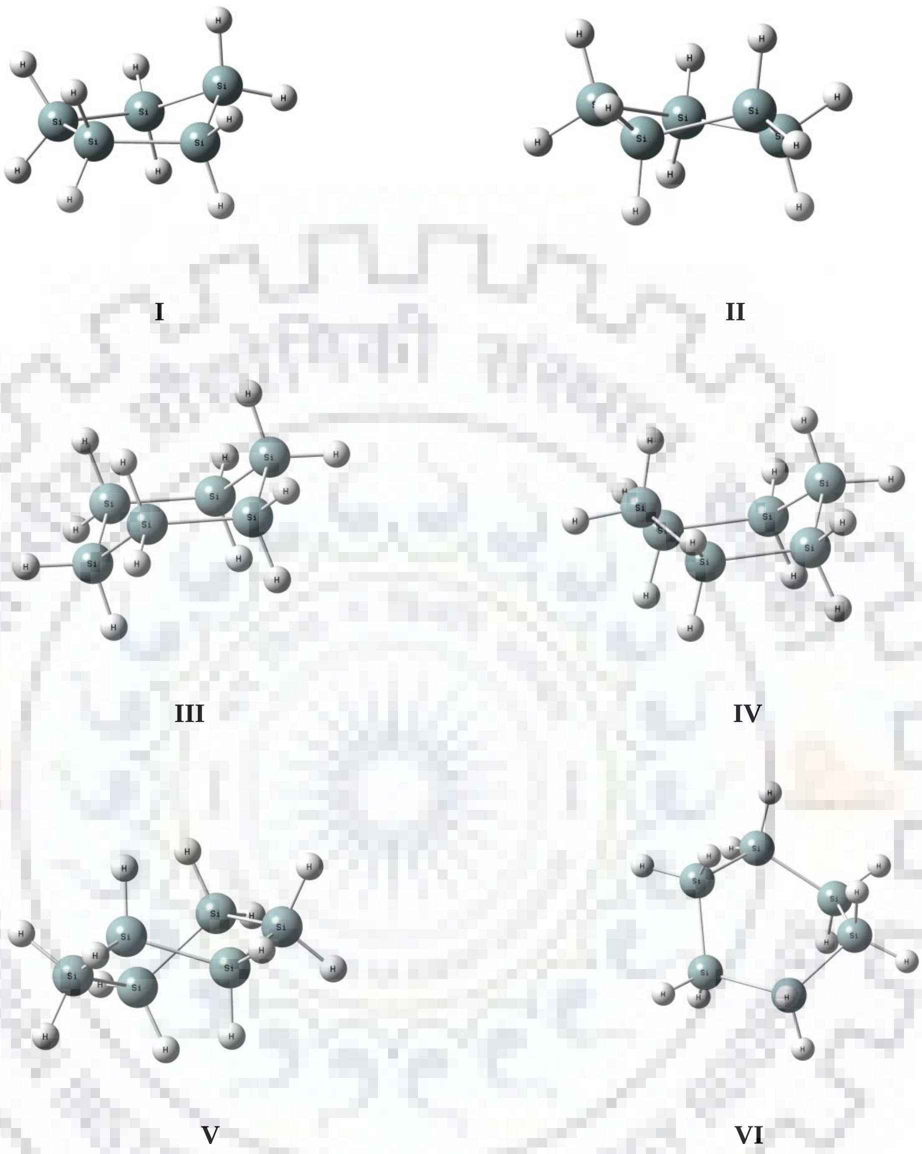

I II III IV V VI

Fig. 3.3 Gas phase optimized geometries of cyclic silanes, Si_nH_{2n} (n=5 and 6) at B3LYP/6-31G(d) level of theory in gas phase. I- *envelope*- Si_5H_{10} (C_s), II- *twist*-Si_5H_{10}(C_2), III- *chair*-Si_6H_{12} (D_{3d}), IV- *boat*- Si_6H_{12}(C_{2V}), V- *twist boat*- Si_6H_{12} (D_2) and VI- *half chair*- Si_6H_{12} (C_2).

The HOMO-LUMO gaps of the linear silanes *n*-Si_5H_{12} and *n*-Si_6H_{14} with the corresponding isomers of cyclic silanes, cyclopentasilane and cyclohexasilane at different levels of theory are shown in Table 3.3 and Table 3.4 respectively.

When we compare the linear Si_5H_{12} with two isomers of cyclopentasilane, Si_5H_{10}, namely twist with C_2 symmetry and envelope with C_s symmetry (see Table 3.3), the results are not uniform but vary with the method. This may be due to the methods representing the strain due to cyclization to differing levels of accuracy along with the changed number of hydrogens.

Table 3.3 HOMO-LUMO gaps (eV) of linear Si_5H_{12} and cyclic Si_5H_{10} at different levels of theory

Method/Basis-set	***n*- Si_5H_{12}**	***twist*-Si_5H_{10}**	***envelope*-Si_5H_{10}**
HF/6-31G(d)	9.94	12.2479	12.2473
MP2/6-31G(d)	12.82	12.3162	12.3156
B3LYP/6-31G(d)	6.92	6.5536	6.5541
PBE/6-31G(d)	5.48	5.1114	5.1125
B3LYP/LANL2DZ	7.50	7.3204	7.3207
B3LYP/D95	7.09	7.0853	7.0842
B3LYP/SHC	6.97	6.9844	6.9841
PM3	9.12	7.8116	7.8116

It is shown in Table 3.4, the HOMO-LUMO gaps increase as we go from the 6-membered linear system to the stable chair form of cyclohexasilane at any level of theory used. This is expected from the consideration that the cyclic system is more compact and its effective size is less than that of the analogous linear structure, the effect of size being reflected through the increase of HOMO-LUMO gaps upon cyclization. However, the less stable isomers do not satisfy this criterion uniformly. The boat forms show gaps consistently below that of the linear form, while the twist and half chair forms confirm to expectation only in the *ab-initio* cases. The half chair conformer is a transition state between the chair and twist conformers which corresponds to exactly one negative imaginary frequency at the potential energy surface. The twist and half chair forms show gaps differing from one another only at the fourth place of decimals. In making these comparisons one has to make allowances for the changed number of hydrogens too.

Table 3.4 HOMO-LUMO gaps (eV) of linear Si_6H_{14} and conformers of cyclohexasilane, Si_6H_{12} at different levels of theory

Method/Basis-set	***n*-Si_6H_{14}**	***chair*-Si_6H_{12}**	***boat*-Si_6H_{12}**	***twist*-Si_6H_{12}**	***half-chair*-Si_6H_{12}**
HF/6-31G(d)	12.65	12.86	12.64	12.7410	12.7415
MP2/6-31G(d)	12.77	12.95	12.67	12.8085	12.8093
B3LYP/6-31G(d)	6.90	7.11	6.78	6.8600	6.8581
PBE/6-31G(d)	5.46	5.64	5.27	5.3655	5.3620
B3LYP/LANL2DZ	7.47	7.78	7.32	7.3830	7.3822
B3LYP/D95	7.07	7.47	6.96	7.0257	7.0254
B3LYP/SHC	6.95	7.31	6.89	6.9531	6.9517
PM3	7.15	7.26	7.04	7.0573	7.0570

3.4. Conclusion

For the present systems investigated by various methods, it seems that the best estimates of HOMO-LUMO gaps were found to be given by the PBE functional. Pseudopotential methods overestimate the HOMO-LUMO gaps.

भारतीय प्रौद्योगिकी संस्थान रुड़की
INDIAN INSTITUTE OF TECHNOLOGY ROORKEE

Chapter 4

Structural, Electronic and Optical properties of Model Silicon Quantum Dots: a Computational Study

4.1 Introduction

In the present chapter, we compute the static mean polarizabilities and optical constants of chosen model SiNCs of two types namely polycyclic systems of the set of sila-diamondoids and several acyclic silanes. The size dependence of the static mean polarizabilities and correlation with HOMO-LUMO gaps and the variation of the optical constants as a function of photon energy of these systems are examined. We employed Vanderbilt ultrasoft pseudopotentials (USPPs) [123, 144] calculate the optical properties of SiNCs. We have chosen these properties for study as they are related to the absorption spectra.

4.2 Computational Details

Ground state geometry of the clusters studied has been optimized using density functional methods. Both B3LYP [49] and PBE [115] functional were used in conjunction with 6-31G (d)

Adapted from Ref. [74]

basis set as implemented in Gaussian 09 software package [132]. All the optimized geometries correspond to true minima on the potential energy surface as confirmed by frequency calculations. The polarizability calculations have been performed using restricted Coulomb-attenuating method Becke 3-parameter Lee-Yang-Parr (CAM-B3LYP) functional [117, 118] in conjunction with cc-pVDZ basis set and the 6-31++G (d, p) basis set.

The investigation of the optical properties of the selected systems was done by DFT calculations based on Plane waves basis set [122] using CASTEP code with ultrasoft pseudopotentials. We have used PBE functional under Generalized Gradient approximation (GGA) [115]. The kinetic energy cutoff for plane wave expansion is 180 eV. The calculations have been performed at Gamma point only. The Kohn Sham wave functions have real eigenvalues at Gamma points making it easy to perform the linear algebra involved. Gamma point only calculations give a good approximation for qualitative studies of isolated (non-periodic) systems and recent literature deals with such calculations [145]. The SCF convergence tolerance for all the calculations has been chosen as 0.2000×10^{-5} eV. The supercell approach has been used in the calculations for isolated systems with a length of supercell almost three times the size of the nanocluster [146]. The large supercell has been chosen to ensure a separation distance between neighboring molecules sufficient enough to minimize any interactions among neighboring molecules. Each molecule placed in the virtually periodic system is surrounded by vacuum. The large supercell provides a virtual periodic environment to isolated molecules and serves as a mathematical construct to perform plane waves based calculations for an isolated system. The optical properties have been calculated using the DFT approach as implemented in CASTEP. In this approach excited states are represented as unoccupied Kohn Sham states. The transitions between occupied and unoccupied states are caused by the electric field of the electromagnetic radiation. In the CASTEP procedure, the electronic transitions are described by matrix elements of momentum operator allowing direct calculations in the reciprocal space.

The matrix elements are given by

$$< \psi_k^c|\mathbf{r}|\psi_k^v >= \frac{1}{i\omega m} < \psi_k^c|\mathbf{P}|\psi_k^v > + \frac{1}{\hbar\omega} < \psi_k^c\,(|\mathbf{V_{nl}}|,\mathbf{r})\psi_k^v > \tag{4.1}$$

The imaginary part of the dielectric function, ε_2 is given by the expression [147]

$$\boldsymbol{\varepsilon_2(hv)} = \frac{2\pi e^2}{\Omega\varepsilon_0}\sum_{k,v,c} | < \psi^c|\mathbf{u.r}|\,\psi^v > |^2\,\delta(E_c - \mathrm{E}_\upsilon - \mathrm{E}) \tag{4.2}$$

where, **u** is the vector defining the polarization of the incident electric field. The expression is similar to Fermi's Golden rule for time-dependent perturbations, and ε_2 (hν) details the actual transitions between occupied and unoccupied electronic states. The real and imaginary parts are linked by a Kramers-Kronig transform as the dielectric constant describes a causal response. Hence, the real part of the dielectric function, ε_1 is evaluated through this transformation.

4.3. Results and Discussion

4.3.1 Polycyclic Silanes

The energy gap between HOMO and LUMO energy levels is expected to vary when the number of rings changes in polycyclic systems. We studied the homologous series of silicon analogues of diamondoids called sila-diamondoids which are cage-like ultrastable molecules. They all have a silicon cage structure containing six-membered cyclohexasilane rings all in the most stable chair conformation. In general, the homologous series can be represented by the general formula

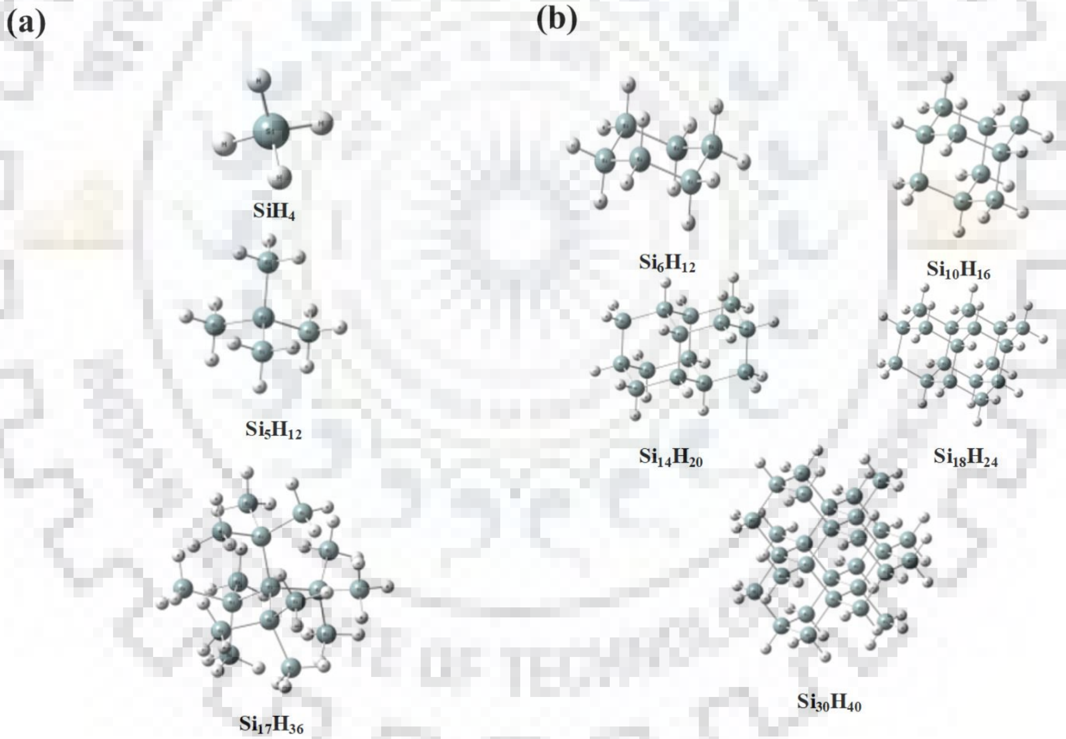

Fig. 4.1 Gas phase optimized geometries of (a) acyclic clusters containing diamond like core and (b) series of sila-diamondoids, $Si_{2(2n+1)}H_{4(n+2)}$ (n = 1, 2,…4) at B3LYP/6-31G (d) level of theory.

$Si_{2(2n+1)}\,H_{4(n+2)}$ where n = 1, 2, 3 etc.

The first few members of the series are Si_6H_{12} (n=1), sila-adamantane [148], $Si_{10}H_{16}$ (n=2), sila-diamantane, $Si_{14}H_{20}$ (n=3) and sila-trimentane, $Si_{18}H_{24}$ (n=4) etc. A polymentane internally has a diamond structure.

4.4 Studies of Static mean Polarizability of model SiNCs

Dipole moments and Polarizability are important properties in connection with spectroscopy. Polarizability determines the change of dipole moment on application of an electric field. Denoting the dipole moment by **P** and the electric field by **E** we may formally expand the dipole moment about the permanent dipole moment, $\mathbf{P_0}$ in a Taylor series as

$$\mathbf{P} - \mathbf{P_0} = \alpha\mathbf{E} + \text{higher terms} \tag{4.3}$$

The quantity $\mathbf{P} - \mathbf{P_0}$ is the induced dipole moment and has its origin in the displacement or redistribution of the charged particles (electrons and nuclei) on application of the field. For low electric fields, only the first term explicitly shown on the right hand side above is significant.

The polarizability $\boldsymbol{\alpha}$ is a second rank tensor, represented as

$$\begin{pmatrix} \boldsymbol{\alpha}_{xx} & \boldsymbol{\alpha}_{xy} & \boldsymbol{\alpha}_{xz} \\ \boldsymbol{\alpha}_{yx} & \boldsymbol{\alpha}_{yy} & \boldsymbol{\alpha}_{yz} \\ \boldsymbol{\alpha}_{zx} & \boldsymbol{\alpha}_{xy} & \boldsymbol{\alpha}_{zz} \end{pmatrix}$$

It is a symmetric tensor [149] (i.e. $\alpha_{xy} = \alpha_{yx}$ etc) and so is diagonalizable i.e., on choosing a rotated coordinated system the off-diagonal elements can be made zero, such a coordinate system being called the principal axes system of the tensor and the diagonal elements are the principal components. However, the diagonalization does not change the sum of the diagonal elements, and so the quantity $\bar{\alpha} = (\alpha_{xx}+\alpha_{yy}+\alpha_{zz})/3$ called the static mean polarizability is unchanged and is meaningful. Polarizability is related to the shape and symmetry characteristics of a molecular species. Structural parameters like size, shape and geometry are responsible for the overall nature of the nanocluster and are associated with all the physical and chemical properties of the nanocluster [150-153]. Variation in the structural parameters might impart a significant change in the physical properties of the nanocluster.

The bulk limit of polarizability can be estimated from the Clausius Mossotti relation as

$$\alpha_{bulk} = \frac{3}{4\pi}\left(\frac{\varepsilon_b - 1}{\varepsilon_b + 2}\right)\mathrm{v}_{at} \tag{4.4}$$

where v_{at} = 2x10^{-23} cm^3 is the elementary volume per atom of Si in the crystal state and ε_b is the bulk dielectric constant with a value of 11.9.This leads to a value of α_{bulk} of 3.75 Å^3 /atom for silicon. The polarizability values obtained from our calculations are in atomic units (a.u.) which are converted to volume units using the conversion factor 1a.u. = 0.148184 Å^3. To compare with the bulk property we need to estimate the polarizability per atom of Si. In this we are faced with two obvious choices: use the total number of atoms or just the number of Si atoms in the cluster. The use of the total number of atoms following the approach of S. Schlecht et al. [154] who studied the dependence of polarizability on the size (n+m) of $Ga_n As_m$ clusters seems inappropriate in this case as Si and H are atoms of widely different mass and size. The use of the number of Si atoms alone underestimates seriously the contribution of large number of hydrogens present in the systems under study. Therefore we adopt a middle course by adding to the number of Si atoms a fraction of the total number of hydrogens. Because the polarizability is expressed in volume units we decided to use the fraction as the cube of the ratio of Van der Waals radii of H and Si atoms, which works out as 0.18659. This

Table 4.1(a) Static mean polarizabilities (Å^3), static mean polarizability per atom and HOMO-LUMO gaps (eV) in a series of sila-diamondoids.

Molecule (Si_nH_m)	**$\bar{\alpha}$ (Å^3)**	***n_c= n+0.1866m**	**$\bar{\alpha}/n_c$**	**E_{gap} (eV)**
Si_6H_{12}	24.925	8.239	3.025	7.11
$Si_{10}H_{16}$	40,355	12.985	3.107	6.87
$Si_{14}H_{20}$	56.919	17,733	3.210	6.03
$Si_{18}H_{24}$	73.932	22.478	3.289	5.55

* n_c denotes non-integer number representing contribution from the total number atoms in SiNC.

leads to a non-integer number which we denote by the symbol n_c. The values of mean static dipole polarizability $\bar{\alpha}$ computed and $\bar{\alpha}/n_c$ and the HOMO-LUMO gaps (computed at the CAM-B3LYP/cc-pVDZ level of theory) of the sila-diamondoids are shown in Table 4.1(a). It is seen that the static mean polarizability per atom increases with size whereas the HOMO-LUMO gaps decrease with increasing size (as was expected). To see if inclusion of diffuse functions in the basis set affects the static mean polarizabilities of these systems seriously, we calculated these properties using the 6-31++G (d, p) basis set also. These results are shown in Table 4.1(b). Table 4.2(a) and 4.2(b) shows the corresponding results for a set of acyclic silanes with tetrahedral geometry. These tables clearly show that both for the sila-

Table 4.1(b) Static mean polarizability ᾱ (Å^3), Static mean polarizability per atom ᾱ/n_c (Å^3) and HOMO-LUMO gaps (eV) in a series of sila-Diamondoids calculated at CAM-B3LYP/6-31++G** level of theory

Molecule (Si_nH_m)	ᾱ(Å^3)	n_c= n+0.1866m	ᾱ/n_c (Å^3)	E_{gap} (eV)
Si_6H_{12}	25.140	8.239	3.051	9.16
$Si_{10}H_{16}$	40.755	12.985	3.138	8.73
$Si_{14}H_{20}$	57.473	17.733	3.241	8.11
$Si_{18}H_{24}$	74.607	22.478	3.319	7.79

Table 4.2(a) Static mean polarizabilities (Å^3), polarizability per atom and HOMO-LUMO gaps (eV) in a series of acyclic silanes with tetrahedral geometry.

Molecule (Si_nH_m)	ᾱ (Å^3)	n_c= n+0.1866m	ᾱ/n_c	E_{gap} (eV)
SiH_4	3.928	1.746	2.250	10.99
Si_5H_{12}	21.081	7.239	2.912	8.11
$Si_{17}H_{36}$	71.657	23.717	3.021	5.83

diamondoids and for the acyclic silanes the trends are similar with both the basis sets chosen. The static mean polarizabilities are not very different in the larger basis set, being higher by less than 1% .Where we are concerned with qualitative comparisons, we infer that the use of diffuse functions in the basis set does not make a serious difference where α is concerned. The coefficient of correlation between static mean polarizability per atom and the energy gap has the value -0.987 for the sila-diamondoids and -0.947 for the acyclic systems studied in the case of the first basis set used.

Table 4.2(b) Static mean polarizaability, ᾱ (Å^3), Static mean polarizability per atom and HOMO-LUMO gaps, E_{gap} (eV) in a series of the acyclic silanes at CAM-B3LYP/6-31++G** level of theory

Molecule (Si_nH_m)	ᾱ (Å^3)	n_c= n+0.1866m	ᾱ/n_c	E_{gap} (eV)
SiH_4	3.841	1.746	2.200	11.87
Si_5H_{12}	21.558	7.239	2.978	9.52
$Si_{17}H_{36}$	73.405	23.717	3.095	8.23

The static mean polarizability values per atom for the cyclic systems (Tables 4.1(a) or 4.2(a)) or for the open systems studied (Tables 4.1(b) or 4.2(b)) clearly increase steadily with the number of Si atoms involved. In either case, it makes it reasonable to suspect that ultimately these are tending to the bulk value of 3.75Å^3 per atom estimated above from the Clausius-Mossotti relation.

4.5. Optical Properties

The inverse correlation between optical gaps and the size of nanoclusters has triggered the idea of tuning the optical response as a function of size and surface [155-158] in order to design silicon-based electronic devices suitable for the desired applications like optoelectronics [159], Si-based light emitting devices [160], photovoltaics [161], solar cells [162], biological applications [163] etc.

In this work, we investigate the optical properties of SiNCs. We calculated the optical constants namely, refractive index (n), extinction coefficient (k), absorption coefficient (α), the complex dielectric function (real part, ε_1 and imaginary part, ε_2) both for a few non-cyclic nanoclusters viz., SiH_4, Si_5H_{12} and $Si_{17}H_{36}$ and the series of hydrogenated and dehydrogenated sila-diamondoids [59].

The polarization **P** that is induced by the externally applied electric field, allows us to describe various processes like reflection, emission, or elastic and non-elastic scattering which occur when light interacts with matter. The complex Dielectric function, ε (hν) is the most important quantity which describes the dielectric behavior of a material [164]. It is determined experimentally using ellipsometry [165]. The remaining optical constants, refractive index (n), extinction coefficient (k), absorption coefficient (α), are calculated through fundamental relations in optics [166, 167], as outlined below.

Absorption coefficient (α) is one of the optical constants which is frequently measured experimentally and is related to the dielectric function through the relation:

$$\varepsilon_2 = \frac{n\alpha\lambda}{2\pi} \tag{4.5}$$

It is a characteristic of a material which defines the amount of light absorbed by it and the average distance travelled by a photon before it gets absorbed is given by the inverse of α i.e α^{-1}. In the limiting region of the spectrum of complex refractive index ($N = n + ik$) versus energy (hν), the complex dielectric function ($\varepsilon = \varepsilon_1 + i\varepsilon_2$) is related to linear refractive index (n) and extinction coefficient (k) through the following relations [168, 169]

$$N = \sqrt{\varepsilon} \tag{4.6}$$

$$\varepsilon_1 = n^2 - \mathrm{k}^2 \tag{4.7}$$

$$\varepsilon_2 = 2nk \tag{4.8}$$

Also, the absorption coefficient can be given in terms of extinction coefficient as

$$\alpha = \frac{4\pi \mathrm{k}}{\lambda\,(\mathrm{nm})} \tag{4.9}$$

The ε_2 (hν) versus energy (hν) spectrum reflects the absorption spectrum of the material.

4.5.1. Optical Spectra

4.5.1.1. Dielectric Function

Fig. 4.2 shows the size dependence of the imaginary part of the complex dielectric function, ϵ_2 as a function of photon energy, hν for both the classes of clusters studied namely, acyclic clusters, SiH_4, Si_5H_{12} and $Si_{17}H_{36}$ with T_d symmetry (see Fig. 4.2(a)) and *sila*-diamondoids, Si_6H_{12}, $Si_{10}H_{16}$, $Si_{14}H_{20}$ and $Si_{18}H_{24}$ (see Fig. 4.2(b)). The variation of ϵ_2 (hν) as a function of hν for acyclic clusters possessing T_d symmetry displays multiple peaks as shown in Fig 4.2(a). It is observed that the peak height decreases as the size increases from SiH_4 to Si_5H_{12} to $Si_{17}H_{36}$ with a concomitant shift of the energy corresponding to the maximum towards the lower energy region. The appearance of multiple peaks may be attributed to the free rotation of the sp^3 hybridized –SiH_3 moieties present at the terminals of the open chains of silanes. It is also observed that the smaller peak is located at a lower energy in case of $Si_{17}H_{36}$ whereas for Si_5H_{12} and SiH_4 the smaller peak is located at a higher energy. The decrease of the intensity of peak with increasing size is consistent with the experimental observation of the absence of any absorption of photons in bulk silicon with energy value below 3.0eV [170, 171].

It is seen from Fig. 4.2(b) that in the case of sila-diamondoids, with the exception of sila-diamantane the maximum value of ε_2 decreases as the size of the cluster increases with a concomitant shift of respective energy values towards lower energy region [170]. sila-diamantane, $Si_{14}H_{20}$ behaves as an exception showing a higher value of ε_2 (0.169) at energy (5.31 eV) compared to sila-adamantane, $Si_{10}H_{16}$ with ε_2 value (0.147) at energy (6.0 eV) and sila-trimentane, $Si_{18}H_{24}$ with ε_2 value (0.048) at energy (5.66 eV), whereas cyclohexasilane, Si_6H_{12} has the highest value of ε_2 (0.206) at energy (7.4 eV). A possible reason for this anomaly lies in the fact that sila-diamantane has a relatively more compact structure than the others (see Fig. 4.1(a)).

The imaginary part of the dielectric function is directly related to absorption. The plot of ε_2 as a function of hν can be seen to be analogous to the absorption spectrum. We obtained the

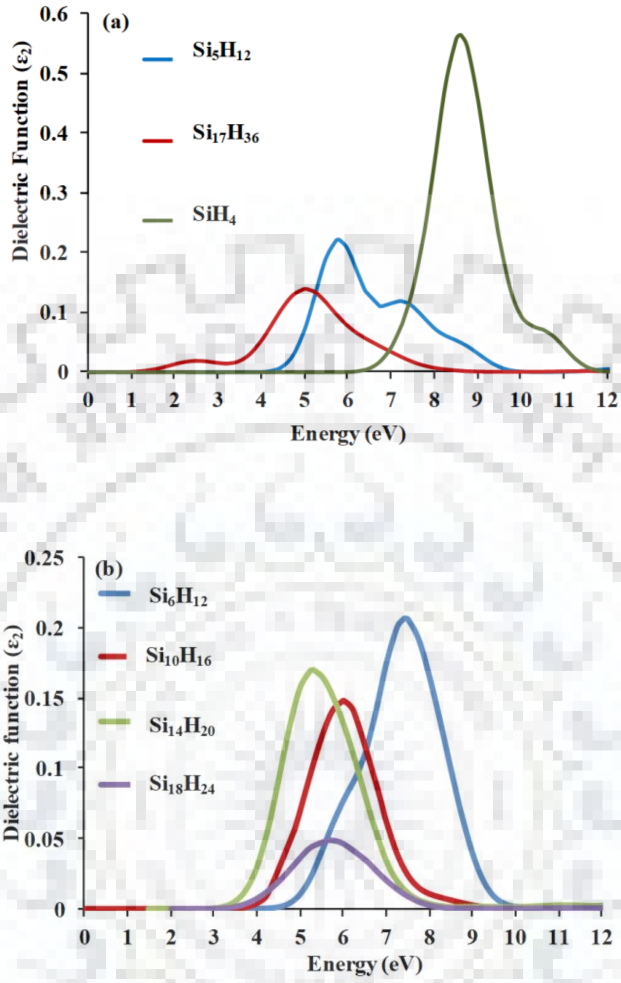

Fig. 4.2 Imaginary part (ε_2) of the complex dielectric function of (a) acyclic SiNCs, SiH_4, Si_5H_{12} and $Si_{17}H_{36}$ (b) hydrogenated sila-diamondoids, Si_6H_{12}, $Si_{10}H_{16}$, $Si_{14}H_{20}$, $Si_{18}H_{24}$.

absorption energies designated as E_p as the energy corresponding to the maximum of ε_2 following the method used by Ghoshal et al. [171] and compared it with the calculated energy gaps, E_g from bandstructure calculation (see Table 4.3). It is seen that the absorption energy E_p is always greater than the calculated energy gap, E_g. The E_p of sila-diamantane falls anomalously below that of sila-trimentane; with this exception, the values E_p and E_g both are found to decrease with increase in the size of the cluster which is consistent with the usual trend observed in nanoclusters owing to quantum size effects [172]. The conventionally measured optical bandgaps of materials correspond to the threshold of absorption rather than the maximum as obtained here (which is more convenient from the functional dependence of ε_2 on radiation frequency as computed here). Hence usually optical bandgaps are lower than E_g values except in the case of indirect bandgaps.

Table 4.3 HOMO-LUMO gap, E_g (eV) of sila-diamondoids and non-cyclic SiNCs with T_d symmetry at B3LYP/6-31G (d) level of theory, optical bandgap, E_p (eV) obtained from the maximum of the plot of ε_2 as a function of photon energy and the maximum value of imaginary part of the complex dielectric function ($\varepsilon_{2\,(max)}$).

Nanocluster	E_g	E_p	$\varepsilon_{2\,(max)}$
Si_6H_{12}	5.20	7.43	0.206
$Si_{10}H_{16}$	4.59	6.00	0.147
$Si_{14}H_{20}$	4.27	5.31	0.169
$Si_{18}H_{24}$	3.91	5.66	0.048
SiH_4	7.62	8.59	0.564
Si_5H_{12}	5.73	5.80	0.221
$Si_{17}H_{36}$	1.179	5.04	0.137

4.5.1.2. Refractive Index (n)

Bulk Silicon is interesting as it has a very high refractive index (close to 3.75) in the visible part of the electromagnetic spectrum. Computationally we obtain the complex refractive index of the material studied while the measured refractive index corresponds to the real part only. The real part of the complex refractive index (n) of the first four sila-diamondoids as a function of the photon energy (hν) is shown in Fig. 4.3. It signifies the dispersion of the incident radiation falling on the material and the slowing down of the propagation of the wave inside the material. Fig 4.3 shows that the dispersive region lies within the ultraviolet region of the electromagnetic spectrum in the energy range of 3-11 eV. The maximum value of n for all the clusters is close to one. At higher energies, the value of n is less than unity but this does not violate the relativity.

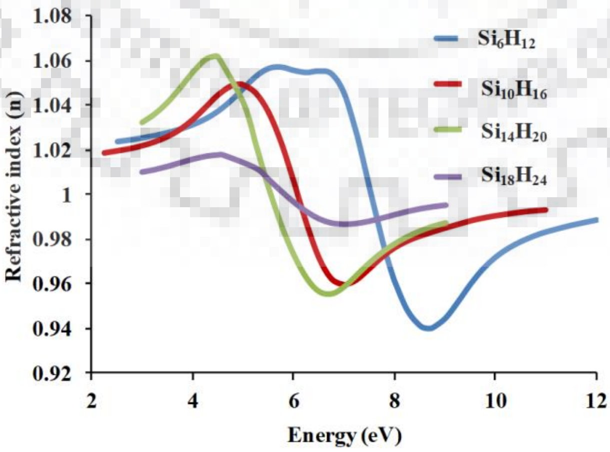

Fig 4.3 Frequency dependence of the real part of the refractive index (n) of hydrogenated sila-diamondoids, Si_6H_{12}, $Si_{10}H_{16}$, $Si_{14}H_{20}$, $Si_{18}H_{24}$.

We note that the values of n are very low compared to bulk silicon which is recognized as a material of very high refractive index.

The Fig. 4.3 also demonstrates a shift of the maximum value of refractive index, n_{max} towards a lower value of energy with a simultaneous decline of the maximum value of refractive index with increase in size with the exception of sila-diamantane which has the highest n_{max} in the dispersive region among the series of 1.062 at the lowest energy of 4.42 eV. sila-trimentane possesses the lowest n_{max} of 1.017 at 4.59 eV.

We also calculated the refractive index for the relatively larger $Si_{30}H_{40}$ cluster possessing a T_d core (see Fig. 4.1(b)) and found a n_{max} value 1.154 at energy 1.11 eV and a limiting value of 1.121 at low energies. These values being higher than that of the series of sila-diamondoids, we may infer that ultimately the refractive index increases with the size of the SiNCs, apparently tending to the bulk value.

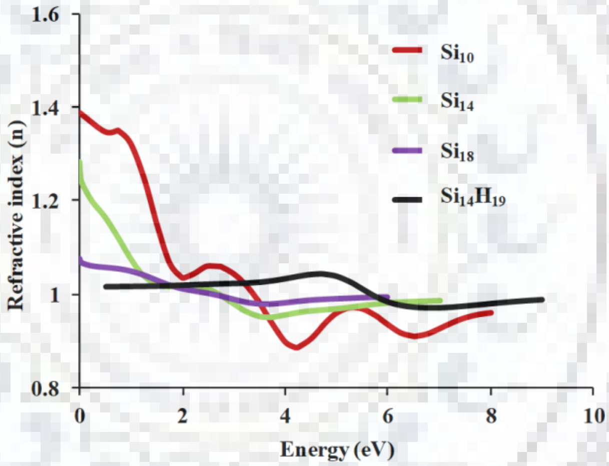

Fig. 4.4 Size dependence of the real part of the refractive index (n) of dehydrogenated sila-diamondoids, Si_{10}, Si_{14}, Si_{18} and sila-diamantane, $Si_{14}H_{19}$ with one apical hydrogen missing (one surface dangling bond).

The optical properties of the system can be tuned through surface manipulation. Surface functionalization [172, 173] with selective choice of the ligands [174] can make the cluster a potential candidate for a wide range of applications [175].

Next, we study the behavior of n as a function of photon energy for clusters possessing no hydrogen capping and free surface states. We have also included in the study the sila-diamantane moiety with one apical H removed. The plots showing energy dependency are presented in Fig. 4.4. In the case of sila-diamantane with only one hydrogen removed i.e. $Si_{14}H_{19}$, the bandgap is reduced from 4.27 eV to 1.14 eV as a consequence of removal of one hydrogen, owing to the generation of surface states [176, 177], with the existence of dangling bonds [178, 179]. The bandgap is further reduced to 0.009eV for the Si_{14} cluster. Fig. 4.4 demonstrates higher values of refractive index of non-hydrogenated clusters compared to the fully hydrogenated counterparts in the low energy regions. This is counter-intuitive as one would expect the opposite trend to hold in view of the high refractive index of bulk Si in the visible region of the electromagnetic spectrum. The maximum value of n also shifts downwards with an increase of the size of the cluster in the order $Si_{10} < Si_{14} < Si_{18}$. The spectrum shows more than one maxima. The bandgap for $Si_{10}H_{16}$ is 4.59eV as against 0.07eV for Si_{10} cluster and the bandgap for $Si_{18}H_{24}$ of 3.91eV compared to 0.133eV for Si_{18} cluster. The lowering of bandgaps upon removal of all hydrogens is again due to the encroachment of additional surface states between the valence band and the conduction band. Further consequences like appearance of multiple peaks in the active spectral region for non-hydrogenated clusters demonstrate the interference of surface states during interband transitions.

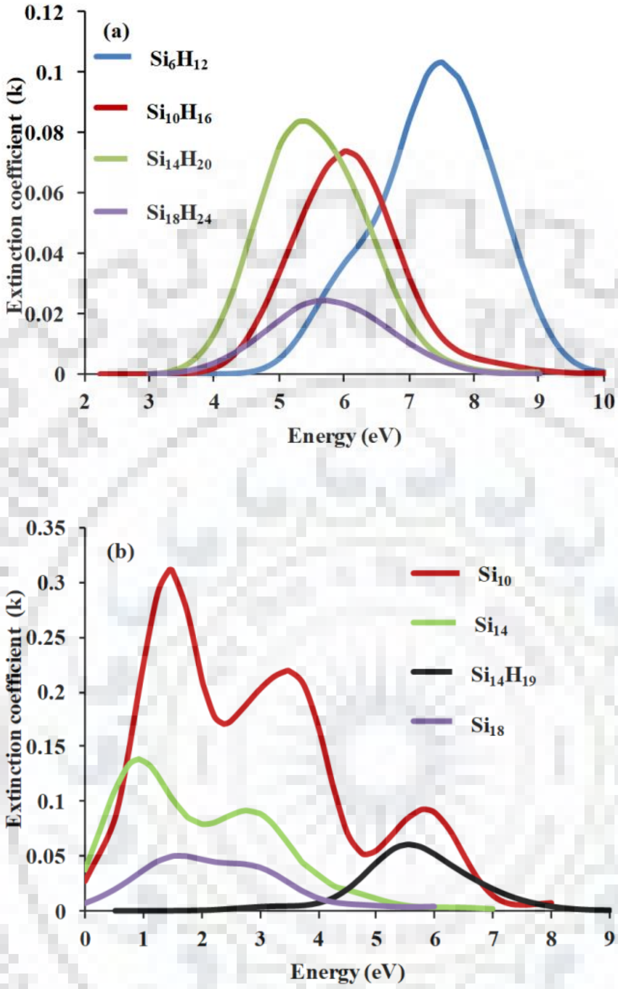

Fig. 4.5 Frequency dependence of Extinction coefficient (k) (a) hydrogenated sila-diamondoids (b) dehydrogenated sila-diamondoids.

4.5.1.3. Extinction Coefficient (k)

The imaginary part of the complex refractive index represents the extinction coefficient (k) of the material and governs the absorption of incident light by the material. The frequency dependence of the extinction coefficient of hydrogenated sila-diamondoids and dehydrogenated sila-diamondoids are shown in Fig. 4.5 (a) and Fig. 4.5 (b) respectively. Fig. 4.5(a) shows a maxima towards lower side of the ultraviolet spectral region with increasing order of size with the exception of sila-diamantane with a concomitant broadness of the curve. We attribute the exceptional behavior of sila-diamantane to its relatively more compact structure. The peaks do not show the δ-function type behavior expected from theory but show considerable gaussian broadening, probably due to involvement of states close to the lowest excited state as well. The extinction coefficient (k) as a function of photon energy (Fig. 4.6(a)) and the imaginary part of the dielectric function (ε_2) as a function of photon energy (Fig. 4.2(a)) show similar behavior

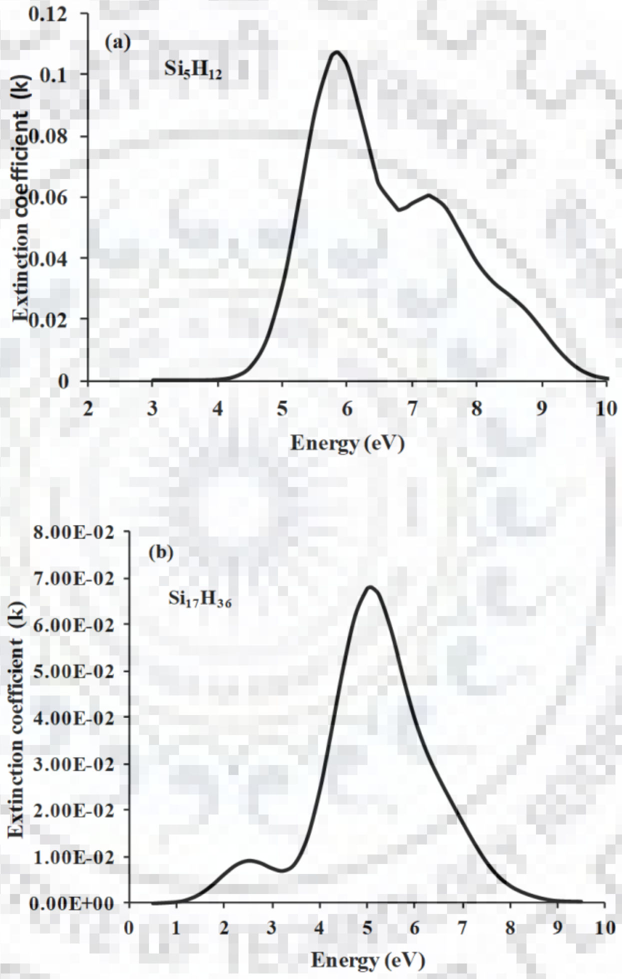

Fig. 4.6 Extinction coefficient, **k** (imaginary part of refractive index) of acyclic SiNCs (a) Si_5H_{12} and (b) $Si_{17}H_{36}$.

qualitatively. The absorption spectra are directly related to k (or ε_2) and they also do not show vibrational structure etc. We suspect that this is due to overlap of the resulting levels and lines due to the transitions involving states close to HOMO and LUMO in the energy scale involved (see Appendix A). In the case where all hydrogens are removed the imaginary part of refractive index shows multiple peaks. This behavior is qualitatively reflected in the absorption spectra as well (see Appendix B).

A similar behavior is shown by the acyclic systems studied too (see Fig. 4.6 (a,b)). In this case, auxiliary peaks or shoulders appear in the hydrogenated species as well which is probably attributable to the silyl groups present. The auxiliary peaks shift to the lower energy side in the larger species, probably due to the larger number of silyl groups present. The spectra also show similar behavior (see Appendix B).

4.6 Conclusion

In the present work, we have initiated the investigation of some important properties of model silicon quantum dots, such as the polarizability, the (complex) dielectric function and the (complex) refractive index with a view to see their frequency dependence and variation with size. It is observed that the peak height decreases as the size increases from cyclohexasilane to sila-trimentane with a concomitant shift of the energy corresponding to the maximum towards the lower energy region. We have observed an anomalous behavior of sila-diamantane among the set of sila- diamondoids studied. We have also studied the optical constants as a function of photon energy for dehydrogenated sila-diamondoids. Further investigations including calculations of hyperpolarizabilities are in progress.

Appendix 4.I

The absorption spectra of hydrogenated and dehydrogenated sila-diamondoids as a function of photon energy.

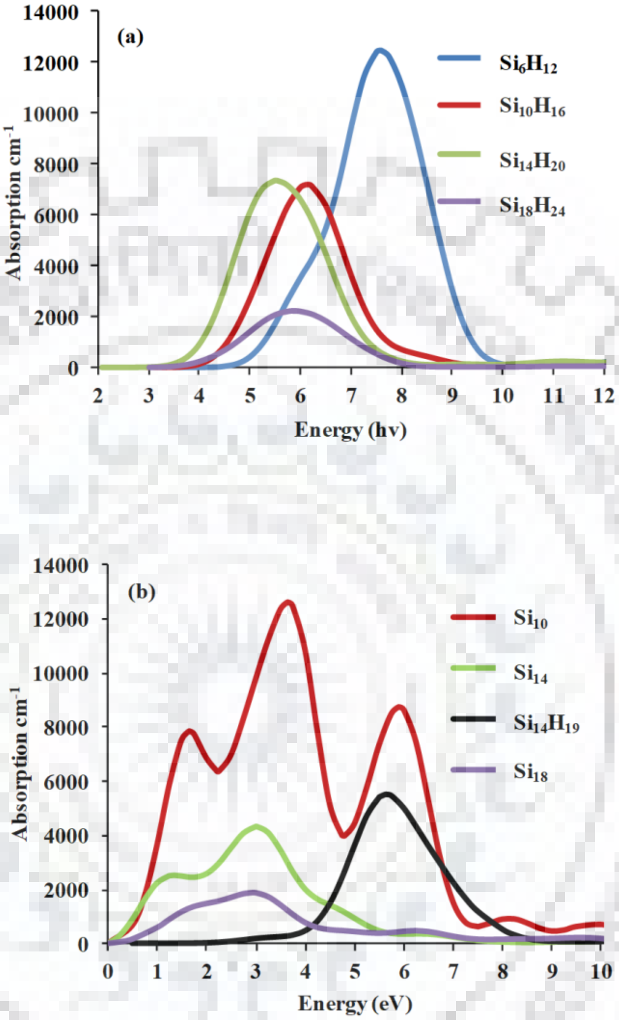

Fig. 4.I.1 Absorption spectrum of (a) hydrogenated sila-diamondoids, (b) dehydrogenated sila-diamondoids.

Appendix 4.II

The absorption spectra of acyclic silicon nanoclusteres with T_d core as a function of photon energy.

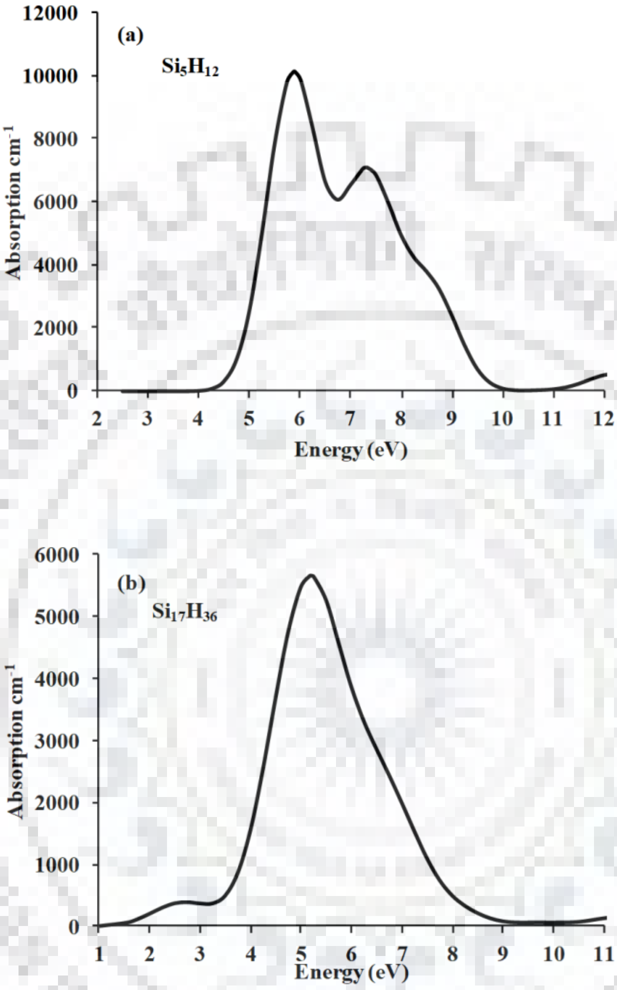

Fig. 4.II.1 Absorption spectrum of acyclic SiNCs (a) Si_5H_{12} (b) $Si_{17}H_{36}$.

Chapter 5

Bandgap Tuning and Two-Photon Activity of Push-Pull Derivatives of Silyl Substituted Silicene Monolayer

5.1 Introduction

It is known that conjugated planar hydrocarbon systems with electron donor/acceptor substituents show significant two-photon absorption (TPA) probabilities [180-184]. Silicene nanosheets with hydrogens or silyl groups saturating the edges would be expected to be planar (analogous to graphene), and those with suitable donor/acceptor substituent pairs 180° apart relative to the centre show significant two-photon activity. However, in contrast to graphene monolayers these systems are found to be puckered [185] on geometry optimization, which implies that they are not perfectly conjugated and hence TPA activity is not obvious, but our studies show TPA properties in them. In this chapter, we discuss the OPA and TPA activity of model silicene systems computationally and attempt to tune their bandgaps to the UV-Visible region of the electromagnetic spectrum with choice of donor/acceptor groups.

5.2 Computational Details

Our model systems comprises of silicene monolayer containing 24 silicon atoms, with edges saturated with hydrogen [186] and sometimes substituted with silyl groups as shown in Fig. 5.1. These are linked with different donor–acceptor groups at a separation of 180 degrees. Fig. 5.2 shows the chosen acceptor and donor groups and their positions in the monolayer. The optimization of all the model systems has been performed using PBE functional in conjunction with 6-31G(d) basis set, in gas phase. Contrary to expectation the silicene unit turns out to be puckered in contrast to the analogous graphene. The optimized geometries of the model systems correspond to minima in their potential energy surfaces, obtained from frequency calculations. The optimization and frequency calculations are done using the Gaussian 09 program package [132]. We used these optimized geometries to calculate optical parameters for linear and non-linear absorption using response theory and TDDFT simulations. These optical property calculations have been done using CAMB3LYP functional [117, 118] in conjunction with cc-pVDZ basis set, as implemented in the DALTON 2013 package [187].

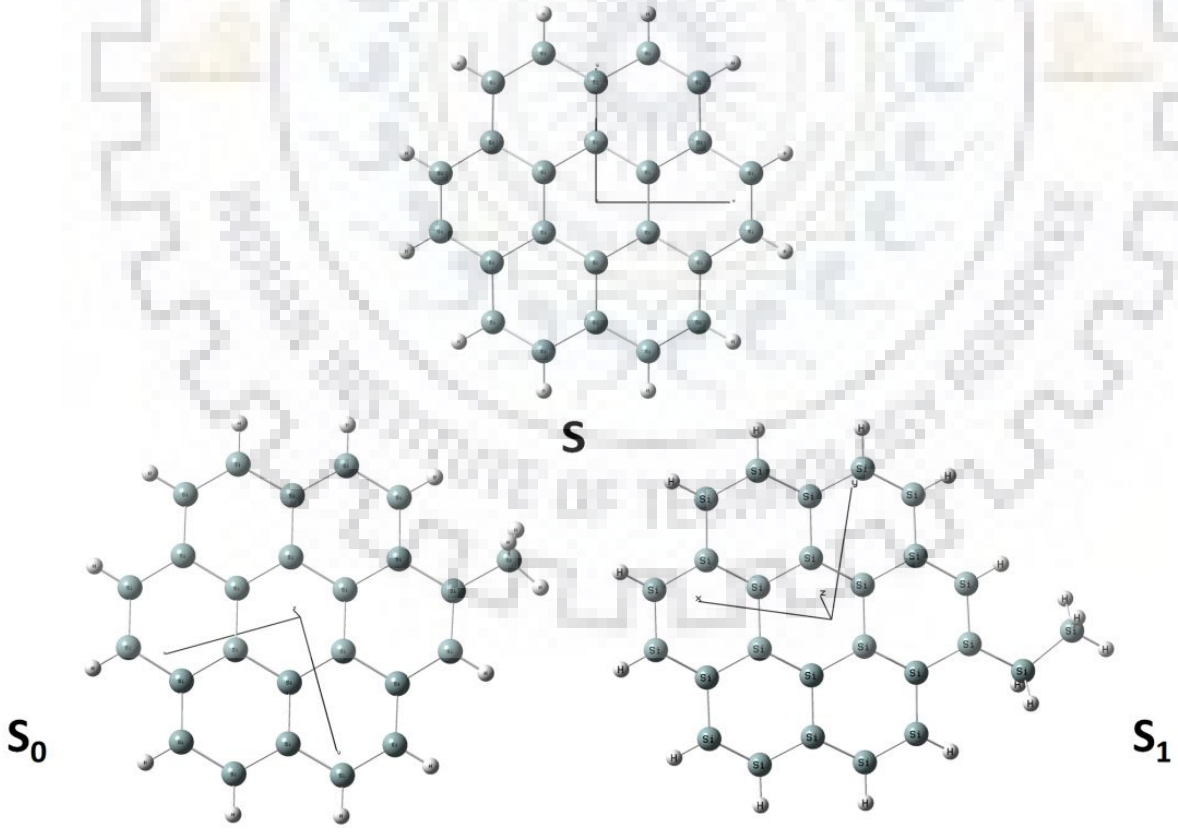

Fig 5.1 Optimized geometries of silicene systems terminated at the edges by hydrogen or by H and one $-SiH_3$ or $–SiH_2SiH_3$ groups denoted as S, S_0 and S_1 respectively. The lines correspond to the coordinate axes.

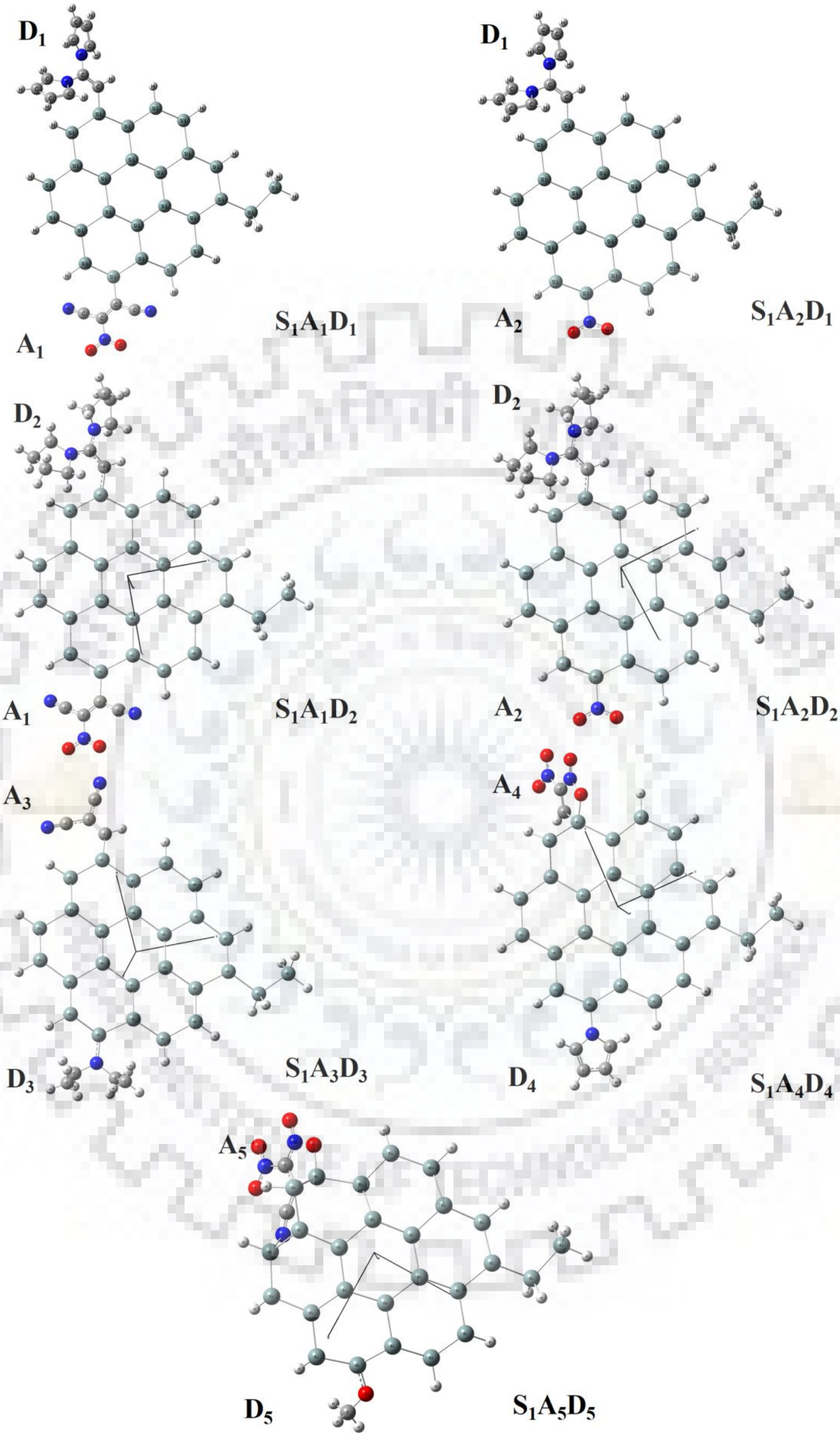
D_1
A_1
$S_1A_1D_1$
D_1
A_2
$S_1A_2D_1$
D_2
A_1
$S_1A_1D_2$
D_2
A_2
$S_1A_2D_2$
A_3
D_3
$S_1A_3D_3$
A_4
D_4
$S_1A_4D_4$
A_5
D_5
$S_1A_5D_5$

Fig. 5.2 Gas phase optimized geometries of the model systems S_1 substituted with D/A pair at PBE/6-31G(d) level of theory. In ball and stick model, Blue color: N atom, Red color: O atom

5.3 Model Silicene Systems

5.3.1 Unsubstituted

Unsubstituted silicene systems comprises $Si_{24}H_{12}$ unit terminated at the edges by hydrogen, or by H and one $-SiH_3$ or $–SiH_2SiH_3$ groups. The optimized structures of these systems calculated at PBE/6-31G(d) level of theory in the gas phase are given in Fig 5.1. S represents the 24 Si atom unsubstituted silicene monolayer terminated with H atoms. S_0 and S_1 represent silyl derivatives with one hydrogen replaced with $-SiH_3$ and $–SiH_2SiH_3$ groups respectively. In the optimized structure of the $Si_{24}H_{12}$ monolayer of silicene the Si-Si bond length in the interior of the layer is 2.28 Å, and in the periphery is 2.23 Å. Si-H bond length is 1.50 Å, Si-Si-Si bond angle is 116° in the interior of the monolayer while at the periphery, it symmetrically varies from 116°-118°, and Si-Si-H bond angle is between 115°-116°. These values are comparable with the experimental values on silicenes and suggest similar extents of puckering. We also performed optimizations of $Si_{24}H_{12}$ including both polarization and diffusion at PBE/6-31G(d), PBE/cc-pVDZ and PBE/aug-cc-pVDZ levels of theory and found that the structural parameters do not vary much.

Table 5.1 The nomenclature of model substituted silicene systems, different acceptor and donor groups, and their structure.

System	**Substituent**	**Donor (D_i)**	**Acceptor (D_j)**
$S_1A_1D_1$	A_1D_1	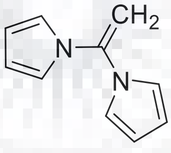	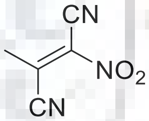
$S_1A_2D_1$	A_2D_1		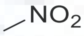
$S_1A_1D_2$	A_1D_2	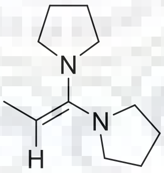	A_1
$S_1A_2D_2$	A_2D_2	D_2	A_2
$S_1A_3D_3$	A_3D_3	$—N(C_2H_5)_2$	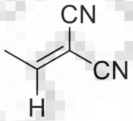
$S_1A_4D_4$	A_4D_4	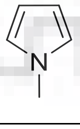	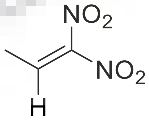
$S_1A_5D_5$	A_5D_5	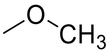	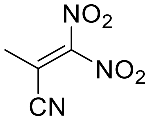

5.3.2 Substituted

Nomenclature, basic structure of the model substituted silicene systems, and different donor-acceptor groups is shown in Table 5.1. The letters D and A denote donor and acceptor group respectively. $S_1A_iD_j$ represents the S_1 derivative substituted with donor and acceptor group (where index *i*(*j*) = 1-5). The minimum energy geometries of the model silicene systems S_1 substituted with D/A pair optimized at PBE/6-31G(d) level of theory in gas phase are shown in Fig 5.2.

5.4 Theoretical Concepts

5.4.1 One -Photon Absorption (OPA) Process

OPA is defined as the process in which excitation between two electronic states takes place by absorption of one incident photon. This process is characterized by oscillator strength (δ_{OPA}) which depends on the excitation energy ω_{pq} and transition dipole moment magnitude μ^{of} between the ground ($|0\rangle$), and excited ($|f\rangle$) states involved in the transition. The value of, (δ_{OPA}) for such a transition is given by [188]

$$\delta_{OPA} = \frac{2\omega_{of}}{3} |\mu^{of}|^2 \,. \tag{5.1}$$

5.4.2 Two -Photon Absorption (TPA) Process

TPA is defined to be a process [189] in which excitation of a molecule between two states occurs via a virtual intermediate state, when two photons of same or different frequencies are absorbed simultaneously. Theoretically, the virtual intermediate state can be written as a linear combination of all states of the system involved during the process of excitation. For a monochromatic (linearly polarized) light, TP tensor elements ($S_{\alpha,\beta}$) and (δ_{TPA}) are expressed in terms of sum-over states (SOS) [190]

$$\delta_{TPA} = \sum_{\alpha,\beta} (2S_{\alpha\alpha}S_{\beta\beta} + 4S_{\alpha\beta}^2) \tag{5.2}$$

where $\alpha, \beta = x, y, z$.

$$S_{\alpha,\beta} = \sum_i \frac{\mu_\alpha^{0i}\mu_\beta^{if} + \mu_\beta^{0i}\mu_\alpha^{if}}{\omega_{0i} - {\omega_{0f}}/_2} \tag{5.3}$$

Where *i* denotes electronic states over which summation is carried out. The other terms have their usual meaning. The TPA process is described by TPA- transition probability, also called as TPA strength [191]. Theoretically, the rotationally averaged TP transition probability $\langle\delta_{TPA}\rangle$ is calculated as:

$$\delta_{TPA} = \frac{1}{30}\sum_{\alpha,\beta}\left(FS_{\alpha\alpha}\bar{S}_{\beta\beta} + GS_{\alpha\beta}\bar{S}_{\alpha\beta} + HS_{\alpha\beta}\bar{S}_{\beta\alpha}\right) \tag{5.4}$$

where $\alpha, \beta = x, y, z$. $S_{\alpha\beta}$ corresponds to the TP-tensor components, bar denotes the complex conjugation where, F, G, H components depend upon the polarization of the incident laser beam. For, parallel linearly polarized light $F = G = H = 2$ (i.e. two photons of equal frequency), while for perpendicularly linearly polarized light $F = -1$, $G = 4$, $H = 1$, and for circularly polarized light $F = -1$, $G = H = 3$. TPA cross-section σ_{TPA} in a.u. units and Goeppert Mayer (GM) units are related as [192]

$$\sigma_{TPA}(GM) = \frac{4\pi^2\alpha a_0^5\omega^2}{15c\Gamma}\sigma_{TPA} \tag{5.5}$$

where, α, a_0, and c denotes the fine structure constant, Bohr radius, and speed of light, respectively. ω denotes exciting photon energy (in TPA process, ω is half times the excitation energy) and Γ corresponds to excited state lifetime, set at 0.1 eV (for microscopic studies).

5.4.3 Λ Parameter

A numerical criterion that decides the nature of transition, whether short-range or long range, is provided by the Λ test [196, 197]. For a given occupied orbital *i* and virtual orbital *a*, an index of spatial overlap avoiding cancellations due to sign differences is given by

$$O_{ia} = \int |\chi_i(\boldsymbol{r})|\,|\chi_a(\boldsymbol{r})|d\boldsymbol{r} \tag{5.6}$$

Many occupied and virtual orbitals contribute to a given TDDFT excitation. Contribution from each occupied-real combination is represented by κ_{ia} and the parameter representing spatial overlap is defined as

$$\Lambda = \frac{\sum_{i,a} \kappa_{ia}^2 \, O_{ia}}{\sum_{i,a} \kappa_{ia}^2}, \text{where}, 0 \le \Lambda \le 1 \quad (5.7)$$

A large value of Λ corresponds to a short-range and small value to a long-range excitation. In a transition, it predicts the extent of localization of involved orbitals. For instance, a Λ value, close to 0, indicates that the orbitals involved are localized at different sites of the molecule, and are unapproachable to one another, whereas a value close to 1 indicates that the orbitals involved are approachable, hence, are delocalized.

5.5 Results and discussion

The property calculations (gas phase) of both unsubstituted and substituted model silicene systems are done and the level of theory is CAM-B3LYP/cc-pVDZ using the gas phase optimized geometries (as in Fig. 5.1 and Fig. 5.2 obtained at level of theory PBE/6-31G(d)). We also calculated polarizability of Si_2H_2, and C_2H_2 molecules at CAM-B3LYP/aug-cc-pVDZ, and CAM-B3LYP/cc-pVDZ. We found that diffused functions in basis set aug-cc-pVDZ yield higher values compared to that for cc-pVDZ, but was highly time consuming. We rather used cc-pVDZ in our calcuations to reduce computational time.

5.5.1 Unsubstituted

The OPA parameters for the first five excited states f_i, where, $i = 1, 2, \ldots, 5$, of the systems, S, S_0 and S_1, calculated at CAM-B3LYP/cc-pVDZ level of theory in the gas phase are shown in Table 5.2. This table contains excitation energy (ω_{of}), magnitude of transition dipole moment (μ^{of}), from ground to excited state, Λ-parameter—a measure of whether the interaction is of short range or long range in nature (see section 5.4.3), and the orbital transitions involved with the corresponding weight and percent contribution of orbital transition (last column). It is observed that oscillator strengths of all the systems are very low in each excited state. The Molecular orbital (MO) contour plots of the orbitals involved in the transition from the ground state to the first five excited states of the model system S_1 are shown in the Table 5.2. MO contour plots qualitatively describe the intra-molecular charge-transfer taking place in molecular systems. It is observed from these contour plots that in S_1 molecule unsubstituted with D/A groups, charge is uniformly distributed over the whole Si=Si backbone.

Table 5.2 OPA parameters of first five excited states f_i (i = 1, 2, …, 5) of the model systems, S, S_0 and S_1 (with representative MO picture of S_1) calculated at level of theory CAMB3LYP/cc-pVDZ in gas phase.

System	**Excited States (f_i)**	ω_{of} **(a.u.)**	μ^{of} **(a.u.)**	δ_{OPA} **(a.u.)**	**Λ**	**Orbital transitions (weight, contribution)**
S	1	1.512	0.005	$9.206\text{x}10^{-7}$	0.711	H-1→ L+1 (0.300, 0.216)
	2	1.646	0.815	$2.680\ \text{x}10^{-2}$	0.821	H-4→ L+1 (0.274, 0.227)
	3	2.119	0.001	$8.852\text{x}10^{-8}$	0.697	H→ L+2 (0.157, 0.103)
	4	2.169	3.534	0.476	0.720	H-1 → L-1 (0.147, 0.105)
	5	2.169	3.535	0.476	0.791	H→ L+1 (0.146, 0.121)
S_0	1	1.511	0.105	$4.0\ \text{x}10^{-4}$	0.743	H→L (0.248, 0.181) H-1→L+1(0.227,0.169)
	2	1.643	0.794	$2.4\ \text{x}10^{-2}$	0.785	H-1→L (0.221,0.175) H→L+1(0.212, 0.172)
	3	2.105	0.413	$8.0\ \text{x}10^{-3}$	0.644	H→L+3 (0.255,0.162)
	4	2.112	0.673	$1.6\ \text{x}10^{-2}$	0.694	H-1→L+3 (0.117,0.082) H→L+2 (0.154, 0.102)
	5	2.121	0.233	$2.0\ \text{x}10^{-3}$	0.664	H-1→L+2(0.235,0.145)
S_1	1	1.511	0.116	$4.0\ \text{x}10^{-4}$	0.747	H → L (0.235, 0.172)
	2	1.643	0.800	$2.6\ \text{x}10^{-2}$	0.779	H-1 → L (0.210, 0.165)
	3	2.105	0.448	$1.0\ \text{x}10^{-2}$	0.646	H → L+3 (0.255, 0.162)
	4	2.112	0.646	$1.5\ \text{x}10^{-2}$	0.694	H→ L+2 (0.156, 0.102)
	5	2.123	0.004	0.344	0.664	H-1→ L+2 (0.235, 0.146)

ω_{of} = Excitation energy,
μ^{of} = magnitude of transition dipole moment vector,
δ_{OPA}=oscillator strength

MO-contour plots of model system S_1

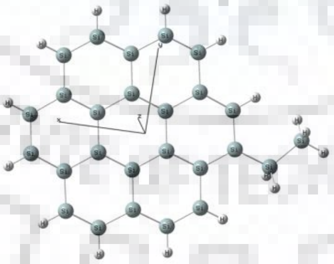

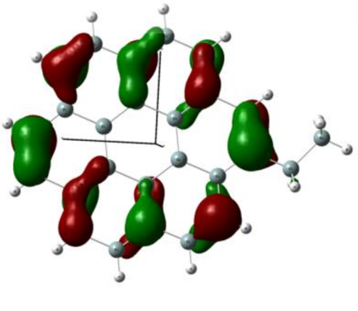

HOMO-1

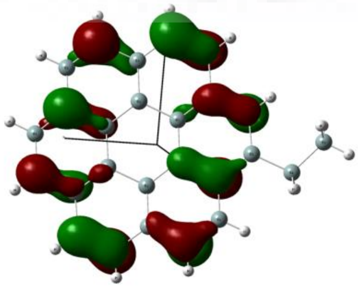

HOMO

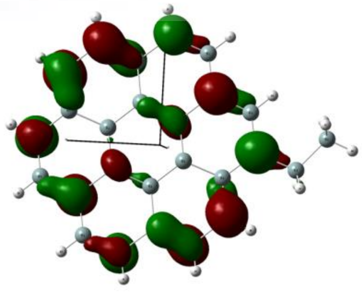

LUMO

The response theory results for TP transition probability (δ_{TPA}) and TP tensor components ($S_{\alpha,\beta}$) of the first five excited states of the systems S, S_0 and S_1 calculated at CAMB3LYP/cc-pVDZ level of theory in gas phase are shown in Table 5.3 and Table 5.4 respectively. From Table 5.3, it is observed that $Si_{24}H_{12}$ has very low TPA transition probability (δ_{TPA}) in all the five excited states (~ 10^{-4} – 10^{-5}) with extremely low TPA cross-section of the order of 10^{-7}, implying $Si_{24}H_{12}$ is TPA inactive. In case of derivative containing one H substituted with a SiH_2SiH_3 group, Si_{24} $(SiH_2SiH_3)H_{11}$, δ_{TPA} and σ_{TPA} values are slightly increased when silyl group is introduced with a slight extension of Si=Si bonding in the direction of the substituent. However, the transition probability still remains very low of the order of 10^1, and the molecule is TPA inactive.

Table 5.3 Parameters for TPA of first five excited states f_i (i = 1, 2, …, 5) of the systems S, S_0 and S_1 in gas phase calculated at the level of theory CAMB3LYP/cc-pVDZ: HOMO, LUMO energies (a.u.), (HL)gap (eV), Excitation energy (E), TPA cross-section (σ_{TPA}) and transition probability (δ_{TPA}).

System	Excited States (f_i)	HOMO (a.u.)	LUMO (a.u.)	(HL)gap (eV)	δ_{TPA}	E(eV)	σ_{TPA} (G.M.)
S	1				7.51×10^{-5}	1.51	1.26×10^{-7}
	2				5.40×10^{-5}	1.65	1.07×10^{-7}
	3				1.89×10^{1}	2.12	6.21×10^{-2}
	4				4.72×10^{-4}	2.17	1.63×10^{-6}
	5	-0.222	-0.098	3.364	1.19×10^{-4}	2.17	4.11×10^{-7}
S_0	1				1.44×10^{1}	1.51	2.41×10^{-2}
	2				1.23×10^{1}	1.64	2.44×10^{-2}
	3				3.57	2.11	1.16×10^{-2}
	4				5.76×10^{1}	2.11	1.88×10^{-1}
	5	-0.222	-0.099	3.338	5.76×10^{1}	2.12	1.90×10^{-1}
S_1	1				2.67×10^{1}	1.51	4.46×10^{-2}
	2				1.13×10^{1}	1.64	2.23×10^{-2}
	3				3.64	2.11	1.18×10^{-2}
	4				7.10×10^{1}	2.11	0.232
	5	-0.221	-0.098	3.335	7.35×10^{1}	2.12	0.243

The corresponding TP tensor components ($S_{\alpha,\beta}$) are shown in Table 5.4. It is observed that in all the excited states, the S_{ij} components have zero value except a few with almost insignificant non-zero value in unsubstituted silicene monolayer, S. The S_1 derivative has all the non-zero S_{ij} components with S_{xx} component being more significant but has very low magnitude, it seems that the charge is spread over the whole system (see MO-contour plots of model system, S_1 Table 5.2).

The remaining molecules in this study are taken by substituting donor and acceptor groups 180° apart on the silicene but with one SiH_2SiH_3 along the edge in S_1 because S has virtually zero TPA activity and S_0 has higher δ_{TPA} but S_1 shows a significant value of δ_{TPA} at least for the fifth excited state (see Table 5.3)

Table 5.4 TPA tensor components (S_{ij}) of the first five excited states f_i ($i = 1, 2, \ldots, 5$) of silicene systems, S, S_0 and S_1 the systems calculated at level of theory CAM-B3LYP/cc-pVDZ in gas phase.

Molecule	f_i	S_{xx}	S_{yy}	S_{zz}	S_{xy}	S_{xz}	S_{yz}
S	1	0.0	-0.0	0.0	-0.0	-0.0	-0.0
	2	-0.0	0.0	-0.0	-0.0	-0.0	0.0
	3	0.8	-1.8	-0.1	-5.9	4.8	3.3
	4	-0.0	-0.0	-0.0	0.0	0.0	0.0
	5	0.0	-0.0	0.0	0.0	0.0	0.0
S_0	1	-3.4	-2.2	0.1	-5.7	0.3	-2.3
	2	7.4	-2.8	-0.9	3.2	0.9	-0.5
	3	-2.3	2.8	0.3	0.4	0.0	2.6
	4	13.8	-1.8	0.4	5.5	-6.5	2.9
	5	-13.6	1.8	0.1	-7.1	-0.4	-6.1
S_1	1	-6.5	-3.0	0.1	6.8	-0.1	-2.3
	2	-7.5	2.8	0.9	2.1	1.1	0.6
	3	1.8	-2.9	-0.2	1.1	0.3	-2.5
	4	15.8	-1.8	0.5	-5.7	6.5	3.4
	5	-17.6	3.0	0.2	5.4	0.8	-5.9

5.5.2 Substituted

5.5.2.1 Bandgap tuning

A schematic pictorial representation of the energy gaps obtained from TPA calculations (Table 5.3 and Table 5.6) of different derivatives of silicene is summarized in Fig 5.3. Calculated E_{gap} values clearly show that the energy gaps lie in UV-Visible region of electromagnetic spectrum. Introduction of lateral donor-acceptor pair in the silicene monolayer greatly influences the HOMO-LUMO energy levels, resulting in tuning of bandgaps [193]. The bandgap of unsubstituted $Si_{24}H_{12}$ monolayer is 3.364 eV, is slightly reduced by replacing one H with SiH_3 group (S_0) and further reduced when H is replaced with SiH_2SiH_3 group (S_1).

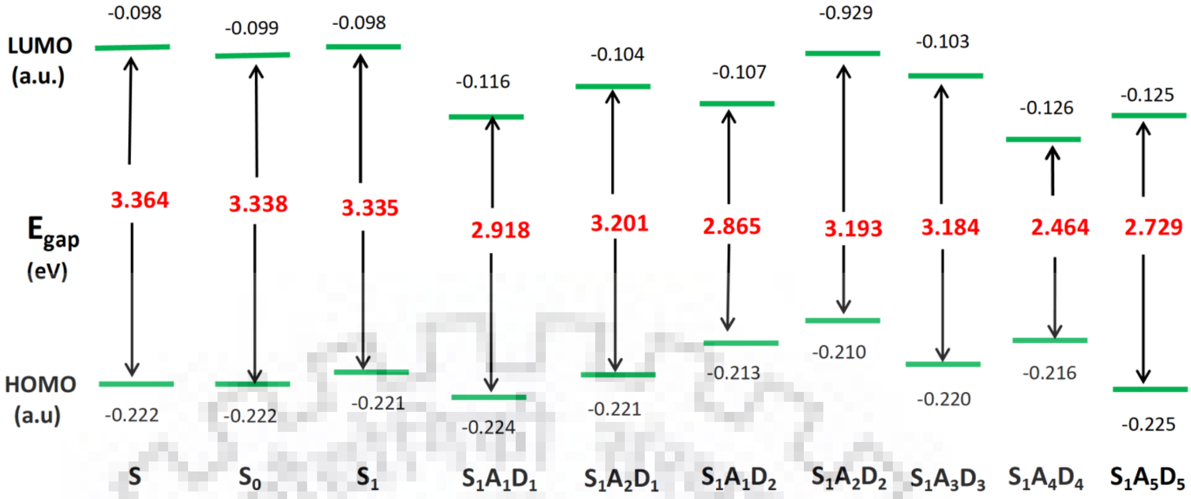
LUMO (a.u.)
Egap (eV)
HOMO (a.u)
-0.098
3.364
-0.222
S
-0.099
3.338
-0.222
S0
-0.098
3.335
-0.221
S1
-0.116
2.918
-0.224
S1A1D1
-0.104
3.201
-0.221
S1A2D1
-0.107
2.865
-0.213
S1A1D2
-0.929
3.193
-0.210
S1A2D2
-0.103
3.184
-0.220
S1A3D3
-0.126
2.464
-0.216
S1A4D4
-0.125
2.729
-0.225
S1A5D5

Fig 5.3 A schematic representation of the tuned HOMO, LUMO energy levels and HOMO-LUMO energy gaps of silicene derivatives (summarized from Table 5.3 and Table 5.6).

In case of $S_1A_1D_1$, A_1D_1 is a strong donor-acceptor pair, reduces the energy of both HOMO and LUMO level, and thus, the energy gap shrinks to 2.91 eV. In $S_1A_1D_2$ with acceptor A_1 and donor D_2 containing pyrrolidine rings is a stronger donor than D_1 which contains pyrrole rings, the gap is further reduced to 2.86 eV. Similarly, in case of $S_1A_2D_1$ and $S_1A_2D_2$, it is the combined effect of donor-acceptor pair which influences the energy gap by altering the HOMO and LUMO energies. $S_1A_3D_3$, $S_1A_4D_4$ and $S_1A_5D_5$ comprises of three different donor-acceptor pairs, A_3D_3, A_4D_4 and A_5D_5 respectively. For pair A_4D_4 and A_5D_5 the gaps are reduced to 2.46 eV and 2.72 eV, respectively. In model system $S_1A_5D_5$ intramolecular interaction in the vicinity of lateral acceptor group is observed which consequently causes distortion in the Si=Si framework as shown in Fig 5.2. The combined effect of donor acceptor pair and intramolecular interactions results in reduction of energy gap. In all, the energy gaps lie in the near UV and Visible region of the electromagnetic spectrum for all the derivatives, hence, tuning of bandgap opens up an opportunity for these model systems to behave as potential candidate in electronic applications [194]. With selective choice of donor-acceptor pair and proper assessment of donor and acceptor strengths model systems having desirable energy gaps can be designed. Moreover, functionalization of silicene unit with organic ligands could be interesting in the synthesis point of view as organo-functionalization provides easy dispersion of the material in organic solvents [195].

5.5.2.2 OPA/TPA properties

The OPA parameters of the model systems, $S_1A_1D_1$, $S_1A_2D_1$, $S_1A_1D_2$, $S_1A_2D_2$, $S_1A_3D_3$, $S_1A_4D_4$ and $S_1A_5D_5$ (see Fig 5.2) are calculated at CAMB3LYP/cc-pVDZ level of theory in the gas phase for the first five excited states f_i, where, $i = 1, 2, \ldots, 5$, as shown in Table 5.5 (a-g), such that the calculated values in Table 5.5 (a) correspond to the model system $S_1A_1D_1$, while Table 5.5 (b) correspond to $S_1A_2D_1$, and so on. The OPA parameters include, excited state (f_i),

Table 5.5(a): OPA parameters of first five excited states f_i ($i = 1, 2, \ldots, 5$) of the model silicene system $S_1A_1D_1$ in gas phase calculated at level of theory CAMB3LYP/cc-pVDZ, and MO contour plots of $S_1A_1D_1$.

Excited States (f_i)	**ω_{of} (a.u.)**	**μ^{of} (a.u.)**	**δ_{OPA} (a.u.)**	**Λ**	**Orbital transitions (weight, contribution)**
1	1.426	0.659	1.4 x10^{-2}	0.621	H-1→L (0.293, 0.161) H→L+1 (0.209, 0.149)
2	1.461	0.191	0.191	0.669	H→L (0.362, 0.230)
3	1.798	1.898	0.147	0.677	H→L+2 (0.106, 0.079)
4	1.867	2.102	0.148	0.689	H-1→L+1 (0.134, 0.111)
5	2.022	0.847	3.0 x10^{-2}	0.540	H-2→L (0.215, 0.088)

MO-contour plots of $S_1A_1D_1$

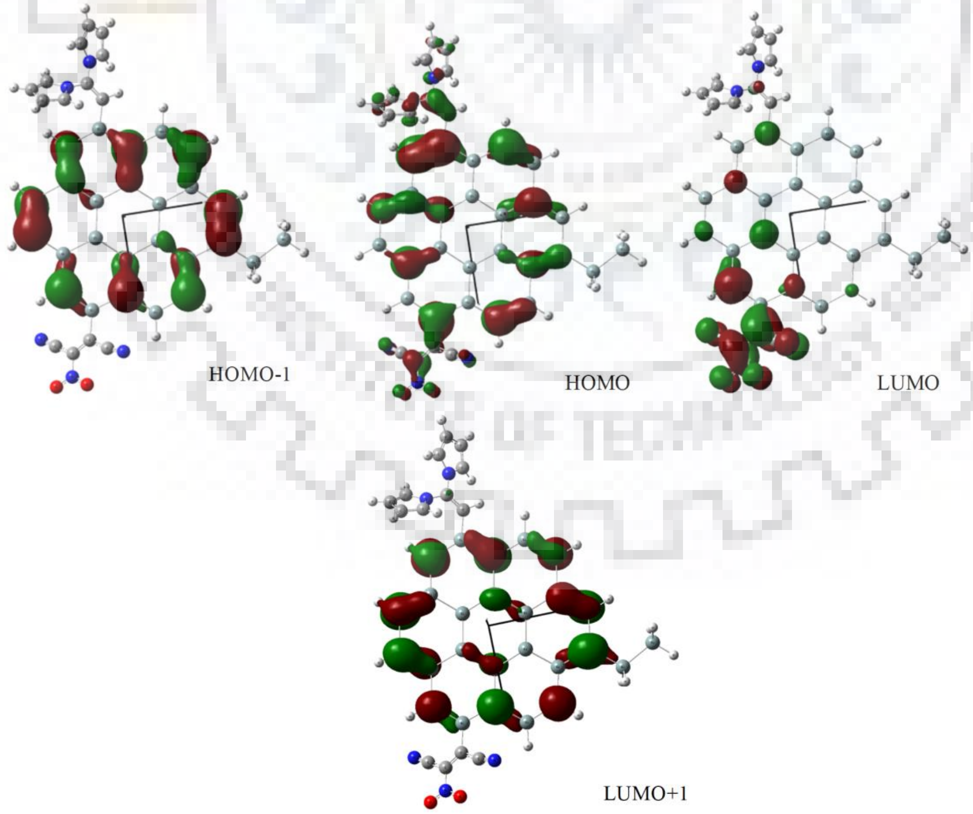

excitation energy (ω_{of}), magnitude of transition dipole moment (μ^{of}), oscillator strength (δ_{OPA}), Λ parameter—a measure for the nature of charge transfer, orbital transitions with corresponding weight and contribution of the orbital pair. MO contour plots of the relevant orbitals involved in the electronic transitions from ground state to first five excited states for all the model systems have been incorporated in Table 5.5(a-g)].

Table 5.5(a) shows that, in case of $S_1A_1D_1$, H→L transition in the second excited state makes the maximum contribution of 23% towards the charge transfer from donor to acceptor group. Quantitatively, the charge transfer is in moderate range as indicated by Λ value of 0.669. The A_1D_1 makes a strong donor-acceptor pair and the directive force due to the push-

Table 5.5(b) Parameters for OPA of first five excited states f_i ($i = 1, 2, \ldots, 5$) of the model silicene system $S_1A_2D_1$ in gas phase calculated at level of theory CAMB3LYP/cc-pVDZ, and MO-contour plots of $S_1A_2D_1$.

Excited States (f_i)	**ω_{of} (a.u.)**	**μ^{of} (a.u.)**	**δ_{OPA} (a.u.)**	**Λ**	**Orbital transitions (weight, contribution)**
1	1.474	0.094	2.6 x10^{-4}	0.702	(H-L) →L (0.308,0.217) H→ (L+1) (0.286,0.202)
2	1.583	1.231	3.7 x10^{-2}	0.796	H→L (0.335,0.267) H→ (L+1) (0.205,0.171)
3	2.024	2.295	0.209	0.660	H→L+3 (0.169, 0.100)
4	2.043	1.934	0.187	0.668	(H-1)→(L+3)(0.139,0.085)
5	2.070	2.821	0.376	0.681	H → (L+1) (0.059, 0.041)

MO-contour plots of $S_1A_2D_1$

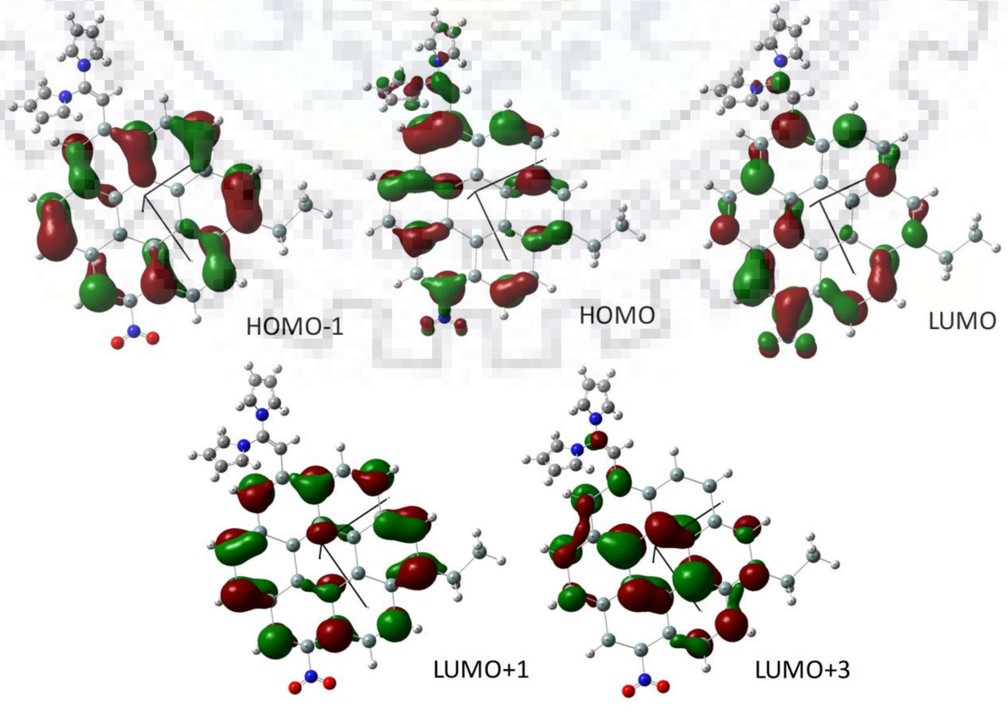

pull effect of the pair is strong such that the whole charge-density is seen to be pulled towards the acceptor moiety through Si=Si bonds present in silicene monolayer.

Table 5.5(b) shows that, in $S_1A_2D_1$ the OP transitions are significant in the higher excited state $f_1 \rightarrow f_3$, $f_1 \rightarrow f_4$ and $f_1 \rightarrow f_5$ contributing 10%, 8% and 4%, although oscillator strength is low with higher μ^{of} values. The H→L transiton is short range in nature as indicated by Λ value of 0.8 and electron density is delocalized over the backbone as well as on the acceptor group. The μ^{of} for H→L+3 transition in excited state $f_1 \rightarrow f_3$ is quite large with 10% contribution. The

Table 5.5(c) Parameters for OPA of first five excited states f_i (i = 1, 2, …, 5) of the model silicene system $S_1A_1D_2$ in gas phase calculated at level of theory CAMB3LYP/cc-pVDZ, and MO-contour plots of $S_1A_1D_2$.

Excited States (f_i)	$\boldsymbol{\omega_{of}}$ **(a.u.)**	$\boldsymbol{\mu^{of}}$ **(a.u.)**	$\boldsymbol{\delta_{OPA}}$ **(a.u.)**	**Λ**	**Orbital transitions (weight, contribution)**
1	1.434	2.673	0.234	0.636	H→L (0.355, 0.213)
2	1.462	1.137	4.4 x10^{-2}	0.635	H→(L+1) (0.261, 0.189)
3	1.767	1.462	8.2 x10^{-2}	0.700	H→(L+2) (0.215, 0.157)
4	1.837	2.424	0.195	0.635	(H-1) →L (0.160, 0.082)
5	1.998	2.059	0.148	0.669	(H-1)→(L+1)(0.083, 0.068)

MO-contour plots of $S_1A_1D_2$

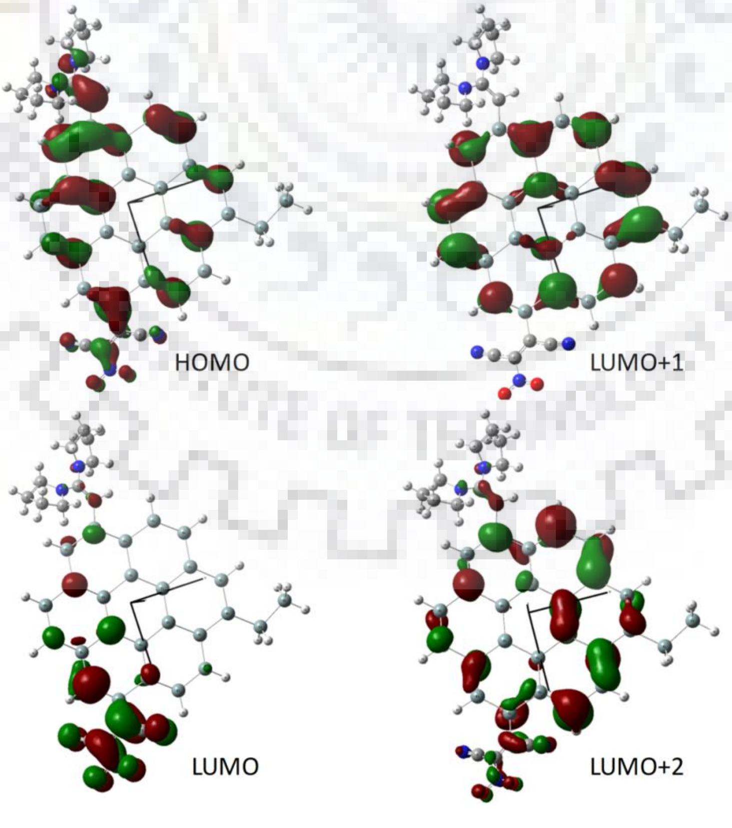

directive force due to donor-acceptor pair is not strong enough to push the electron density towards the acceptor moiety, as a result charge is delocalized within the backbone and the acceptor site is still electron deficient.

MO contour plots in Table 5.5(c) show that the charge is uniformly distributed over the whole assembly at the HOMO level in $S_1A_1D_2$. The charge transfer is most significant in the

Table 5.5(d) Parameters for OPA of first five excited states f_i ($i = 1, 2, \ldots, 5$) of the model silicene system $S_1A_2D_2$ in gas phase calculated at level of theory CAMB3LYP/cc-pVDZ, and MO-contour plots of $S_1A_2D_2$.

Excited States (f_i)	ω_{of} (a.u.)	μ^{of} (a.u.)	δ_{OPA} (a.u.)	Λ	Orbital transitions (weight, contribution)
1	1.484	0.483	8.0 x10^{-3}	0.743	H→L (0.153, 0.117) H→(L+1) (0.194, 0.142)
2	1.583	1.348	5.5 x10^{-2}	0.745	H→L (0.202, 0.155) H→(L+1) (0.145, 0.107)
3	1.972	0.284	3.0 x10^{-3}	0.636	H→(L+2) (0.325, 0.198)
4	1.997	3.027	0.386	0.704	(H-1) →L (0.127, 0.095) H→(L+3) (0.103, 0.073)
5	2.03	2.892	0.294	0.722	(H-1)→(L+1)(0.196, 0.150) H→L (0.071, 0.055)

MO-contour plots of $S_1A_2D_2$

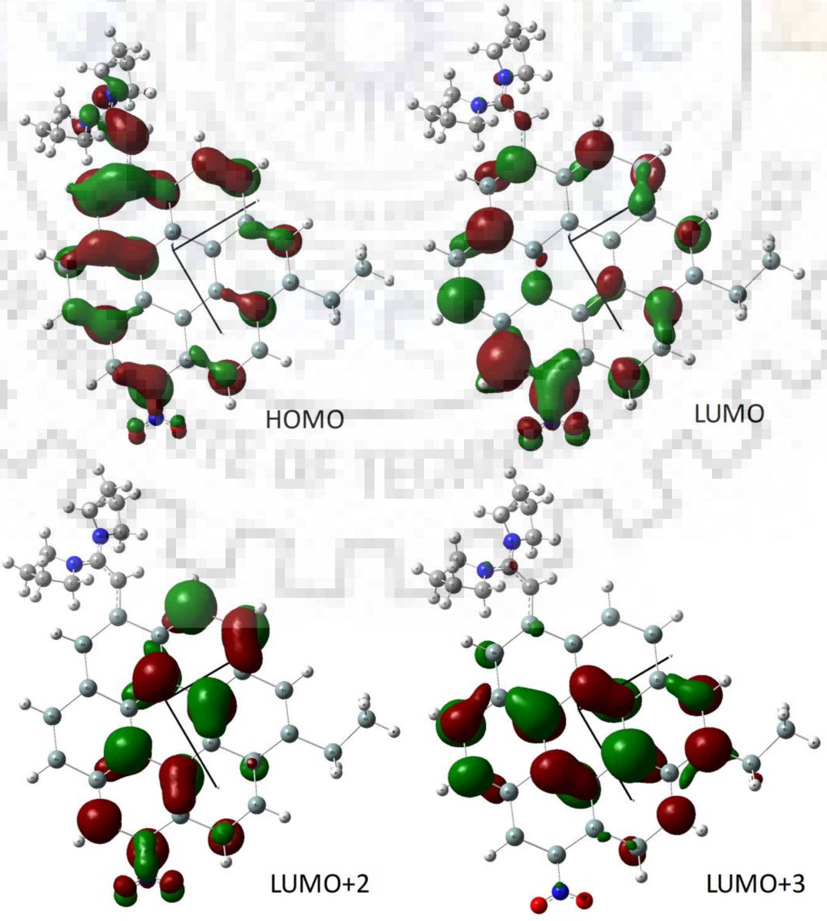

first three excited states among which H→L transition makes maximum contribution of 21% with a Λ value of 0.66 indicating a moderate charge transfer, as seen in the calculated values of Table 5.5(c). A maximum pulling of charge from the acceptor moiety through the Si=Si channel is seen in this case. The electron density is found to be localized over acceptor moiety in MO-picture of LUMO level in the first excited state. The H→L+1 and H→L+2 transition in the f_2 and f_3 excited state also make significant contribution of 19% and 16%, respectively. However, the

Table 5.5(e) Parameters for OPA of first five excited states f_i (i = 1, 2, …, 5) of the model silicene system $S_1A_3D_3$ in gas phase calculated at level of theory CAMB3LYP/cc-pVDZ, and MO-contour plots of $S_1A_3D_3$.

Excited States (f_i)	ω_{of} (a.u.)	μ^{of} (a.u.)	δ_{OPA} (a.u.)	Λ	Orbital transitions (weight, contribution)
1	1.487	7.223	1.6 x10^{-2}	0.738	H→L (0.232, 0.179) H→(L+1) (0.129, 0.095)
2	1.610	1.372	5.2 x10^{-2}	0.737	H→L (0.131, 0.100) H→(L+1) (0.208, 0.153) (H-1) →L (0.122, 0.092)
3	1.923	5.478	0.202	0.667	H→(L+2) (0.279, 0.180)
4	1.982	2.988	0.223	0.686	(H-1) →L (0.108, 0.082)
5	2.073	2.685	0.353	0.705	(H-1)→(L+1)(0.197,0.143)

MO-contour plots of $S_1A_3D_3$

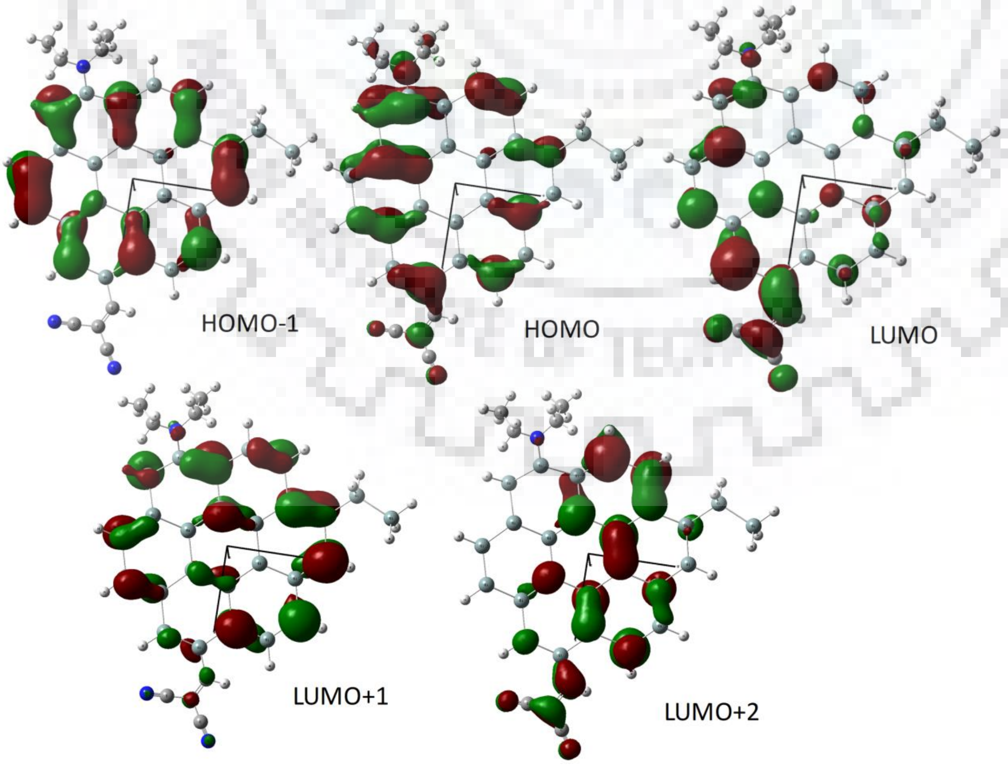

charge is localized more in the interior of the Si=Si framework in L+1 level in the f_2 excited state, while in case of L+2 level of f_3 excited state charge is partially spread over the acceptor moiety. A_1D_2 is a strong donor-acceptor pair. The strong donating tendency of pyrrolidine ring in donor group and electron deficiency in acceptor group results in strong push-pull effect through the ring.

MO contour plots in Table 5.5(d) show that, $S_1A_2D_2$ at the HOMO level the charge is delocalized over the whole system with more electron density in the vicinity of donor moiety.

Table 5.5 (f) Parameters for OPA of first five excited states f_i (i = 1, 2, …, 5) of the model silicene system $S_1A_4D_4$ in gas phase calculated at level of theory CAMB3LYP/cc-pVDZ, and MO-contour plots of $S_1A_4D_4$.

Excited States (f_i)	ω_{of} (a.u.)	μ^{of} (a.u.)	δ_{OPA} (a.u.)	Λ	Orbital transitions (weight, contribution)
1	1.064	2.386	0.142	0.721	H→L (0.314, 0.232)
2	1.318	0.795	1.4×10^{-2}	0.663	H→(L+1) (0.294, 0.217) (H-1) →L (0.182, 0.098)
3	1.659	2.601	0.184	0.654	H→(L+1) (0.100, 0.074)
4	1.693	1.075	3.5×10^{-2}	0.665	H→(L+2) (0.130, 0.086)
5	1.779	0.587	1.1×10^{-2}	0.660	(H-2) →L (0.190, 0.127)

MO-contour plots of $S_1A_4D_4$

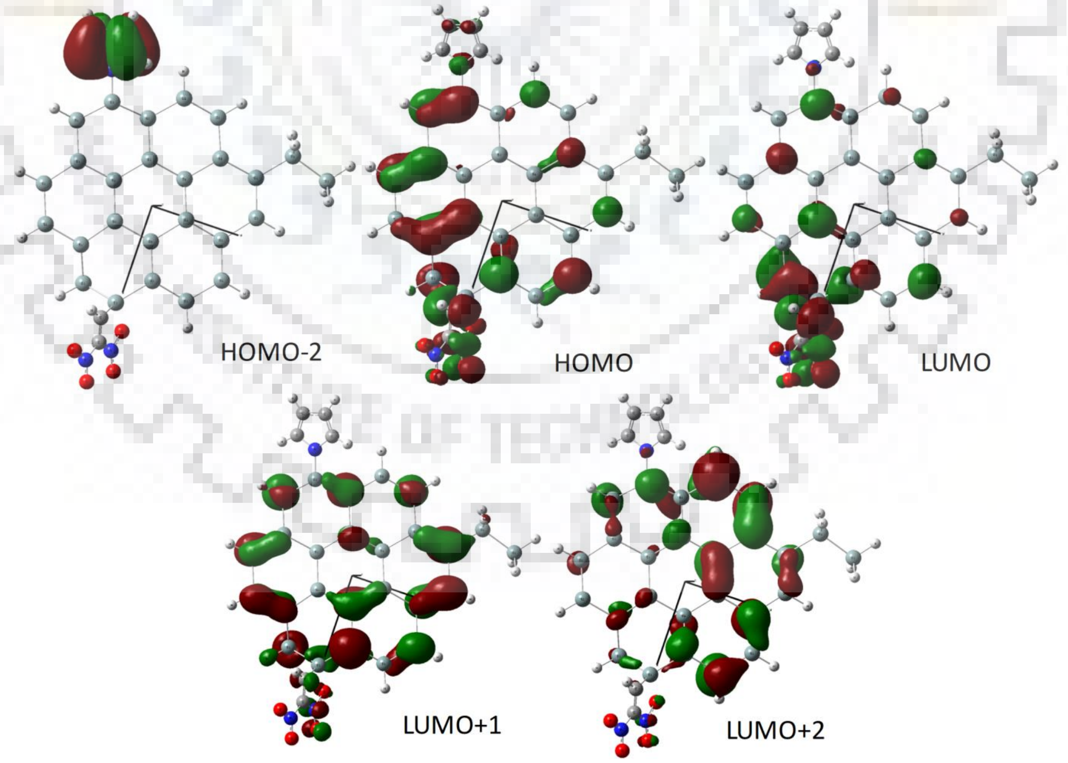

D_2 is a strong donor group. The maximum contribution of 20% is observed for H→L+2 transition in the f_3 excited state with Λ value of 0.636. The charge transfer is taking place through the interior Si=Si bonds while H→L transition in the f_1 excited state makes 12% contribution and the peripheral Si=Si bonds are involved in the charge transfer.

MO contour plots in Table 5.5(e) show that, the orbitals that are significantly involved in the charge-transfer are H, L, H-1, L+1, L+2, in case of $S_1A_3D_3$. In HOMO orbital, the charge is fully delocalized over the molecule while in H−1 it is uniformly concentrated on silicone framework. MO picture of transition from H→L demonstrates localization of charge on the acceptor group, although the charge transfer is short-range in nature and the Si=Si bonds at the periphery are involved. In L+1 level charge is delocalized over the interior of Si=Si framework.

Table 5.5(f) shows that, in case of $S_1A_4D_4$ almost complete charge transfer is seen as demonstrated from the molecular orbital picture of transition from H−2→L. HOMO orbital

Table 5.5 (g) Parameters for OPA of first five excited states f_i ($i = 1, 2, \ldots, 5$) of the model silicene system $S_1A_5D_5$ in gas phase calculated at level of theory CAMB3LYP/cc-pVDZ, and MO-contour plots of $S_1A_5D_5$.

Excited States (f_i)	ω_{of} (a.u.)	μ^{of} (a.u.)	δ_{OPA} (a.u.)	Λ	Orbital transitions (weight, contribution)
1	1.055	1.303	4.4 x10^{-2}	0.674	H→L (0.389, 0.269)
2	1.451	1.394	6.9 x10^{-2}	0.674	(H-1) →L (0.256, 0.178) (H-2) →L (0.103, 0.069)
3	1.556	0.927	2.9 x10^{-2}	0.627	H→(L+1) (0.161, 0.090) H→(L+2) (0.088, 0.053)
4	1.726	1.016	3.3 x10^{-2}	0.617	H→(L+1) (0.189, 0.105)
5	1.843	1.337	6.0 x10^{-2}	0.617	(H-3) →L (0.208, 0.140)

MO-contour plots of $S_1A_5D_5$

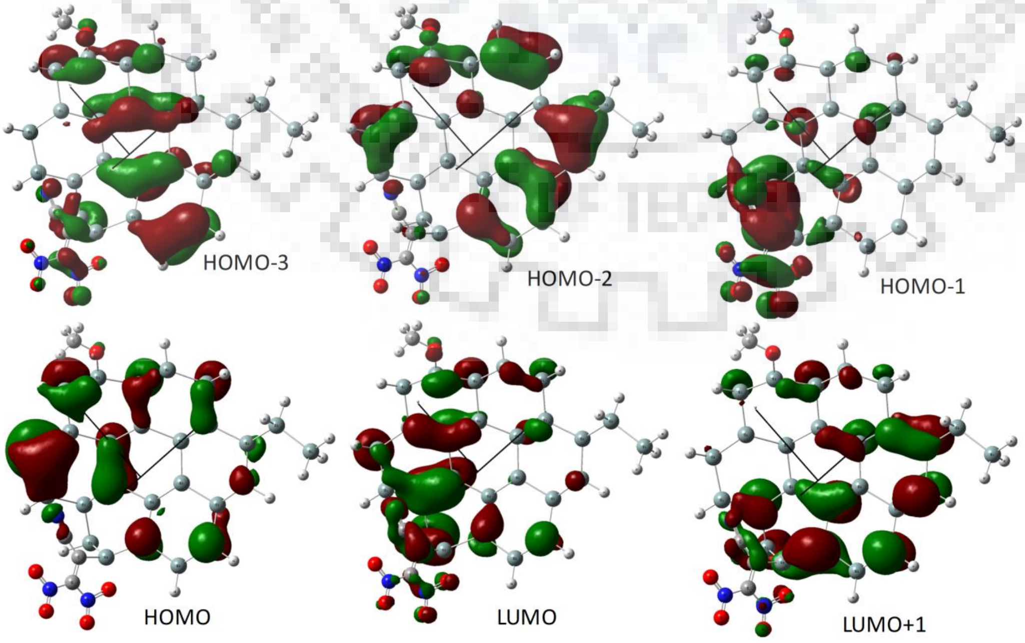

shows delocalization of charge over the whole system while at the LUMO level the charge is localized mostly over the vicinity of acceptor group.

Table 5.5(g) shows that, in the system $S_1A_5D_5$, structural distortion is seen in the vicinity of lateral acceptor group due to intramolecular interaction. The charge density is delocalized over the Si=Si backbone with more weight at the periphery. The charge-transfer is of short-range in nature.

In our results it can be seen that the Λ value lies within the range of 0.6-0.7, which indicates short-range character of the transition and further implies that in most of the cases the orbitals that are involved in the transition are partially localized over specific part the molecule. For the complete charge-transfer from donor to the acceptor moiety, Λ values should indicate values <0.5. The charge-transfer is taking place through Si=Si bonds in silicene monolayer. Unlike, carbon-based system like graphene in which all the carbon atoms are in one plane, Si atoms in silicene are located in different planes. Furthermore, the buckling due to pseudo Jahn-Tellar distortion imposes non-planarity in silicene, which hinders the free motion of electron density through the Si=Si channel. It is revealed in the MO-pictures that the charge is partially promoted to the acceptor group and partially localized over other areas of the Si=Si framework, which may provide additional sites from where the charge can be extracted by another acceptor group. In all, it can be suggested that such silicene based systems can be helpful in charge transport. The constitutive-affinity of Si makes it more compatible with the present Si-based technology.

The TPA parameters of the first five excited states of molecules chosen for study of TPA activity calculated in the gas phase at CAM-B3LYP/cc-pVDZ level of theory are shown in Table 5.6. The table comprises of excited state (f_i), HOMO energy (a.u.), LUMO energy (a.u.), HOMO-LUMO energy gap, $(HL)_{gap}$ (eV), two-photon transition probability (δ_{TPA}), Excitation energy, E (eV) and TPA cross-section (σ_{TPA}) (G.M.). In the molecule, $S_1A_1D_1$, the TPA transition probability is enhanced unexpectedly, on substituting S_1 skeleton with strong donor-acceptor pair. The values of δ_{TPA} are of the order of $10^3 - 10^5$, and σ_{TPA} values are of the order of 10^1. The maximum transition probability is seen in the first excited state. All the five excited states show fairly good TPA transition probability, hence the molecule is TPA active.

In the molecule $S_1A_2D_1$, first excited state f_1 and f_4 show less TPA transition probability, however, excited states f_2, f_3 and f_4 show transition probability of the order of 10^3 which is significant enough to term the molecule TPA active. If we compare $S_1A_1D_1$ and $S_1A_2D_1$, it can be stated that the nature of the acceptor group influences the TPA activity. The accepting tendency of NO_2 (A_2) is less than that of the A_1, therefore the A_1D_1 makes a strong donor-acceptor pair compared to the A_2D_1 and works better for the enhancement of TPA activity.

In $S_1A_1D_2$, excited state f_1 has maximum δ_{TPA} value of 6.51x10^4 and σ_{TPA} is 98.1. The other excited states also show TPA transition probability of the order of 10^4 except excited state

Table 5.6 TPA parameters of first five excited states f_i (i = 1, 2, …, 5) of all the systems S_1 substituted with D/A pair in gas phase calculated at level of theory CAMB3LYP/cc-pVDZ: HOMO, LUMO energies (a.u.), (HL)gap (eV), Excitation energy (E), TPA cross-section (σ_{TPA}) and transition probability (δ_{TPA}).

System	Excited States (f_i)	HOMO (a.u.)	LUMO (a.u)	$(HL)_{gap}$ (eV)	δ_{TPA}	E(eV)	σ_{TPA} (G.M.)
$S_1A_1D_1$	1				1.91x10^5	1.43	2.84
	2				5.41x10^4	1.46	84.6
	3				3.36x10^4	1.8	79.6
	4				3.01x10^4	1.87	76.9
	5	-0.224	-0.116	2.918	3.60x10^3	2.02	10.8
$S_1A_2D_1$	1				5.48x10^2	1.47	0.873
	2				1.70x10^3	1.58	3.12
	3				1.92x10^3	2.02	5.77
	4				9.72x10^1	2.04	0.297
	5	-0.221	-0.104	3.201	1.27x10^3	2.07	3.98
$S_1A_1D_2$	1				6.51x10^4	1.43	98.1
	2				2.42x10^4	1.46	38.0
	3				3.43x10^4	1.77	78.6
	4				1.48x10^4	1.84	36.7
	5	0.213	-0.107	2.865	1.56x10^3	2.00	4.56
$S_1A_2D_2$	1				5.38x10^2	1.48	0.86
	2				5.58x10^3	1.58	10.3
	3				2.13x10^3	1.97	6.06
	4				3.75x10^3	2.00	11.00
	5	-0.210	-0.929	3.193	2.67x10^3	2.04	8.12
$S_1A_3D_3$	1				1.36x10^3	1.49	2.21
	2				6.76x10^3	1.61	12.80
	3				1.07x10^4	1.92	29.00
	4				6.50x10^2	1.98	1.87
	5	-0.220	-0.103	3.184	2.52x10^3	2.07	7.93
$S_1A_4D_4$	1				9.73x10^3	1.06	8.08
	2				1.54x10^4	1.32	19.7
	3				1.29x10^4	1.66	26.0
	4				2.61x10^4	1.69	54.8
	5	-0.216	-0.126	2.464	2.56x10^4	1.78	59.4
$S_1A_5D_5$	1				9.50x10^2	1.06	0.77
	2				4.69x10^3	1.45	7.24
	3				1.59x10^3	1.56	2.81
	4				1.25x10^4	1.73	27.3
	5	-0.225	-0.125	2.729	6.45x10^4	1.84	161.00

Table 5.7 TPA tensor components (S_{ij}) of the first five excited states f_i (i = 1, 2, …, 5) of system, S_1 substituted with D/A pair calculated at level of theory CAM-B3LYP/cc-pVDZ in gas phase.

Molecule	f_i	S_{xx}	S_{yy}	S_{zz}	S_{xy}	S_{xz}	S_{yz}
$S_1A_1D_1$	1	0.8	79.7	-83.8	3.2	-6.8	-20.0
	2	-4.3	74.6	438.5	0.9	8.1	197.5
	3	-1.4	26.3	367.7	-12.6	6.6	139.1
	4	-0.1	-148.0	-240.5	-2.0	18.7	-186.6
	5	0.1	-90.4	120.3	16.3	-9.7	-40.1
$S_1A_2D_1$	1	0.3	22.7	33.7	-0.5	1.5	-20.6
	2	2.8	12.5	-79.3	0.2	-0.2	-46.1
	3	0.7	-4.5	-68.5	2.0	8.9	-58.7
	4	0.2	14.8	-12.3	9.7	-6.9	-5.8
	5	0.4	-8.6	80.2	-12.2	-5.8	4.0
$S_1A_1D_2$	1	-4.2	-22.9	544.9	7.8	34.5	164.6
	2	3.3	-90.2	-284.3	-7.3	-14.4	-108.3
	3	2.0	12.8	365.7	-8.0	15.4	159.0
	4	0.9	-78.0	-199.1	-13.5	4.8	-116.2
	5	1.4	61.9	11.1	-13.6	-0.5	47.9
$S_1A_2D_2$	1	0.1	-33.2	-22.7	3.8	-2.7	20.2
	2	-6.3	-37.4	168.6	2.1	5.6	45.4
	3	0.9	14.2	-62.9	2.9	0.7	-72.9
	4	-3.0	-29.4	140.8	5.4	-10.4	25.6
	5	1.9	6.2	109.1	-23.9	-4.9	1.8
$S_1A_3D_3$	1	53.3	37.2	-0.9	-31.5	2.3	-0.6
	2	175.0	-7.8	-6.5	57.7	13.7	0.8
	3	-238.0	38.9	0.7	-34.6	-6.3	-3.1
	4	-45.4	-17.6	0.5	7.9	-4.5	13.9
	5	102.8	13.3	2.1	8.0	-12.8	18.5
$S_1A_4D_4$	1	224.6	-40.0	1.1	42.7	5.1	-3.5
	2	-196.8	-91.6	6.7	117.4	18.4	16.7
	3	-241.2	-27.6	1.6	1.9	31.2	-3.9
	4	-347.4	13.8	5.3	96.5	32.2	0.5
	5	316.0	91.6	-5.6	-32.1	-20.2	-3.3
$S_1A_5D_5$	1	5.0	-60.5	2.8	-31.7	-3.5	-2.2
	2	97.2	22.4	28.3	70.6	-39.6	-13.0
	3	55.3	-31.3	4.5	-46.2	0.1	-39.7
	4	-154.8	79.3	-7.2	-169.1	22.0	-29.9
	5	-36.0	548.5	-0.4	-156.9	-22.9	-0.5

f_5. All the states are TPA active. The δ_{TPA} of $S_1A_1D_1$ is 10 times higher than $S_1A_1D_2$ in the excited state f_1, probably due to the different nature of donor groups D_1 and D_2, which may influence the TPA activity.

The δ_{OPA} value of $S_1A_2D_2$ is low of the order of 10^2 in first excited state and 10^3 in all other excited states, unlike other derivatives. It appears that the acceptor group NO_2 has less electron pulling tendency and the overall push-pull effect of the donor-acceptor pair is weaker. The derivatives $S_1A_3D_3$, $S_1A_4D_4$ and $S_1A_5D_5$ have fairly good TPA transition probability of the order of 10^3–10^4 in most of the excited states. $S_1A_5D_5$ has quite high value of TPA cross-section σ_{TPA}=161.

All these combinations of donor-acceptor pairs are found to be able to enhance the TPA activity of S_1 unit which is otherwise TPA inactive. Most importantly, the higher excited states which contribute to the TPA activity of silicene derivatives can be identified from our study. We also show that an appropriate choice of donor-acceptor pair plays a vital role in enhancing the TPA activity in silicene derivatives studied.

Further insights into the TPA activity of the molecule can be drawn from the analysis of TP tensor elements S_{ij} of the first five excited states of all the systems S_1 substituted with D/A pair in gas phase calculated at CAM-B3LYP/cc-pVDZ level of theory as shown in Table 5.7**.** The derivatives in which S_1 unit is appended with donor-acceptor pair (180° apart), anisotropy in the charge distribution is observed in all the excited states. In derivatives $S_1A_1D_1$, $S_1A_2D_1$, $S_1A_1D_2$ and $S_1A_2D_2$, the contribution of the S_{zz} component is seen to be prominent. The higher excited states, f_2, f_3, f_4 in $S_1A_1D_1$, show signs of TPA activity and significant involvement of S_{yz} component. Similar results are obtained for derivatives, $S_1A_2D_1$, $S_1A_1D_2$ and $S_1A_2D_2$. In case of derivatives, $S_1A_3D_3$, $S_1A_4D_4$ and $S_1A_5D_5$, the S_{xx} component makes the most significant contribution. However, S_{xy} component also contributes in higher states.

5.6 Conclusion

To summarize, it can be inferred from the MO-picture analysis, that the push-pull effect is not strong enough to export the charge from donor to the acceptor group completely through Si=Si channel connected between DA-pair. It is due to the fact that Si=Si channel is less effective in charge-transportation. The Si-atoms, while not strictly planar are of a nearly planar arrangement and partial aromatic character persists and supports charge-transfer through Si=Si channel to good extent and the presence of lateral donor-acceptor pairs further directs the flow of charge-transfer fairly well.

The silicene systems having non-planar buckled structure show signatures of two-photon activity; is an important finding of the present study. Such push-pull derivatives of silicene can be employed in the manufacture of architectures which can serve as potential non-linear optical materials. To the best of our knowledge studies of silicene frameworks showing non-linear behavior are very rare and the relevant research is still in its infancy. We have made an attempt to explore new possibilities of designing silicene based systems which can contribute to applications in non-linear optical device making. Also, the bandgap tuning through functionalization of silicene framework with different ligands can be very helpful in silicon-based technology.

Chapter 6

Concluding Remarks

The present thesis is mainly an attempt to calculate theoretically some properties related to spectra of SiNCs and to see how the one-photon and two-photon absorption probabilities of silicenes are affected by substitution by electron donor/acceptor groups. HOMO-LUMO gaps of some small systems are also investigated preliminarily, essentially to choose functionals and basis sets that give good fits with experimental estimates of the band gaps in small systems.

The calculation of mean static polarizabilities is performed on two classes of compounds. One, near spherical open clusters beginning with SiH_4, each derived from the previous by replacing each H by SiH_3 units. However we have only used three members of this sequence, as the next member of this sequence, $Si_{53}H_{108}$, would take too much time for optimization of geometry with the computational resources at hand. The other class is a set of sila-diamondoids, again terminated with sila- trimentane since subsequent members have isomers with attendant complications. The major innovation in this section is in calculation of mean static atomic polarizability per atom; since Si and H have widely different volumes, for $Si_n H_m$ we find $n_c = n+0.1866m$ (0.1866 being the cube of the ratio of the van Der Waals Radii) and obtain the mean static polarizabilliy per atom by dividing the computed mean static polarizability by n_c. This results in numbers that apparently tend to the estimate for bulk Si for both classes. Both sets correlate inversely with E_{gap} values.

The same classes of compounds are used for calculating complex dielectric constants and refractive indices using CASTEP. Among the set of sila-diamondoids, sila-diamantane gave irregular behaviour in these and in absorption spectra. We have ascribed it to the relatively more compact structure of sila-diamantane. To make it more explicit, sila-diamantane has a structure which has two cages fused along a face and has a centre of symmetry.

In studying the OPA and TPA of silicenes we have chosen a 24-Si fragment terminated along the edges by H or Silyl groups. Time constraints prevented use of larger fragments. That the presence of electron Donor/Acceptor groups made changes in OPA and TPA despite the buckled structures was satisfactory.

As far as future work goes, we are currently engaged in calculating and interpreting the hyperpolarizability tensor components of the systems studied in Ch. V. We are also looking at methods for calculating spectra with higher resolution.

INDIAN INSTITUTE OF TECHNOLOGY ROORKEE

References

[1] R. P. Feynman, *Plenty of Room at the Bottom*, American Physical Society, 1959.

[2] A. D. Yoffe, Low-dimensional systems: quantum size effects and electronic properties of semiconductor microcrystallites (zero-dimensional systems) and some quasi-two-dimensional systems, *Adv. Phys.*, 2006, **42**, 173.

[3] E. Chukwuocha, M. Onyeaju and T. Harry, Theoretical Studies on the Effect of Confinement on Quantum Dots Using the Brus Equation, *W. J. Conden. Matter Phy.*, 2012, **2**, 96.

[4] L. E. Brus, Electron-Electron and Electron-Hole Interactions in Small Semiconductor Crystallites: The Size Dependence of the Lowest Excited Electronic State, *J. Chem. Phys.*, 1984, **80**, 4403.

[5] M. A. Reed, R. T. Bate, K. Bradshaw, W. M. Duncan, W. R. Frensley, J. W. Lee and H. D. Shih, Spatial quantization in GaAs–AlGaAs multiple quantum dots, *J. Vac. Sci. Technol. B*, 1986, **4**, 358.

[6] E. V. Kolobkova, N. V. Nikonorov and V. A. Aseev, Optical Technologies Silver Nanoclusters Influence on Formation of Quantum Dots in Fluorine Phosphate Glasses, *Sci. Tech. J. Inf. Technol., Mech Opt.*, 2012, **5**, 1.

[7] A. Ekimov, A. Efros and A. Onushchenko, Quantum size effect in semiconductor microcrystals, *Solid State Commun.*, 1985, **56**, 921.

[8] R. Rossetti, S. Nakahara and L. E. Brus, Quantum size effects in the redox potentials, resonance Raman spectra, and electronic spectra of CdS crystallites in aqueous solution, *J. Chem. Phys.*, 1983, **79**, 1086.

[9] L. E. Brus, Electron–electron and electron-hole interactions in small semiconductor crystallites: The size dependence of the lowest excited electronic state, *J. Chem. Phys.*, 1984, **80**, 4403.

[10] A. Ekimov and A. Onushchenko, Quantum size effect in the optical-spectra of semiconductor micro-crystals, *Sov. Phys. Semicond.-USSR*, 1982, **16**, 775.

[11] C. Dong, X. Li and J. Qi, First-Principles Investigation on Electronic Properties of Quantum Dot-Sensitized Solar Cells Based on Anatase TiO_2 Nanotubes *J. Phys. Chem. C*, 2011, **115**, 20307.

[12] R. G. Parr and W. Yang, *Density Functional Theory of Atoms and Molecules*, Oxford University Press, Oxford, 1989.

[13] A. J. Karttunen, D. Usvyat, M. Schutz and L. Maschio, Dispersion interaction in silicon allotropes, *Phys. Chem. Chem. Phys*, 2017, **19**, 7699.

[14] D. Ghosh, A. Roy, R. Seidel, B. Winter, S. Bradforth and A. I. Krylov, First-Principle Protocol for Calculating Ionization Energies and Redox Potentials of Solvated Molecules and Ions: Theory and Application to Aqueous Phenol and Phenolate, *J. Phys. Chem. B*, 2012, **116**, 7269.

[15] S. V. Shedge, S. P. Joshi and S. Pal, Behaviour of density functional theory for electric response properties at distorted geometries of molecules, *Theor. Chem. Acc.*, 2012, **131**, 1094.

[16] S. K. Bhattacharya and A. Kshirsagar, Defect studies in small CdTe clusters, *Eur. Phys. J. D*, 2011, **61**, 609.

[17] S. K. Bhattacharya and A. Kshirsagar, Ab initio calculations of the structural and electronic properties of CdTe clusters, *Phys. Rev. B*, 2007, **75**, 035402.

[18] M. Das, Computational investigation on tunable optical band gap in armchair polyacenes, *J. Chem. Phys.*, 2015, **143**, 064704.

[19] D. Ghosh, Hybrid Equation-of-Motion Coupled-Cluster/Effective Fragment Potential Method: A Route toward Understanding Photoprocesses in the Condensed Phase, *J. Phys. Chem. A*, 2017, **121**, 741.

[20] D. Ghosh, Multiscale modelling: hybrid quantum mechanics/molecular mechanics as an example and some recent developments, *Curr. Sci.*, 2017, **112**, 1455.

[21] K. B. Sophy, P. Calaminici and S. Pal, Density Functional Static Dipole Polarizability and First-Hyperpolarizability Calculations of Na_n (n = 2, 4, 6, 8) Clusters Using an Approximate CPKS Method and its Comparison with MP2 Calculations, *J. Chem. Theory and Comput.*, 2007, **3**, 716.

[22] P. Banarjee, B. Pathak, R. Ahuja and G. P. Das, First Principles Design of Li Functionalized Hydrogenated h-BN Nanosheet for Hydrogen Storage, *Int. J. Hydrog. Energy*, 2016, **41**, 14437.

[23] P. Garg, S. Kumar, I. Choudhuri, A. Mahata and B. Pathak, Hexagonal Planar CdS Monolayer Sheet for Visible Light Photo-Catalysis, *J. Phys. Chem. C*, 2016, **120**, 7052.

[24] E. N. Koukaras, A. D. Zdetsis, P. Karamanis, C. Pouchan, A. Avramopoulos and A. G. Papadopoulos, Structural and Static Electric Response Properties of Highly Symmetric Lithiated Silicon Cages: Theoretical Predictions, *J. Comput. Chem*, 2012, **33**, 1068.

[25] A. J. Karttunen, U. Denis, S. Martin and M. Lorenzo, Dispersion interactions in silicon allotropes, *Phys. Chem. Chem. Phys*, 2017, **19**, 7699.

[26] B. Goller, S. Polisski, H. Wiggers and D. Kovalev, Freestanding spherical silicon nanocrystals: A model system for studying confined excitons, *Appl. Phys. Lett.* 2010, **97**, 041110.

[27] L. T. Canham, Silicon quantum wire array fabrication by electrochemical and chemical dissolution of wafers, *Appl. Phys. Lett.* 1990, **57**, 1046.

[28] S. Tripathy, R. K. Soni, S. K. Ghoshal and K. P. Jain, Optical properties of nano-silicon, *Bull. Mater. Sci.*, 2001, **24**, 285.

[29] M. Larsson, A. Elfving, P. O. Holtz, G. V. Hansson and W. X. Ni, Spatially direct and indirect transitions observed for Si/Ge quantum dots, *Appl. Phys. Lett.*, 2003, **82**, 4785.

[30] A. N. Poddubny, A. A. Prokofiev and I. N. Yassievich, Optical transitions and energy relaxation of hot carriers in Si nanocrystals, *App. Phys. Lett.*, 2010, **97**, 231116.

[31] A. Smith, Z. H. Yamani, N. Roberts, J. Turner, S. R. Habbal, S. Granick and M. H. Nayfeh, Observation of strong direct-like oscillator strength in the photoluminescence of Si nanoparticles, *Phys. Rev. B*, 2005, **72**, 205307.

[32] A. Puzder, A. J.Williamson, J. C. Grossman and G. Galli, Surface control of optical properties in silicon nanoclusters, *J. Chem. Phys.*, 2002, **117**, 6721.

[33] N. M. Abdul-ameer and M. C. Abdulrida, Direct Optical Energy Gap in Amorphous Silicon Quantum Dots, *J. Mod. Phys.*, 2011, **2**, 1530.

[34] V. Baturin, S. Lepeshkin, N. Matsko and Y. Uspenskii, Electronic Properties and Stability of Silicon Nanoclusters Passivated by Hydrogen, *Solid State Phenom.* 2015, **233-234**, 562.

[35] M. M. Anas, A. P. Othman and G. Gopir, Structural and Electronic Properties of Hydrogen Passivated Silicon Quantum Dots: Density Functional Calculations, *Adv. Mat. Res.*, 2015, **1107**, 571.

[36] B. Marsen, M. Lonfat, P. Scheier and K. Sattler, The energy gap of pristine silicon clusters, *J. Electron Spectros. Relat. Phenomena*, 2000, **109**, 157.

[37] S. K. Ghoshal, K. P. Jain and R. Elliott, Optical and Electron Correlation Effects in Silicon Quantum Dots, *J. Metastable Nanocryst. Mater.*, 2005, **23**, 129.

[38] M. Lannoo, C. Delerue and G. Allan, Theory of radiative and nonradiative transitions for semiconductor nanocrystals, *J. Lumin.*, 1996, **70**, 170.

[39] A. N. Poddubny, A. A. Prokofiev and I. N. Yassievich, Optical transitions and energy relaxation of hot carriers in Si nanocrystals, *App. Phys. Lett.*, 2010, **97**, 231116.

[40] M. Lannoo, C. Delerue and G. Allan, Nonradiative recombination on dangling bonds in silicon crystallites, *J. Lumin.*, 1993, **57**, 243.

[41] N. M. Abdul-ameer and M. C. Abdulrida, Direct Optical Energy Gap in Amorphous Silicon Quantum Dots, *J. Mod. Phys.*, 2011, **2**, 1530.

[42] F. Koch, V. Petrova-Koch and T. Muschik, The luminescence of porous Si: the case for the surface state mechanism, *J. Lumin.*, 1993, **57**, 271.

[43] G. Allan, C. Delerue and M. Lannoo, Nature of Luminescent Surface States of Semiconductor Nanocrystallites, *Phys. Rev. Lett.*, 1996, **76**, 2961.

[44] G. Allan, C. Delerue and Y. M. Niquet, Luminescent polarization of silicon nanocrystals, *Phys. Rev. B*, 2001, **63**, 205301.

[45] S. De, S. A. Ghasemi, A. Willand, L. Genovese, D. Kanhere and S. Goedecker, The effect of ionization on the global minima of small and medium sized silicon and magnesium clusters, *J. Chem. Phys*., 2011, **134**, 124302.

[46] N. L. Matsko, E. V. Tikhonov, V. S. Baturin, S. V. Lepeshkin and A. R. Oganov, The impact of electron correlations on the energetic and stability of silicon nanoclusters, *J. Chem. Phys.*, 2016, **145**, 074313.

[47] W. Kohn and L. J. Sham, Self-Consistent Equations Including Exchange and Correlation Effects, *Phys. Rev. A*, 1965, **140**, 1133.

[48] J. P. Perdew, J. A. Chevary, S. H. Vosko, K. A. Jackson, M. R. Pederson, D. J. Singh and C. Fiolhais. Atoms, molecules, solids, and surfaces: Applications of the generalized gradient approximation for exchange and correlation, *Phys. Rev. B*, 1996, **46**, 6671.

[49] C. Lee, C. Hill and N. Carolina, Development of the Colle-Salvetti correlation energy formula into a functional of the electron density, *Phys. Rev. B*, 1988, **37**, 785.

[50] J. C. Grossman, Benchmark quantum Monte Carlo calculations, *J. Chem. Phys.*, 2002, **117**, 1434.

[51] M. Sonia, Aguilera-Segura and J. M. Seminario, Ab initio analysis of silicon nanoclusters, *J. Phys. Chem. C*, 2014, **118**, 1397.

[52] O. Lehtonen and D. Sundholm, Density-functional studies of excited states of silicon nanoclusters, *Phys. Rev. B*, 2005, **72**, 085424.

[53] O. Lehtonen and D. Sundholm, Optical properties of sila-adamantane nanoclusters from density functional theory, *Phys. Rev. B,* 2006, **74**, 045433.

[54] S. Niaz and A. D. Zdetsis, Comprehensive Ab Initio Study of Electronic, Optical, and Cohesive Properties of Silicon Quantum Dots of Various Morphologies and Sizes up to Infinity, *J. Phys. Chem. C,* 2016, **120**, 11288.

[55] M. M. Anas, A. P. Othman and G. Gopir, First-principle study of quantum confinement effect on small sized silicon quantum dots using density-functional theory, *AIP Conference Proceedings*, 2014, **104**, 1614.

[56] V. S. Baturin, S. V. Lepeshkin, N. L. Matsko, A. R. Oganov and Y.A. Uspenskii, Prediction of the atomic structure and stability for the ensemble of silicon nanoclusters passivated by hydrogen, *Europhys. Lett.*, 2014, **106,** 37002.

[57] V. Petkov, C. M. Hessel, J. Ovtchinnikoff, A. Guillaussier, B. A. Korgel, X. Liu, and C. Giordano, Structure-Properties Correlation in Si Nanoparticles by Total Scattering and Computer Simulations, *Chem. Mater*. 2013, **25**, 2365.

[58] A. Kshirsagar and N. Kumbhojkar, Empirical pseudo-potential studies on electronic structure of semiconducting quantum dots, *Bull. Mater. Sc.*, 2008, **31**, 297.

[59] S. K. Ghoshal, M. R. Sahar and M. S. Rohani, Investigation of optical effects in silicon quantum dots by using empirical pseudopotential method, *J. Korean Phys. Soc.*, 2011, **58**, 256.

[60] L. Wang, and A. Zunger, Solving Schrödinger's equation around a desired energy: Application to silicon quantum dots, *J. Chem. Phys.*, 1994, **100**, 2394.

[61] A. D. Corso, Pseudopotentials periodic table: from H to Pu, *Comput. Mater. Sci.*, 2014**,** **95**, 337.

[62] S. R. K. C. Yamijala, M. Mukhopadhyay and S. K. Pati, Linear and Nonlinear Optical Properties of Graphene Quantum Dots: A Computational Study, *J. Phys. Chem. C,* 2015, **119**, 12079.

[63] W. L. Yang, J. D. Fabbri, T. M. Willey, J. R. I. Lee, J. E. Dahl, R. M. K. Carlson, P. R. Schreiner, A. A. Fokin, B. A. Tkachenko, N. A. Fokina, W. Meevasana, N. Mannella, K. Tanaka, X. J. Zhou, T. van Buuren, M. A. Kelly, Z. Hussain, N. A. Melosh and Z.-X. Shen: Monochromatic Electron Photoemission from Diamondoid Monolayers, *Science,* 2007, **316**, 1460.

[64] P. Rodgers, Diamondoids: Carbon emissions, *Nat. Nanotechnol.*, 2007, DOI: 10.1038/nnano.2007.212.

[65] N. D. Drummond, Diamondoids display their potential, *Nat. Nanotechnol.*, 2007, **2**, 462.

[66] W. L. Yang, J. D. Fabbri, T. M. Willey, J. R. I. Lee, J. E. Dahl, R. M. K. Carlson, P. R. Schreiner, A. A. Fokin, B. A. Tkachenko, N. A. Fokina, W. Meevasana, N. Mannella, K. Tanaka, X. J. Zhou, T. van Buuren, M. A. Kelly, Z. Hussain, N. A. Melosh and Z.-X. Shen, Monochromatic electron Photoemission from Diamondoids monolayes, *Science*, 2007, **316**, 1460.

[67] J. Fischer, J. Baumgartner and C. Marschner, Synthesis and structure of Sila-Adamantane, *Science*, 2005, **310**, 825.

[68] O. Lehtonen and D. Sundholm, Optical properties of sila-adamantane nanoclusters from density-functional theory, *Phys. Rev. B*, 2006, **74**, 045433.

[69] R. R. Zope, T. Baruah, S. L. Richardson, M. R. Pederson and B. I. Dunlap, Optical excitation energies, Stokes shift, and spin-splitting of $C_{24}H_{72}Si_{14}$, *J. Chem. Phys.*, 2010, **133**, 34301.

[70] S. Prusty, H. S. Mavi and A. K. Shukla, Optical nonlinearity in silicon nanoparticles: Effect of size and probing intensity, *Phys. Rev. B*, 2005, **71**, 113313.

[71] F. Marsusi, K. Mirabbaszadeh and G. A. Mansoori, Optoelectronic properties of adamantane and hydrogen terminated sila- and germa- adamantane: A comparative study, *Physica E*, 2009, **41**, 1151-1156.

[72] W. D. S. A. Miranda, S. S. Coutinho, M. S. Tavares, E. Moreira, and D. L. Azevedo, *Ab initio* vibrational and thermodynamic properties of adamantane, sila-adamantane ($Si_{10}H_{16}$), and $C_9S_1H_{16}$ isomers, *J. Mol. Struct.*, 2016, **1122**, 299-308.

[73] M. V. Gordeychuk, K. P. Katin, K. S. Grishakov and M. M. Maslov, Silicon buckyballs versus prismanes: Influence of spatial confinement on the structural properties and optical spectra of the $Si_{18}H_{12}$ and $Si_{19}H_{12}$ clusters, *Int. J. Quantum Chem.*, 2018, DOI:10.1002/qua.25609.

[74] S. Bondwal, P. Debnath, and P. P. Thankachan, Structural, electronic and optical properties of model silicon quantum dots: A computational study, *Phys. E: Low Dimens. Syst.*, 2018, **103**, 194.

[75] H. Zhang, R. Zhang, K. S. Schramke, N. M. Bedford, K. Hunter, U. R. Kortshagen and P. Nordlander, Doped Silicon Nanocrystal Plasmonics, *ACS Photonics*, 2017, **4**, 963.

[76] T. Chen, B. Skinner, W. Xie, B. I. Shklovskii and U. R. Kortshagen, Carrier Transport in Films of Alkyl-Ligand-Terminated Silicon Nanocrystals, *J. Phys. Chem. C*, 2014, **118**, 19580.

[77] C. C. Tu, K. P. Chen, T. A. Yang, M. Y. Chou, L. Y. Lin and Y. K. Li, Silicon Quantum Dot Nanoparticles with Antifouling Coatings for Immunostaining on Live Cancer Cells, *Appl. Mater. Interfaces*, 2016, **8**, 13714.

[78] P. Chandrachud, B. S. Pujari, S. Haldar and D. Kanhere, A systematic study of electronic structure from graphene to graphane, *J. Phys. Condens. Matter*, 2010, **22**, 465502.

[79] J. Prasongkit, A. Grigoriev, B. Pathak, R. Ahuja and R. H. Scheicher, Theoretical Study of Electronic Transport through DNA Nucleotides in a Double-Functionalized Graphene Nanogap, *J. Phys. Chem. C*, 2013, **117**, 15421.

[80] E. Kogan, Symmetry Classification of Energy Bands in Graphene and Silicene, *Graphene*, 2013, **2**, 74.

[81] K. S. Novoselov, A. K. Geim, S. V. Morozov, Grigorieva IV and A. A. Firsov, Electric field effect in atomically thin carbon films, *Science*, 2004, **306**, 666.

[82] J. Zhuang, X. Xu, H. Feng, Z. Li, X. Wang and Y. Du, Honeycomb silicon: a review of silicone, *Sci. Bull.*, 2015, **60**, 1551.

[83] L.C. Lew Yan. Voon and G. G. Guzmán-Verri, Is silicene the next graphene?, arXiv:1404.5691 [cond-mat.mtrl-sci], 2014, **39**, 366.

[84] L. C. Lew Yan Voon, J. Zhu and U. Schwingenschlögl, Silicene: Recent theoretical advances, *Appl. Phys. Rev.*, 2016, **3**, 040802.

[85] J. Zhao, H. Liu, Z. Yu, R. Quhe, S. Zhou, Y. Wang, C. C. Liu, H. Zhong, N. Han, J. Lu, Y. Yao and K. Wu, Rise of silicene: A competitive 2D material, *Prog. Mater. Sci.,* 2016, **83**, 24.

[86] C. Grazianetti, E. Cinquanta and A. Molle, Two-dimensional silicon: the advent of silicone, *2D Mater.*, 2016, **3**, 012001.

[87] D. Ghosh, P. Parida and S. K. Pati, Stable line defects in silicone, *Phys. Rev. B,* 2015, **92**, 195136.

[88] D. Jose and A. Dutta, Understanding the Buckling Distortion in Silicene, *J. Phys. Chem C*, 2012, **116**, 24639.

[89] M. Houssai, A. Dimoulas and A. Molle, Silicene: a review of recent experimental and theoretical investigations, *J. Phys.: Condens. Matter*, 2015, **27,** 253002.

[90] E. Kogan, Symmetry Classification of Energy Bands in Graphene and Silicene, *Graphene*, 2013, **2**, 74.

[91] W. Ke-Hui, A review of the growth and structures of silicene on Ag (111). *Chin. Phys. B*, 2015, **24**, 086802.

[92] Y. Yamada-Takamura and R. Friedlein, Progress in the material science of silicene. *Sci. Technol. Adv. Mater*., 2014, **15**, 064404.

[93] Z. Hong-Xia, Q. Ru-Ge and W. Yang-Yang, Silicene on substrates: A theoretical perspective, *Chin. Phys. B*, 2015, **24**, 087308.

[94] L. Hui, F. Hui-Xia and M. Sheng, Silicene from monolayer to multilayer-A concise review, *Chin. Phys. B*, 2015, **24**, 086102.

[95] D. Jose and A. Dutta, Structures and electronic properties of silicene clusters: a promising material for FET and hydrogen storage, *Phys. Chem. Chem. Phys.*, 2011, **13**, 7304.

[96] M. Neek-Amal, A. Sadeghi, G. R. Berdiyorov and F. M. Peeters, Realization of free-standing silicene using bilayer grapheme, *Appl. Phys. Lett.*, 2013, **103**, 261904.

[97] Y. Sugiyama, H. Okamoto, T. Mitsuoka, T. Morikawa, K. Nakanishi, T. Ohta and H. Nakano, Synthesis and Optical Properties of Monolayer Organosilicon Nanosheets, *J. Am. Chem. Soc.*, 2010, **132**, 5946.

[98] Y. Du, J. Zhuang, H. Liu, X. Xu, S. Eilers, K. Wu, P. Cheng, J. Zhao, X. Pi, K. W. See, G. Peleckis, X. Wang and S. X. Dou, Tuning the Band Gap in Silicene Oxidation, *ACS Nano*, 2014, **8**, 10019.

[99] J. H, Mokkath and U. Schwingenschlögl, Tunable optical absorption in silicene molecules, *J. Mater. Chem. C*, 2013, **4**, 7387.

[100] R. Das, A. Chowdhury, A. Majumdar and D. Jana, Optical properties of P and Al doped : a first principles study, *RSC Adv.*, 2015, **5**, 41.

[101] R. John and B. Merlin, Optical properties of graphene, silicene, germanene, and stanene from IR to far UV-A first principles study, *J. Phys. Chem. Solids*, 2017, **110**, 307.

[102] N. Saikia, M. Seel and R. Pandey, Stability and Electronic Properties of 2D Nanomaterials Conjugated with Pyraznamine Chemotherapeutic: A First Principles Cluster Study, *J. Phys. Chem. C*, 2016, **120**, 20323.

[103] A. Szabo and N. S. Ostlund, *Modern Quantum Chemistry: Introduction to Advanced Electronic Structure Theory*, Dover Publications Inc., Mineola, 1989.

[104] F. Jensen, *Introduction to Computational Chemistry*, John Wiley & Sons, Chichester, 2013.

[105] P. W. Atkins and R. S. Friedman, *Molecular Quantum Mechanics*, Oxford University Press, Oxford, 2011.

[106] T. Helgaker, P. Jorgensen and J. Olsen, *Molecular Electronic-Structure Theory*, John Wiley & Sons, New York, 2014.

[107] J. J. Sakurai, *Modern Quantum Mechanics*, Addison-Wesley, Reading, 1995.

[108] B. H. Bransden and C. J. Joachain, *Introduction to Quantum Mechanics*, Longman Scientific & Technical, 1994.

[109] C. C. J. Roothaan, New developments in molecular orbital theory. *Rev. Mod. Phys.*, 1951, **23**, 69.

[110] W. Koch and M. C. Holthausen, *A Chemist's Guide to Density Functional Theory*, Wiley-VCH, Weinheim, 2012.

[111] L. H. Thomas, The calculation of atomic fields, Mathematical Proceedings of the Cambridge Philosophical Society, Cambridge Univ. Press, 1927, **23**, 542.

[112] E. Fermi, Statistical method to determine some properties of atoms, *Rend. Accad. Naz. Lincei.*, 1927, **6**, 602.

[113] P. Hohenberg and W Kohn, Density functional theory, *Phys. Rev. B*, 1964, **136**, 864.

[114] W. Kohn and L. J. Sham, Self-Consistent Equations Including Exchange and Correlation Effects, *Phys. Rev.*, 1965, **140**, A1133.

[115] J. P. Perdew, K. Burke and M. Ernzerhof, Generalized Gradient Approximation Made Simple, *Phys. Rev. Lett.*, 1996, 7**7**, 3865.

[116] M. Ernzerhof, G. E. Scuseria, Assesment of the Perdew-Burke-Ernzerhof exchange-correlation functional. *J. Chem. Phys.* 1999, **110**, 5029.

[117] T. Yanai, D. P. Tew and N. C. Handy, A new hybrid exchange-correlation functional using the Coulomb-attenuating method (CAM-B3LYP), *Chem. Phys. Lett.*, 2004, **393**, 51.

[118] J. D. Chai and M. Head-Gordon, Long-range corrected hybrid density functional with damped atom-atom dispersion corrections, *Phys. Chem. Chem. Phys.*, 2008, **10**, 6615.

[119] E. Runge and E. K. Gross, Density-functional theory for time-dependent systems, *Phys. Rev. Lett.*, 1984, **52**, 997.

[120] S. J. Clark, M. D. Segall, C. J. Pickard, P. J. Hasnip, M. I. J. Robert, K. Refson and M. C. Payne, First principles methods using CASTEP, *Z. Kristallogr.*, 2005, **220**, 567.

[121] M. D. Segall, P. J. D. Lindan, M. J. Probert, P. C. James, P. J. Hasnip, S. J. Clark and M. C. Payne, First-principles simulation : ideas , illustrations and the CASTEP code, *Journal of Physics: Condensed Matter*, 2002, **14**, 2717.

[122] J. Paier, R. Hirschl, M. Marsman and G. Kresse, The Perdew-Burke-Ernzerhof exchange-correlation functional applied to the G2-1 test set using a plane-wave basis

set, *J. Chem. Phys.*, 2005, **122**, 234102.

[123] G. Kresse, From ultrasoft pseudopotentials to the projector augmented-wave method, *Phys. Rev. B*, 1999, **59**, 1758.

[124] N. Torres, J. Gracia, J. López, J. García, A. Sánchez, J. Sánchez, D. Luz and F. Morales, Ab Initio Molecular Orbital Calculation for Optical and Electronic Properties Evaluation of Small and Medium Size Silicon Nano-Clusters Found in Silicon Rich Oxide Films, *J. Mod. Phys.*, 2013, **4**,1.

[125] C. Vatankhah and A. Ebadi, Quantum Size Effects on Effective Mass and Band gap of Semiconductor Quantum Dots, *Res. J. Recent Sci.*, 2013, **2,** 21.

[126] A. Kshirsagar and N. Kumbhojkar, Empirical Pseudo- potential studies on electronic structure of semiconducting quantum dots, *Bull. Mater. Sci.*, 2008, **31**, 297.

[127] E. G. Barbagiovanni, D. J. Lockwood, N. L. Rowell, R. N. Costa Filho, I. Berbezier, G.Amiard, L. Favre, A. Ronda, M. Faustini, and D. Grosso, Role of quantum confinement in luminescence efficiency of group IV nanostructures, *J. Appl. Phys.*, 2014, **115**, 044311.

[128] D. K. Yu, R. Q. Zhang and S. T. Lee, Structural transition in nanosized silicon clusters, *Phys. J. Rev. B*, 2002, **65**, 245417.

[129] S. Niaz, E. N. Koukaras, N. P. Katsougrakis, T. G. Kourelis, D. K. Kougias and A. D. Zdetsis, Size dependence of the optical gap of small silicon quantum dots: Ab initio and empirical correlation schemes, *Microelectron. Eng.*, 2013, **112**, 231.

[130] R. Guerra, F. Cigarini and S. Ossicini, Optical absorption and emission of silicon nanocrystals: From single to collective response, *J. Appl. Phys.*, 2013, **113**, 143505.

[131] X. Jiang, J. Zhao and X. Jiang, Tuning the electronic and optical properties of hydrogen-terminated Si nanocluster by uniaxial compression, *J. Nanoparticle Res.*, 2012, **14**, 818.

[132] M. J. Frisch, G. W. Trucks, H. B. Schlegel, G. E. Scuseria, M. A. Robb, Cheeseman, , J. R. G. Scalmani, V. B. Mennucci and G. A.: Petersson, Gaussian, Inc., Wallingford CT (2009).

[133] T. H. Dunning and P. J. Hay, *Modern Theoretical Chemistry*, Plenum, NewYork, 1977.

[134] A. K. Rappe, T. A. Smedly and W. A. Goddard, The shape and Hamiltonian consistent (SHC) effective potentials, *J. Phys. Chem.*, 1981, **85**, 1662.

[135] P. J. Hay and W. R. Wadt, Ab *initio* effective core potentials for molecular calculations. Potentials for the transition metal atoms Sc to Hg, *J.Chem.Phys.*, 1985, **82**, 270.

[136] W. R. Wadt and P. J. Hay, Ab initio effective core potentials for molecular calculations. Potentials for main group elements Na to Bi, *J. Chem. Phys.*, 1985, **82**, 284.

[137] A. Zunger and L. Wang, Theory of silicon nanostructures, *Applied Surface Science*, 1996, **102**, 350.

[138] O. Lehtonen and D. Sundholm, Coupled-cluster studies of the electronic excitation spectra of silanes, *J. Chem. Phys.*, 2006, **125**, 144314.

[139] U. Itoh, Y. Toyoshima and H. Onuki, Vacuum ultraviolet absorption cross sections of SiH_4, GeH_4, Si_2Hs, and Si_3Ha , *J. Chem. Phys.*, 1986, **85**, 4867.

[140] K. A. Jackson, M. Yang, I. Chaudhuri and T. Frauenheim, Shape, polarizability, and metallicity in silicon clusters, *Phys. Rev., A,* 2005, **71**, 033205.

[141] H. Li, M. H. Garner, Z. Shangguan, Q. Zheng, T. A. Su, M. Neupane, P. Li, A. Velian, M. L. Steigerwald, S. Xiao, C. Nuckolls, G. C. Solomon and L. Venkataraman, Conformations of cyclopentasilane stereoisomers control molecular junction conductance, *Chem. Sci.*, 2016, **7**, 5657.

[142] Z. Smith, A. Almenningen, E. Hengge and D. Kovar, Electron-diffraction study of gaseous cyclohexasilane, *J. Am. Chem. Soc.*, 1982, **104**, 4362.

[143] G. Tekautz, A. Binter, K. Hassler and M. Flock, hair, Boat and Twist Conformation of Dodecamethylcyclohexasilane and Undecamethylcyclohexasilane: A Combined DFT and Raman Spectroscopic Study, *Chem. Phys. Chem.*, 2006, **7**, 421.

[144] D. Vanderbilt, Soft self-consistent pseudopotentials in a generalized eigen value formalism, *Phys. Rev. B*, 1990, 41, 7892.

[145] (a) D. Prendergast, J. C. Grossman and G. Galli, The electronic structure of liquid water within density-functional theory. *J. Chem. Phys.*, 2005, **123**, 014501. (b) J. Q. Zeng and H. Yu, Oxidation-Induced Redshifts in the Energy Gap of Silicon, *Key Eng. Mater.*, 2013, **562-565**, 852.

[146] Z. R. Qiu and H. Yu, Optical Properties of Silicon Quantum Dots, *Key Eng. Mater.*, 2011, **483**, 760.

[147] A. Kulkarni, D. Guney, A. Vora, Optical Absorption in Nano-Structures : Classical and Quantum Models, *ISRN Nanomaterials*, 2013, 1.

[148] R. R. Zope, T. Baruah, M. R. Pederson, S. L. Richardson, Equilibrium structure and vibrational spectra of sila-adamantane, arXiv:1005.5381v1 [physics.chem-ph] , 2010.

[149] K. J. Miller, The Molecular Polarizability Tensor, *J. Am. Chem. Soc.*, 1990, **112**, 8543.

[150] X. Chu, M. Yang and K. A. Jackson, The effect of geometry on cluster polarizability: Studies of sodium, copper, and silicon clusters at shape-transition sizes, *J. Chem. Phys.*, 2011, **134**, 234505.

[151] I. Heidari, N. Vaval, S. Pal and D. G. Kanhere, Polarizability of few electron quantum dots: Extended coupled-cluster response approach, *Chem. Phys. Lett.***,** 2016, **4**, 7387.

[152] G. Maroulis, Charge distribution, electric multipole moments, static polarizability and hyperpolarizability of silene, *Chem. Phys. Lett.*, 2011, **505**, 5.

[153] G. Maroulis, Bond length dependence of polarizability and hyperpolarizability of boron hydride, *Int. J. Quantum Chem*., 2011, **111**, 807.

[154] R. Schäfer, S. Schlecht, J. Woenckhaus and J. A. Becker, Polarizabilities of Isolated Semiconductor Clusters, *Phys. Rev. Lett*., 1996, **76**, 471.

[155] M. X. Dung, D. D. Tung, S. Jeong and H. D. Jeong, Tuning optical properties of Si quantum dots by π-conjugated capping molecules, *Chem. Asian J*., 2013, 8, 653.

[156] J. M. Rondinelli and E. Kioupakis, Predicting and Designing Optical Properties of Inorganic Materials, *Annu. Rev. Mater. Res.*, 2015, **45**, 491.

[157] J. P. Proot, C. Delerue and G. Allan, Electronic structure and optical properties of silicon crystallites: Application to porous silicon, *Appl. Phys. Lett.*, 1992, **61**, 1948.

[158] X. Wang, R. Q. Zhang and S. T. Lee, Unusual size dependence of the optical emission gap in small hydrogenated silicon nanoparticles, *Appl. Phys. Lett*., 2007, **90**, 123116.

[159] K. Dohnalová, T. Gregorkiewicz and K. Kůsová, Silicon quantum dots: surface matters, *J. Phys. Condens. Matter*, 2014, **26**, 173201.

[160] M. H. Nayfeh, and L. Mitas, *Nanosilicon*, Vijay Kumar, Elsevier, Amsterdam, 2008.

[161] G. Pucker, E. Serra and Y. Jestin, *Quamtum Dots - A Var. New Appl.*, Dr. Ameenah Al. Ahmadi, Italy, 2012.

[162] K. Surana, PhD Thesis, University of Grenoble, 2011.

[163] Y. He, C. Fan and S. T. Lee, Silicon nanostructures for bioapplications, *Nano Today*, 2010, **5**, 282.

[164] G. E. J. Jr and F. A. Modine, Parameterization of the optical functions of amorphous materials in the interband region, *Appl. Phys. Lett*., 1996, **69**, 371.

[165] R. L. Olmon, B. Slovick, T. W. Johnson, D. Shelton, S. H. Oh, G. D. Boreman and M. B. Raschke, Optical dielectric function of gold, *Phys. Rev. B*, 2012, **86**, 235147.

[166] K. E. Peiponen, E. M. Vartiainen, T. Unuma, J. A. Zeitler, P. Silfsten, T. Venäläinen and H. Kishida, H, Dispersion relations for evaluating the complex refractive index of medium without the information of its thickness, *Appl. Phys. Lett*., 2013, **102**, 181110.

[167] D. E. Aspnes and A. A. Studna, Dielectric functions and optical parameters of Si, Ge, GaP, GaAs, GaSb, InP, InAs, and InSb from 1.5 to 6.0 eV, *Phys. Rev. B*, 1983, **27**, 985.

[168] P. Holmström, L. ThyĺenThylén and A. Bratkovsky, Dielectric function of quantum dots in the

strong confinement regime, *J. Appl. Phys.*, 2010, **107**, 064307.

[169] T. J. Foley and U. Landman, U, Model dielectric function for semiconductors, *Si. Phys. Rev.B*, 1976, **14**, 1597.

[170] F. Huaxiang, Y. Ling and X. Xide, Optical properties of silicon nanostructures, *Phys. Rev. B,* 1993, **48**, 10978.

[171] S. K. Ghoshal, M. R. Sahar and M. S. Rohani, Dielectric Function of Silicon Nanoclusters : Role of Hydrogen, *Chin. Phys. Lett.*, 2011, **28**, 097801.

[172] Q. S. Li, R. Q. Zhang, S. T. Lee, T. A. Niehaus and T. Frauenheim, T, Optimal surface functionalization of silicon quantum dots, *J. Chem. Phys*., 2008, **128**, 244714.

[173] T. Zhou, R. T. Anderson, H. Li, J. Bell, Y. Yang, B. P. Gorman, S. Pylypenko, M. T. Lusk and A. Sellinger, Bandgap Tuning of Silicon Quantum Dots by Surface Functionalization with Conjugated Organic Groups, *Nano Lett*., 2015, **15**, 3657.

[174] M. M. Anas and G. Gopir, Surface Passivation Effect of Hydrogen and Methyl on the Structural and Electronic Properties of Silicon Quantum Dots: Density Functional Calculation. Mater, *Sci. Forum*, 2016, **846**, 375.

[175] J. Wang, Y. Liu, F. Peng, C. Chen, Y. He, H. Ma, L. Cao and S. Sun, A general route to efficient functionalization of silicon quantum dots for high-performance fluorescent probes, *Small*, 2012, **8**, 2430.

[176] F. Koch and T. Muschik, The luminescence of porous Si: the case for the surface state mechanism, *J. Lumin.*, 1993, **57**, 271.

[177] G. Allan, C. Delerue and M. Lannoo, Nature of Luminescent Surface States of Semiconductor Nanocrystallites, *Phys. Rev. Lett.*, 1996, **96**, 2961.

[178] P. Ebert, Coulomb Energy Determination of a Single Si Dangling Bond, *Phys. Rev. Lett*., 2010, **105**, 226404.

[179] S. K. Bhattacharya and A. Kshisagar, First-principle study of free and surface terminated CdTe nanoparticles, *Eur. Phys. J. D*, 2008, **48**, 355.

[180] M. Das, Two-Photon Cross Sections of trans-Stilbene, and 7, 8-Disubstituted Stilbenes in Different Molecular Conformations: A Model Exact Study, *J. Phys. Chem. A*, 2004, **108**, 6279.

[181] Sarkar, A., Das, M., Bagchi, S.: Electronic spectra and hyperpolarizabilities of structurally similar donor-acceptor dyes. A density functional theory analysis. *J. Mol. Struct*. 2011, **1102**, 11.

[182] V. Kundi, M. M. Alam, and P. P. Thankachan, Triply twisted Mobius annulene: a new class of two-photon active material-a computational study, *Phys. Chem. Chem. Phys.*, 2015, **17**, 6827.

[183] V. Kundi and P. P. Thankachan, New trans-stilbene derivatives with large two-photon absorption cross-section and non-linear optical susceptibility values-a theoretical investigation, *Phys. Chem. Chem. Phys*., 2015, **17**, 12299.

[184] V. Kundi and P. P. Thankachan, Packing of Large Two-and Three-Photon Activity into smallest possible unsymmetrical fluorine chromophores, *J. Phys. Chem. A*, 2016, **120**, 2757.

[185] L. Meng, Y. Wang, L. Zhang, S. Du, R. Wu, L. Li, Y. Zhang, G. Li, H. Zhou, W. A. Hofer and H. –J. Gao, Buckled Silicene Formation on Ir (111), *Nano Lett*., 2013, **13**, 685.

[186] G. Liu, X. L. Lei, M. S. Wu, B. Xu and C. Y. Ouyang, Comparision of the stability of free-standing silicene and hydrogenated silicene in oxygen: a first principles investigation, J. *Phys.: Condens. Matter*, 2014, **26** 355007.

[187] DALTON: A Molecular Electronic Structure Program, Release2013.4, 2014.

[188] R. C. Hilborn, Einstein coefficients, cross sections, f values, dipole moments, and all that, *Am. J. Phys.*, 1982, **50**, 982.

[189] A. Rizzo, S. Coriani and K. Ruud, *Computational Strategies for Spectroscopy. From Small Molecules to Nano Systems*, John Wiley and Sons, 2012.

[190] B. J. Orr and J. F. Ward, Perturbation theory of the nonlinear optical polarization of an isolated system, *Mol. Phys*., 1971, **20**, 513.

[191] E. Rudberg, P. Salek, Calculations of two-photon charge-transfer excitations using Coulomb-attenuated density-functional theory, *J. Chem. Phys.*, 2005, 123, 184108.

[192] M. Göppert-Mayer, Elementary processes with two quantum transitions, *Ann. Phys*., 2009, **18**, 466.

[193] Q. Yang, S. L. Zhang, X. P. Chen, M. Cai and C. J. Tan, Fluorosilicene/chlorosilicene bilayer semiconductor with tunable electronic and optical properties, *J. Appl. Phys.*, 2017, **121**, 055701.

[194] P. A. Denis, Stacked functionalized silicene: a powerful system to adjust the electronic structure of silicone, *Phys. Chem. Chem. Phys*., 2015, **17**, 5393.

[195] Y. Sugiyama, H. Okamoto, T. Mitsuoka, T. Morikawa, K. Nakanishi, T. Ohta and H. Nakano, Synthesis and Optical Properties of Monolayer Organosilicon Nanosheets, *J. Am. Chem. Soc*., 2010, **132**, 5946.

[196] M. J. G. Peach, P. Benfield, T. Helgaker and D. J. Tozer, Excitation energies in density functional theory: An evaluation and a diagnostic test, *J. Chem. Phys.*, 2008, **128**, 044118.

[197] M. J. G. Peach, C. R. Le Sueur, K. Ruud, M. Guillaume and D. J. Tozer, TDDFT diagnostic testing and functional assessment for triazene chromophores., *Phys. Chem. Chem. Phys.*, 2009, **11**, 4465.

INDIAN INSTITUTE OF TECHNOLOGY ROORKEE